UNIVERSITÀ
DEGLI STUDI
DI BRESCIA

DOTTORATO DI RICERCA IN
INGEGNERIA MECCANICA E
INDUSTRIALE

settore scientifico disciplinare
ING-IND/15

CICLO XXXVI

METHODS AND TOOLS TO EASE THE ELECTRIFICATION OF OFF-HIGHWAY VEHICLES AND MACHINERY PRODUCED BY SMALL AND MEDIUM-SIZED COMPANIES.

Chiar.mo Prof. Stefano Uberti
Chiar.mo Prof. Paolo Giulio Iora

Daniele Beltrami 707043

Abstract

Methods and Tools to Ease the Electrification of Off-Highway Vehicles and Machinery Produced by Small and Medium-Sized Companies.

Environmental sustainability, greenhouse emissions, and air pollution reduction are among the major drivers for the electrification of the transport and mobility sector. Indeed, the electrification of the consumptions for the automotive industry is in broad daylight, but the same process has just started for the off-highway industry. This process enables new technologies, but it comes also with new challenges and objectives. For instance, it facilitates new off-highway architectures and the development of both incremental and disruptive technology, enabling the emergence of completely new machinery and companies too. In this regard, industry and academia have already started developing electrified solutions, but they come with high development costs.

Small and medium-sized companies can be particularly sensitive to changes, and the expertise, cost, and timeframe related to this process can be extremely challenging. Many of these companies usually work as system integrators, relying on the integration and tuning of off-the-shelf components and systems. On the contrary, leading off-highway manufacturers can design optimized machinery thanks to custom-made products, relying on the economy of scale to return on investments.

Modeling and simulation can greatly help system-level design but building the mathematical model of an entire machinery is not trivial. In this regard, using industry-oriented modeling software like Simscape can simplify it, especially for small manufacturers. Indeed, modeling and simulation shift the design from steady-state design to dynamic and transient-state design, which is an essential step to investigate the potential of electrification: new control strategies, lower energy consumption, higher productivity, better forecast of the machinery hour rate, etc.

After an overview of the industry, its history, and the new challenges, the main components, and architectures typical of the electrification process

are presented. The most interesting electrified machinery are also shown to understand the general trends of both industry and academia. In fact, this analysis shows how much retrofitting can be important for this transition to more electrified machinery, but also how many improvements can be applied.

To investigate how much an industry-oriented modeling software can help small and medium-sized companies, an electrified material handler is modeled using Simscape. The modeling of the main four subsystems is presented (energy storage, electric motor, mechanics, and hydraulics), and the most important movements are compared with experimental data.

While focusing on the real objectives of this work, simulation and real-world testing show a good match. Indeed, even if the modeling of other subsystems is needed for more in-depth and accurate analysis, it is shown how industry-oriented software can be used to model complex subsystems and to get sensible results.

Lastly, two different approaches are analyzed by simulating the model over a personalized and realistic duty cycle. First, without changing anything of the current control strategy of the machinery, one reference velocity is proposed to balance energy consumption and productivity. The empirical results of the manufacturer of the hydraulic material handler confirm this trend, highlighting the good applicability of the model. Second, a new strategy based on the control of the electric motor speed is proposed and simulated. The results show the possibility of reducing energy consumption, but some components need to be modeled more in-depth to reach better accuracy and even lower results.

Nonetheless, it proves how much the system can be improved without changing any component, by relying on transient-state design and using the additional control variables enabled by electrification. Furthermore, it is shown how much an industry-oriented modeling software can help small and medium size enterprises during this important phase.

Metodi e Strumenti per Favorire l'Elettrificazione di Veicoli e Macchinari Off-Highway Prodotti dalla Piccola e Media Industria.

Sostenibilità ambientale, emissione di gas serra, e inquinamento atmosferico sono tra i maggiori driver dell'elettrificazione dei trasporti e della mobilità. Sotto questo punto di vista, l'elettrificazione dei consumi è evidente nell'industria automotive, ma lo stesso processo è iniziato anche per quella dell'Off-Highway. Questo è un passaggio importante per consentire lo sviluppo di alcune nuove tecnologie, ma porta con sé anche nuove sfide e obiettivi. Per esempio, esso facilita l'insorgere di nuove architetture tecniche, così come lo sviluppo di nuove tecnologie, sia evolutive che rivoluzionarie, favorendo anche la nascita di nuovi macchinari e aziende. A questo proposito, sia il mondo industriale che quello accademico hanno già iniziato lo sviluppo di soluzioni elettrificate, a fronte tuttavia di alti costi di sviluppo.

Per le aziende medio-piccole, più sensibili al cambiamento, le competenze, i costi, e i tempi richiesti da questo processo possono essere molto sfidanti. Molte di queste aziende sono solite lavorare come integratori di sistemi, il che significa che comprano dai fornitori componenti e sistemi stock. Al contrario, le aziende più strutturate e leader del mercato possono puntare su prodotti maggiormente ottimizzati e basati su componenti custom, poiché sono poi in grado di rientrare del più elevato investimento iniziale grazie alle maggiori economia di scala.

La modellistica e la simulazione possono aiutare molto la progettazione a livello sistemico, ma lo sviluppo di un modello matematico non è assolutamente banale. Questo processo può tuttavia essere semplificato da software di modellistica indirizzati all'ambiente industriale, specialmente per i produttori più piccoli. Infatti, modellistica e simulazione consentono il passaggio da un approccio steady-state a uno transient-state, che è fondamentale per investigare i vantaggi dell'elettrificazione: nuove strategie di controllo, minori consumi energetici, maggior produttività, miglior previsione dei costi orari di utilizzo, ecc.

Dopo un iniziale visione d'insieme dell'industria, della sua storia, e delle nuove sfide esistenti, sono presentati i componenti principali e le architetture tipiche dei mezzi elettrificati. Sono anche mostrati i macchinari più

interessanti per capire le tendenze dell'industria e dell'ambiente accademico. Per esempio, si capisce quanto il retrofitting dei macchinari possa essere importante per questa fase di transizione, seppur sia vero che possono essere applicate diverse migliorie.

Per investigare quanto un software di modellistica di tipo industry-oriented sia in grado di aiutare le piccole e medie aziende del settore, un sollevatore idraulico elettrificato è creato usando Matlab Simscape. È mostrata la modellizzazione dei quattro sottosistemi principali (accumulo di energia, motore elettrico, meccanica, e idraulica), e i movimenti principali della macchina sono simulati e comparati con i dati sperimentali.

Se ci si concentra sul reale focus di questo lavoro, simulazione e prove reali sono abbastanza affini. Infatti, pur riconoscendo che dei modelli più dettagliati siano necessari per analisi più accurate, è evidente come questa tipologia di software (maggiormente orientato agli ambienti aziendali) possa già essere usata per modellare sistemi complessi e per prendere confidenza con alcuni risultati.

Infine, due diversi approcci sono analizzati simulando il modello su un ciclo di lavoro personalizzato e realistico. Innanzitutto, senza alcun cambiamento al sistema di controllo, viene proposto un valore di velocità che bilanci consumo di energia e produttività della macchina. A questo proposito, lo storico e le osservazioni empiriche del costruttore confermano che tale velocità è sensata, evidenziando quindi la buona applicabilità del modello. In secondo luogo, è implementata e simulata una nuova strategia per il controllo della velocità del motore elettrico, e i risultati mostrano una generale diminuzione del consumo energetico. Tuttavia, per migliorare maggiormente l'accuratezza della previsione e diminuire di più i consumi, è necessario approfondire ulteriormente alcune componenti.

Cionondimeno, i risultati ottenuti testimoniano quanto il sistema attuale possa essere migliorato senza cambiare alcun componente, basandosi solamente su un design di tipo transient-state, e sfruttando i vantaggi dati dall'elettrificazione. Inoltre, è dimostrato quanto un software di modellistica industry-oriented possa essere utile ai produttori più piccoli per affrontare meglio questa importante transizione.

Table of Contents

1 Introductory Chapter

Electrified vehicles have undergone great evolution during the last two decades thanks to the increasing attention on environmental sustainability, greenhouse gas emissions, and air pollution. These are indeed among the major drivers for the electrification of the transport and mobility sector, especially for the automotive industry. On the one hand, consumers are more knowledgeable and careful during the selection process, on the other hand, governments have been tightening emission regulations. The electrification of consumptions for the automotive industry is in broad daylight, but the same process has just started for the off-highway industry (known also as Non-Road Mobile Machinery industry NRMM). In this regard, what happened in the former seems to be happening in the latter, but some key differences exist, among which the heterogeneity of the industry is among the most important ones. Indeed, while the architecture and size of passenger and commercial vehicles are limited in number and variety, as visible in Figure 1.1, the same does not apply to the off-highway industry: agricultural tractors, construction excavators, mining dump trucks, small lawnmowers are all off-highway machinery (Figure 1.2). So, as clearly visible from Figure 1.2, the off-highway machinery can greatly differ from each other, thus their size, architecture, and purpose.

Due to the electrification process, the automotive industry has been facing a great revolution, affecting the traditional European and American automakers, and paving the way for new manufacturers like Tesla, BYD, and many others, which were capable of bringing to the market some disruptive technology and new business models. In a minor way, the electrification process is enabling also new off-highway architectures and the development of both incremental and disruptive technology, enabling the emergence of completely new machinery and companies too. In this regard, a profound difference exists between the automotive and the off-highway industry: even if giant corporations/manufacturers exist also among NRMM, many small

and specialized companies share an essential part of the market, which is unusual in the automotive industry.

(a) (b)

(c) (d)

Figure 1.1 Examples of passenger and commercial vehicles. Light duty passenger vehicle (a), Medium duty passenger vehicle (b), Commercial van (c), Heavy duty truck (d).

(a) (b)

(c) (d)

Figure 1.2 Examples of off-highway machinery. Agricultural tractor (a), excavator (b), mining dump truck (c), riding lawn mower (d).

Electrification can be seen as an enabling technology, but it comes also with new challenges and objectives. For instance, while the focal point of any machinery remains to effectively complete its task, more attention has been given to how efficiently this is accomplished, and, even more importantly, which is the final Total Cost of Ownership (TCO). NRMM are indeed purchased to generate value and income, not for leisure or status, thus this market needs to justify the higher cost of acquisition with lower costs of operation, higher productivity, and/or new purposes. A clear example is the underground mining industry, where the use of battery electric and/or cabled machinery reduces the requirements for ventilation systems and exponentially increases the safety of the work environment.

The higher upfront cost of electrified machinery is due to components' cost (batteries, electric machines, high/voltage equipment, sensors, etc.), and to the investments in research and development to improve and optimize the performance of such components. Moreover, lack of standards is a burden for both suppliers and manufacturers: every component is essentially custom, for low-volume production, or one-offs, and many times it is difficult for manufacturers to understand what to make while thinking about what the standards will be in the future [1].

On the one hand, it allows both industry and academia to look to a wider range of solutions, on the other hand, the expertise is still growing, and defining which solution is best suited for each application is extremely challenging.

Modeling and simulation try to answer these open questions by digitalizing as much as possible of the research and development, but it requires moving from steady-state analyses made using spreadsheets to transient-state simulations. This shifting is indeed a priority to better analyze energy consumption. However, this process is not straightforward, it requires highly specialized employees, it takes time, and it still needs extensive testing campaigns to validate models.

While big manufacturers can afford all the previous thanks to their bigger nominal capitals, Small and Medium size Enterprises (SME) must find a way to stay competitive. In this regard, more and more software houses are developing tools to ease modeling and simulation, by moving from explicit

coding to visual programming to the assembly of pre-compiled components. A clear example of this transition can be seen throughout the portfolio offered by MathWorks with MATLAB, Simulink, and Simscape.

1.1 Off-Highway Machinery

The European Union defines off-highway machinery as [2] :

> *"… any mobile machine, transportable equipment or vehicle with or without bodywork or wheels, not intended for the transport of passengers or goods on roads, and includes machinery installed on the chassis of vehicles intended for the transport of passengers or goods on roads".*

As understandable from the definition, the off-highway machinery industry is extremely broad, and one of the key aspects is the "mission" [3]. The mission defines what the machinery is supposed to do, defining the main tasks to complete, as well as the environments where the machinery is supposed to work. The mission can be extremely specific, as for some extremely specialized machinery like the trencher visible in Figure 1.3a, but it can also be related to multiple tasks, requiring multipurpose capabilities, as for the backhoe loader in Figure 1.3b.

Because defining the mission can be extremely complicated and varied, the off-highway machinery industry is divided into four main categories (Table 1.1). Even if these different categories are universally recognized within the industry, multipurpose machinery can be fitted with different accessories to fulfill duties across the board (e.g., small tractors that can be used during winter as snow removal machinery, or municipal and property maintenance vehicles with many different types of equipment).

(a) (b)

Figure 1.3 Examples of off-highway machinery. Trencher (a), backhoe loader (b).

Category	Machinery
Tractors and agricultural.	Tractors, combine harvesters, field choppers, etc.
Municipal and property maintenance.	Turf cutters, street sweeping machines, etc.
Transportation of goods and material handling.	Forklift machines, material handlers, etc.
Construction, forestry, and mining.	Excavators, front-end loaders, backhoes, etc.

Table 1.1 Off-Highway machinery categories

1.2 History

The off-highway machinery industry is composed of many categories, but its roots can be traced down to the first applications of steam engines for earth moving, the steam shovel, in 1838. (Figure 1.4a) [4]. In 1868 a steam engine tractor was supposed to replace horses to boost productivity, marking the beginning of agricultural tractors and mechanized agriculture [5]. A decade after, in 1876, J. D. Adams paired its leaning-wheel road grader (Figure 1.4b) to a steam traction engine, and at the very beginning of the 20th century, the first gasoline-powered crawler tractor was created (Figure 1.4c) by the Holt Manufacturing Company, which then become the internationally famous Caterpillar Inc [6].

The transition from steam engines to gasoline and, most importantly, diesel engines is one of the most important key points. Indeed, the size and maintenance request of steam engines made it difficult to create mobile self-propelled machinery, while internal combustion engines proved to perfectly fit the needs of off-highway machinery. The World Wars played another significant role in advancing NRMM technology: the construction and earthmoving equipment industry was eager to speed up, the agriculture industry needed to increase food productivity, and obviously, there were many technological interconnections between off-highway machinery and

military vehicles. In these years, the first practical one-man-operated, self-propelled off-highway machinery was created by LeTourneau, the Model B Carryall scraper (Figure 1.4d) [4].

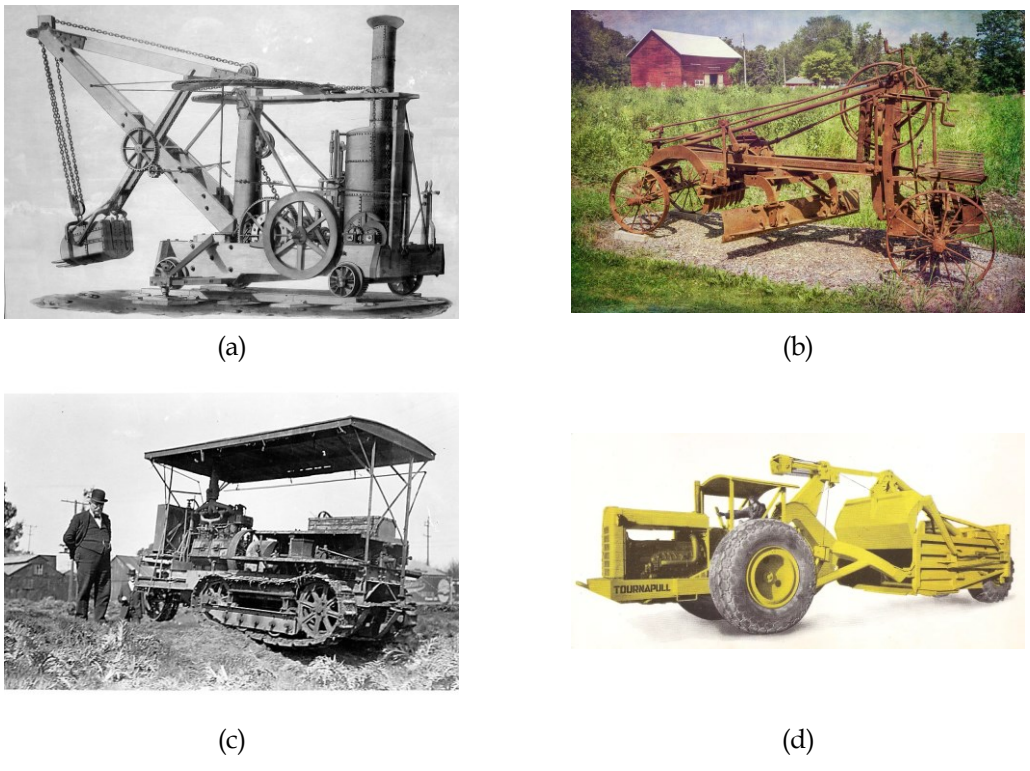

(a) (b)

(c) (d)

Figure 1.4 Ancient off-highway machinery: Otis's first excavator (a), J. D. Adams's leaning-wheel road grader (b), Holt crawler tractor (c), Model B Tournapull (d).

After World War II some important types of machinery were developed, like the front-end loader, which currently is the second most sold NRMM worldwide, but the second huge step forward for the industry was the introduction of hydraulic power, more or less 35 years after the arrival of ICEs. Up until the mid-50s, every excavator relied on cables, like most of the machinery, but in 1954 the German manufacturer Demag (currently part of Komatsu Germany Mining) presented the first fully hydraulic excavator [7].

The combination of mobile hydraulic and diesel engines was essential for the development of light construction equipment, and most of the off-highway machinery are still based on the same powertrain concept. In the last 30 years, the engines and hydraulics have been continuously developed to add functionalities, improve productivity, achieve better controllability, and, due to the advent of emission policies, reduce emissions. Electronics (computerized controls, telematics, GPS systems, etc.) has now become the

focus of most manufacturers. It is indeed fundamental for modern control systems, but it also gives the possibility to acquire and analyze data, which is essential for data-driven technical development, as well as data-driven business and marketing.

Figure 1.5 Demag B504.

1.3 Emission regulations

While in the 1990s the emission of NRMM was considered minor in comparison to the passenger vehicle industry, based on the analysis carried out in [8], the model shown in [9] predicts that NRMM will eventually surpass on-road vehicles as the leading source of mobile pollution in Asia by 2030.

However, the large variety of types of machinery is one of the main difficulties in calculating and/or measuring the emissions of off-highway machinery and vehicles [8]. Considering all the differences among the industry (sizes, engines, fuels, etc.), laboratory emissions measurements are indeed incapable of representing real-life emissions [10]. Furthermore, the use of Portable Emissions Measurement Systems (PEMS) gets more difficult due to extreme working conditions, and, even if in-use exhaust emissions

measurements of construction and agricultural machinery exist [11, 12], it is very difficult to generalize the results to the whole industry.

In the last decade, to reduce emissions throughout the entire industry, emission regulation policies have been requesting the adoption of emission reduction devices to be mounted on NRMM, like Diesel Particulate Filters (DPF), Exhaust Gas Recirculation (EGR), and Selective Catalytic Reduction (SCR), as described in [13]. The use of these technologies and their contribution to emission reduction is cited also in [12], where the consumption of the London construction fleet is discussed by analyzing 29 machinery.

One of the major concerns is indeed about the emissions in urban areas, where construction machinery powered by combustion engines represent significant sources of emissions. London, for instance, was one of the first metropolitan areas to set a Low Emission Zone (LEZ). In these areas, emissions regulations are very rigid also for NRMM and not only for passenger vehicles, buses, and vans [12]. Other important European metropolitan cities like Oslo, Copenhagen, Helsinki, and Barcelona signed a Joint Statement in 2022 requiring fossil-free construction machinery (a.k.a. electric battery machinery) in public project sites from 2025 [14].

The European Union, which historically is on the edge for emission control and regulations, set an emission control and reduction policy for NRMM engines back in 1997 through Stage I regulation [15]. The limits were initially set only for diesel compression ignited (CI) engines, and they were based on engine size, as visible in Table 1.2. Gasoline and/or natural gas spark-ignited (SI) engines below 19 kW were added by means of additional directives.

Net Power	CO	HC	NOx	PM
kW		g/kWh		
$130 \leq P \leq 560$	5.0	1.3	9.2	0.54
$75 \leq P < 130$	5.0	1.3	9.2	0.70
$37 \leq P \leq 75$	6.5	1.3	9.2	0.85

Table 1.2 EU Stage I emission standard for nonroad diesel engines. [16]

Nowadays, the Stage V regulation (Table 1.3) [16] has been effective since 2020 in the European Union and it is fundamental for multiple reasons:

- it includes SI engines above 19 kW;
- it includes CI engines below 19 kW and above 560 kW;
- it categorizes engines not only based on power but also on use cases (e.g. mobile machinery, all-terrain recreational vehicles, hand-held tools, etc.).

Cat.	Ign.	Net Power kW	CO	HC	NOx	PM	PN $1/kWh$
				g/kWh			
NRE-v/c-1	CI	$P < 8$	8.00	$7.50^{a,c}$		0.40^{b}	/
NRE-v/c-2	CI	$8 \leq O < 19$	6.60	$7.50^{a,c}$		0.40	/
NRE-v/c-3	CI	$19 \leq P < 37$	5.00	$4.70^{a,c}$		0.015	1×10^{12}
NRE-v/c-4	CI	$37 \leq P < 56$	5.00	$4.70^{a,c}$		0.015	1×10^{12}
NRE-v/c-5	All	$56 \leq P < 130$	5.00	0.19^{c}	0.40	0.015	1×10^{12}
NRE-v/c-6	All	$130 \leq P \leq 560$	3.50	0.19^{c}	0.40	0.015	1×10^{12}
NRE-v/c-7	All	$P > 560$	3.50	0.19^{d}	3.50	0.045	/

$a \rightarrow$ HC+NOx
$b \rightarrow$ 0.60 for hand-startable, air-cooled direct injection engines
$c \rightarrow A = 1.10$ for gas engines
$d \rightarrow A = 6.00$ for gas engines

Table 1.3 Stage V emission standard for nonroad engines.

In the United States, and more generally speaking in North America, the EPA is the organization responsible for emission regulations policies, and it was the first to promulgate emission standards with the Tier 1 policy in 1994 [17].

The EU Stage policy and the EPA Tier policy have been following a common route since their creation, paving the way for emission standards all over the globe. However, due to the technical challenges and increased costs demanded by the EU Stage V, the EPA has not currently published the new Tier 5 standard, nor there is a hypothetical due date for its release. The difference between the new EU Stage V and older Tier 4 standards is visible in Figure 1.6, however, it is worth mentioning that neither the EU Stage V nor

the U.S. EPA Tier 4 set any limitation for CO2 emissions, which is instead the most common parameter for passenger vehicles.

The evolution of the EU Stage policy is also visible in Figure 1.7, where it is visually clear the magnitude of the emission reduction, remarking the incredible evolution of engine emission control in the past two decades, as well as the technical challenges the industry will encounter by facing further reductions. The PM limit of the Stage V standard is indeed 97 percent lower than that of the Stage I standard, and the hydrocarbon (HC) + nitrogen oxides (NOx) limit is 94 percent lower [18]. The magnitude of this emission reduction is such that further decrease is supposed to be extremely difficult without any implementation of electrified solutions, copying what has been happening in the automotive industry.

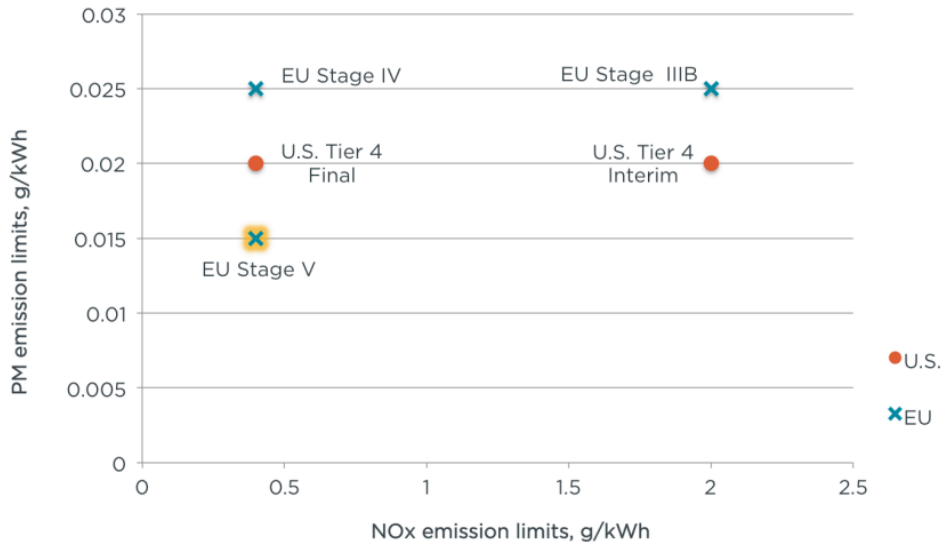

Figure 1.6 Comparison of PM and NOx emission limits between the U.S. and EU.

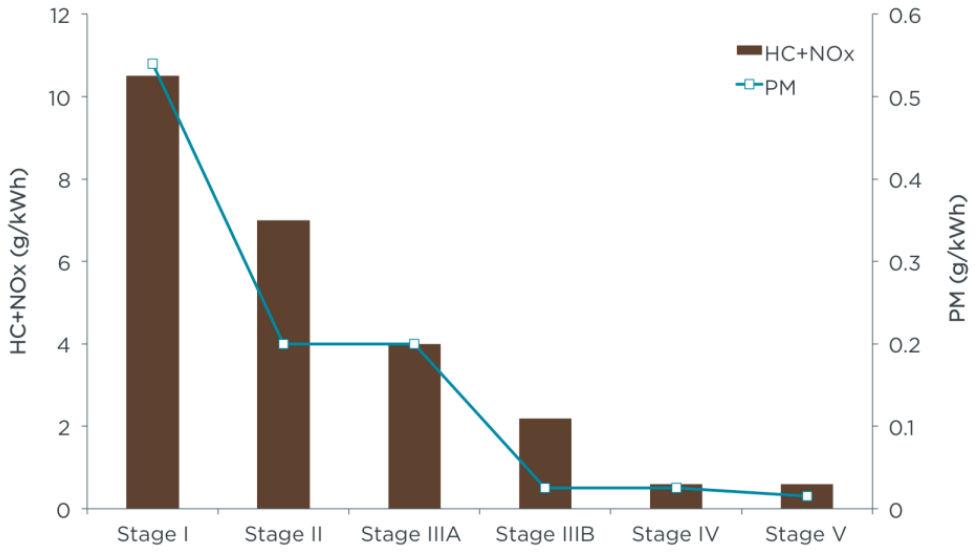

Figure 1.7 Emission limits from Stage I to Stage V for HC + NOx and PM. [18]

1.4 Driving and working cycles

By setting different velocity profiles, driving cycles are useful to set a common ground for the evaluation of the energy consumption of passenger vehicles. The most known sets of driving cycles are the ones decided by the American Environmental Protection Agency (EPA), the ones that were in use in the European Union (EU), and the Japanese ones. In the attempt to create a worldwide recognized driving cycle, the final version of the World harmonized Light-duty vehicles Test Procedure (WLTP) was released in 2015, but not in every market this has been recognized as the common standard yet. For instance, while every vehicle sold in Europe after 2019 must declare the energy consumption based on the WLTP (Figure 1.8a), this is not the case for the US market, where the EPA Federal Testing Procedure is preferred for the EPA window sticker (Figure 1.8b and Figure 1.9). Because some use cases can be more specific, like driving in a very congested metropolitan area like Manhattan or, on the opposite, on highways, more peculiar driving cycles exist, and they are used for technical investigations and not for certification purposes.

In any case, while some differences in procedures exist among automotive driving cycles, the only essential and clear difference is about the

speed profile, as visible in Figure 1.8, because the main power/energy flow of a vehicle is supposed to be completely toward traction. Even thinking about long haul trucks (on-highway heavy-duty vehicles), the velocity profiles are different than for a passenger vehicle, but the order of magnitude is similar: for instance, instead of a maximum velocity of 130 km/h, it is around 100 km/h.

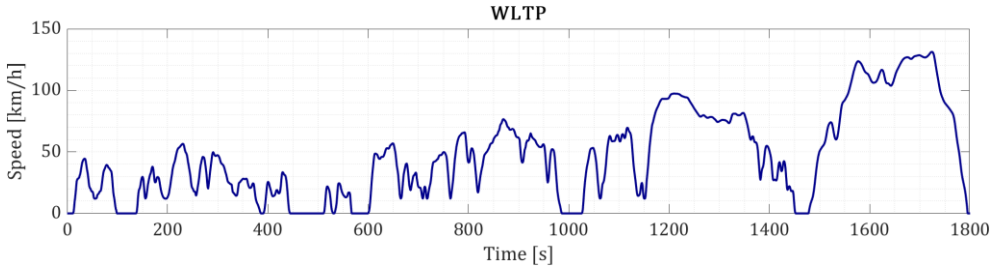

(a)

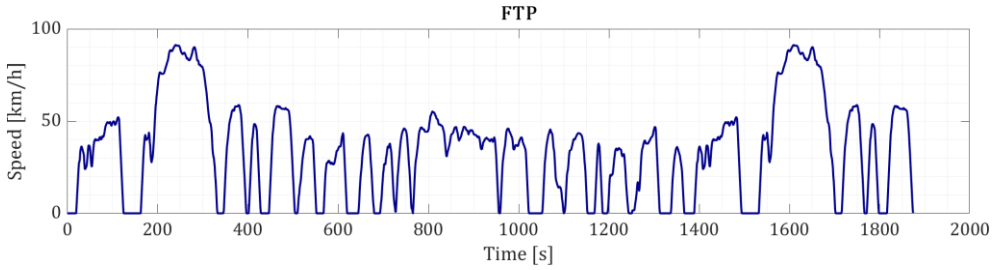

(b)

Figure 1.8 Automotive driving cycles: WLTP (a), FTP (b).

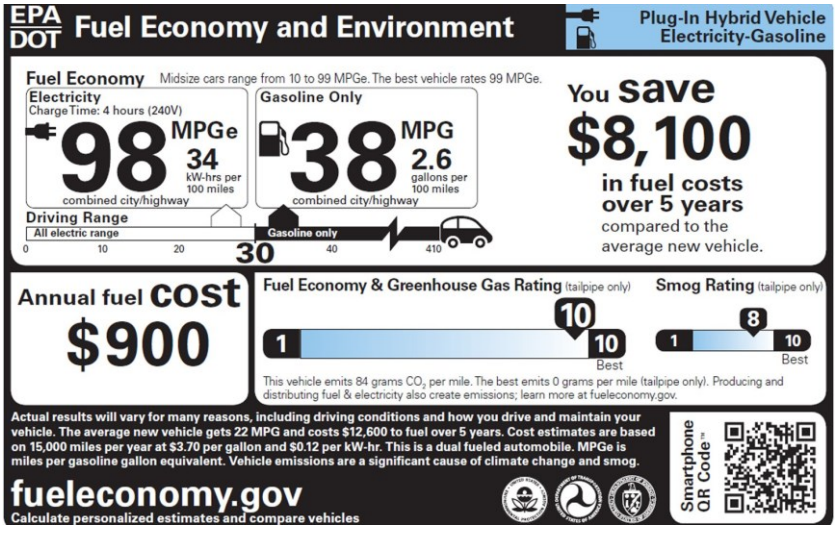

Figure 1.9 Example of the EPA window sticker.

This is not the case for off-highway machinery, where driving cycles are replaced by working cycles (or duty cycles).

First, traction is only one of the many tasks that the machinery must fulfill. Thinking about an agricultural tractor, for instance, much power is directed to ancillaries by use of the Power Take Off (PTO). Indeed, in a very simplified manner, the main mission of this machinery is to be a mobile, pulling-capable power supplier. Another example is a tracked excavator: tracks allow the excavator to move on difficult pavements, but the main power flows are to the arms and the swinging of the upper carriage.

The other big difference is related to the size: as an example, the maximum power requested by a small excavator for in-house renovation is completely different from the one requested by a mining excavator, even if one seems to be a scaled version of the other.

It is then clear how difficult it is for the scientific and technical community to set standardized duty cycles for the off-highway industry.

In this regard some attempts were made by the EPA [19], that designed some duty cycles for some of the most known NRMM, like agricultural tractors (Figure 1.10a), backhoe loaders (Figure 1.10b), excavators (Figure 1.10c), skid steer loaders (Figure 1.10d), etc. All these examples, which descend by experimental campaigns and are not designed a priori, show another key aspect: the frequency of the power peaks is incredibly higher than the frequency of the speed profiles of the driving cycles. Another good attempt at standardization was made by the Japanese Construction Mechanization Association with the test procedure explained in [20], but they are still not globally recognized. The last noteworthy attempt, which may be also the most successful yet, is the DLG PowerMix (Deutsche Landwirtschafts Gesellschaft-German Agricultural Society) [21], which states itself as the de facto standard for agriculture tractors. The PowerMix test consists of 14 test cycles that simulate various loads on the tractor, measuring its fuel and AdBlue consumption, its output power, and its efficiency as the machinery goes through the test cycle. The aim is to replicate typical field and transport applications at half-load and full-load. Nonetheless, this duty cycle has no legal value for the homologation process, and it is mainly used to provide

product information to potential buyers by reporting a synthetic cost per kWh of usage.

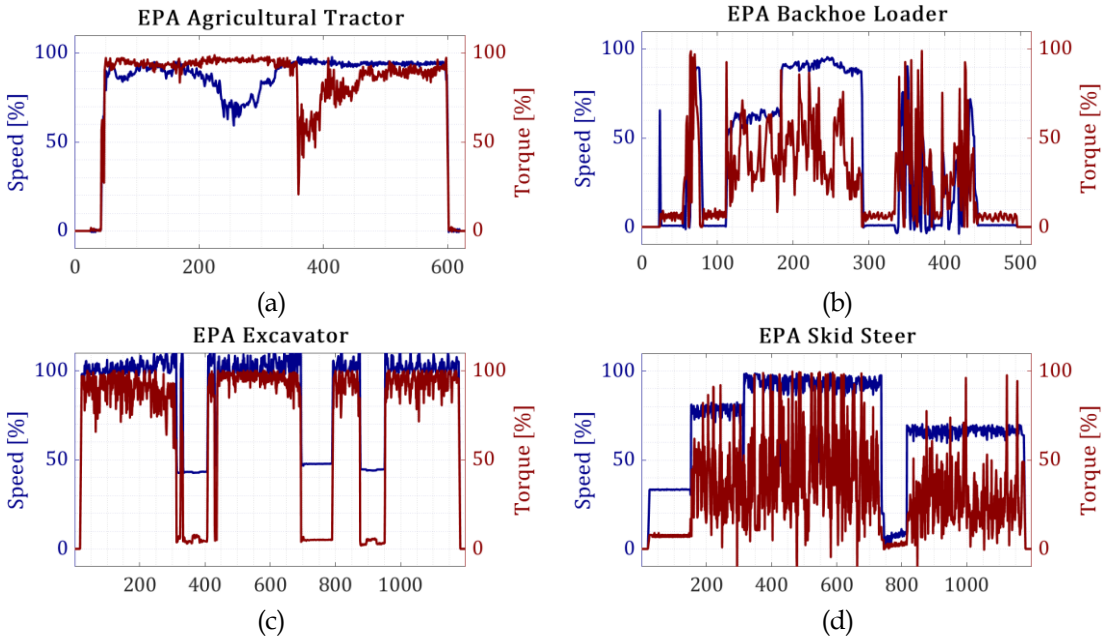

Figure 1.10 EPA nonroad working cycles: agricultural tractor (a), backhoe loader (b), excavator (c), skid steer (d).

In these circumstances, every Original Equipment Manufacturer (OEM) is accustomed to its internal duty cycles and researchers even tend to register specific duty cycles for each vehicle under analysis: in [22–24] the electrification of agricultural tractors is investigated, and some duty cycles are used for the analysis, but no DLG Power Mix or EPA duty cycle are mentioned. Similarly for construction machinery, in [25, 26] the authors define a specific duty cycle for the hybridization process of a skid loader, while in [27–31] different duty cycles are used for compact excavators.

So, driving and/or duty cycles are key points since knowing the power and torque request profiles for each vehicle/machinery allows the correct selection and sizing of the onboard power sources, powertrain layout, and energy storage systems. They all indeed influence the effectiveness, efficiency, and operational runtime of electrified machinery.

1.5 Modeling Software

MATLAB, Simulink, and Simscape are three interconnected tools used for modeling, simulation, analysis, and data visualization.

MATLAB is a high-level programming language and computing environment. It is commonly used by engineers in industry and academia for numerical analysis, data manipulation, and algorithm development, and it is primarily focused on numerical and matrix-based computation [32].

MATLAB is often compared to other programming languages like Fortran or C++, which are low-level general-purpose programming languages. On the one hand, MATLAB uses a simplified syntax, it usually is more friendly to use because it is designed for rapid prototyping, and it provides a wide range of toolboxes to expand its functionalities. On the other hand, it is not as efficient for high-performance computing. In short, MATLAB excels in matrix operations, data manipulation, and visualization, but it is not ideal for modeling complex dynamics systems: being a programming language it requires a lot of coding, and there are other more efficient languages when complex coding is vital.

Simulink is a graphical simulation and model-based design environment based on MATLAB, and it is extremely common for dynamic systems analysis. Being a visual programming software, it employs blocks representing different mathematical components (operators, inputs, functions, etc.) (Figure 1.11) [33]. While MATLAB is capable of analytical computing, Simulink completely relies on numerical computing, which is essential to represent the behavior of complex systems with nonlinear dynamics, time-varying parameters, and interactions among components. After the selection of the proper solver, which is the computational algorithm to numerically solve the differential equation of the system, using Simulink it is possible to observe how the system's signals change over different time steps. Thus, Simulink models are best suited for the development of control systems. Indeed, the visual programming approach allows engineers to quickly understand the structure, dynamics, and interactions. However, Simulink still needs in-depth mathematical knowledge of the phenomena,

and, most importantly, it is necessary to understand and share its visual programming logic.

Simscape is a tool within the Simulink environment, and its purpose is to simplify the modeling of physical systems [34]. The idea is to shift the attention from block diagram modeling (math operators, functions, etc.) to component-based modeling. Thus, instead of visually coding equations and interactions, there are libraries of physical components where to insert proper physical parameters. The requested parameters can range from the simple constant stiffness of a linear spring (Figure 1.12a) to the mechanical and electrical parameters needed to characterize a linear piezoelectric motor (Figure 1.12b). One great advantage of Simscape over Simulink is the visualization of the system and its components more intuitively. Indeed, the components are sequentially placed to replicate the mechanical/electrical/hydraulic scheme of the system, as visible in Figure 1.13, where the same two-degree dynamic system of Figure 1.11 is replicated.

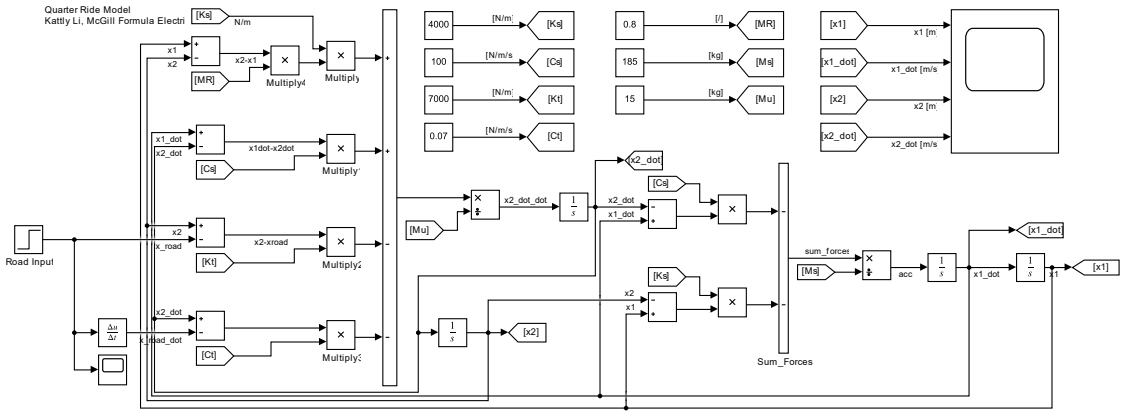

Figure 1.11 Example of visual programming in Simulink for a two-degree freedom system with two springs and two dampers. (Edited from [35])

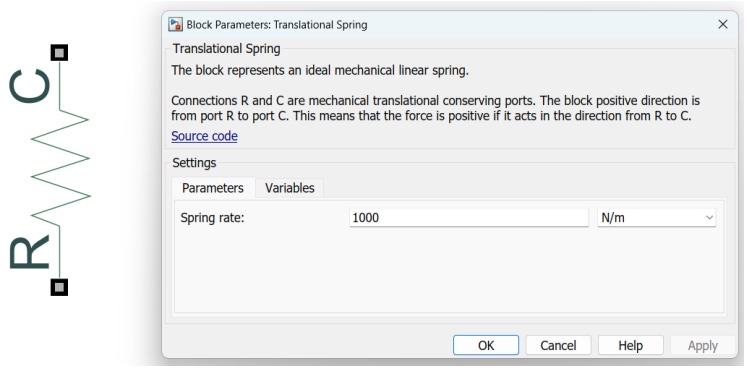

(a)

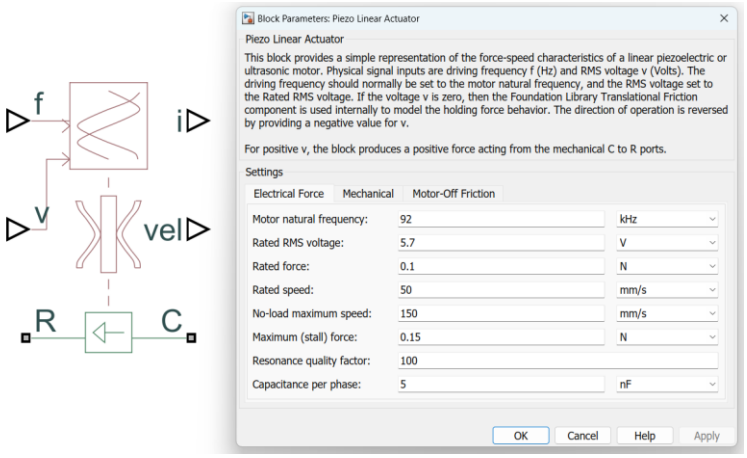

(b)

Figure 1.12 Instances of Simscape components: translational spring (a), piezo linear actuator (b).

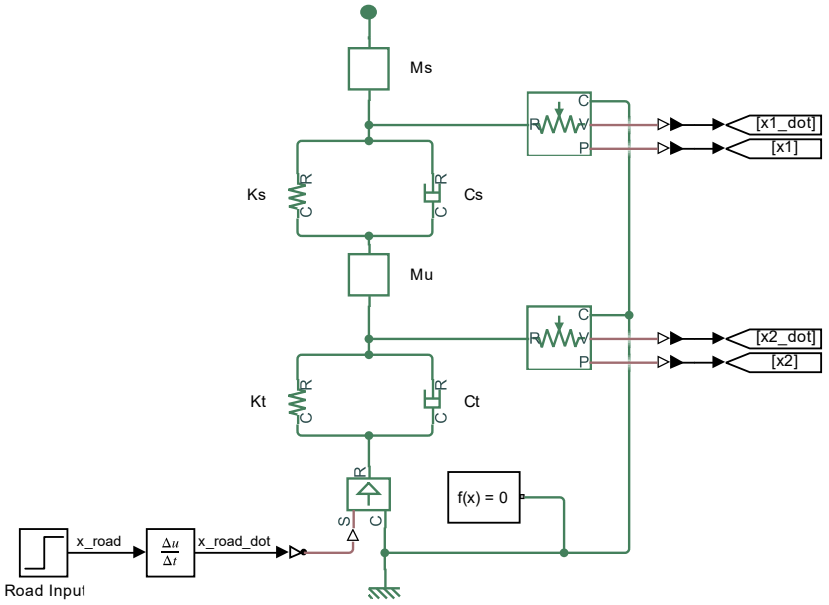

Figure 1.13 Example of modeling in Simscape for a two-degree freedom system with two springs and two dampers.

2 Main Components and Architectures

The very first distinction to make when talking about electrified vehicles and machinery is about electric and hybrid: the distinction between the two depends on the energy sources mounted on the machinery. In the former, the powertrain is characterized by a single energy source of electric power (e.g. battery and/or tethered cable), while hybrid machinery and vehicles have at least two different sources (e.g. ICE and battery, fuel cells and battery, etc.).

Starting with electric machinery, similar to what is reported in [36], they can be divided based on the following architectures:

- Tethered type: The only energy source is the physical connection to an external electric source (e.g. power grid, or external diesel generator). Examples of this machinery are the huge, tethered excavators for mining applications (Figure 2.1). These applications can exploit the boost in efficiency given by electrification [37], but, because of the great amount of requested power, the only feasible solution is the physical connection to the power grid.
- Battery type: The energy storage system provides all the energy. External sources of energy charge the energy storage system, but they are disconnected when the machinery works. This probably is the most common type of electric machinery but working range and charging infrastructure remain important topics of discussion and development.
- Tethered-battery type: The machinery can work either way, while connected to the external source or using only the internal energy storage system, which can potentially overcome the limited working range. For instance, some small excavators for indoor construction take advantage of this solution and they connect to external diesel generators.

Figure 2.1 Example of tethered electric excavator, the Hitachi EX5600E.

Within hybrid machinery, there are many more architectures because of the presence of multiple energy sources. Indeed, they can be divided based on how the energy sources are coupled, on the power ratio between the energy sources, or, considering the traction power flow and the working power flow as two different entities, on which part of the machinery they are intended to provide energy to. The former two methods of splitting the hybrid architectures are common also in the automotive industry [38]:

- Series hybrid: The two power sources are electrically coupled, meaning that they are mechanically disconnected, and the power electronics must balance the energy flow between them. In this case, there must be at least one electric motor and one electric generator. This can also be considered as the simplest hybrid architecture.
- Parallel hybrid: The two power sources are mechanically coupled by a transmission. It is more complex than the series hybrid, but it needs only one electric machine that works both as motor and generator.
- Series-parallel hybrid: The two power sources are electrically and mechanically connected, giving engineers the possibility of creating more working modes to optimize efficiency, because it can work both as series and parallel hybrids. It surely is the most complex architecture, indeed, not only there is both the complex mechanical transmission (usually with one or more Planetary Gear Set PGS) and, at least, two electric machines, but much attention must be given to properly control power recirculation among the sources.

Based on this classic division between hybrid architectures, in the automotive industry, it is common to classify hybrids also based on the power ratio between the sources. This is known as the Hybridization Factor HF [39] (Eq. 1), where P_{EM} is the power coming from the electric motor, while $P_{\mathrm{ICE|FC}}$ comes from an ICE or a FC:

$$HF = \frac{P_{\mathrm{EM}}}{P_{\mathrm{EM}} + P_{\mathrm{ICE\,|\,FC}}} \qquad \text{Eq. 1}$$

Because for off-highway machinery it is important to differentiate the traction effort and the power that goes to hydraulics and implements, in [40] the authors proposed a novel definition of the Hybridization Factor HF, where this is computed as the average of two different factors (Eq. 2). P_{EM1} is the power of the electric motor addressed to traction, P_{EM2} is the one that goes to hydraulics and implements, $P_{\mathrm{ICE|FC}}$ is generated by the ICE or FC.

$$\mathrm{HF} = \frac{1}{2}\left(\frac{P_{\mathrm{EM1}}}{P_{\mathrm{EM1}} + P_{\mathrm{ICE|FC}}} + \frac{P_{\mathrm{EM2}}}{P_{\mathrm{EM2}} + P_{\mathrm{ICE|FC}}}\right) \qquad \text{Eq. 2}$$

The combination of these classifications can be seen in Figure 2.2, where the difference between the driveline and the hydraulics power flows is schematized as done in [41].

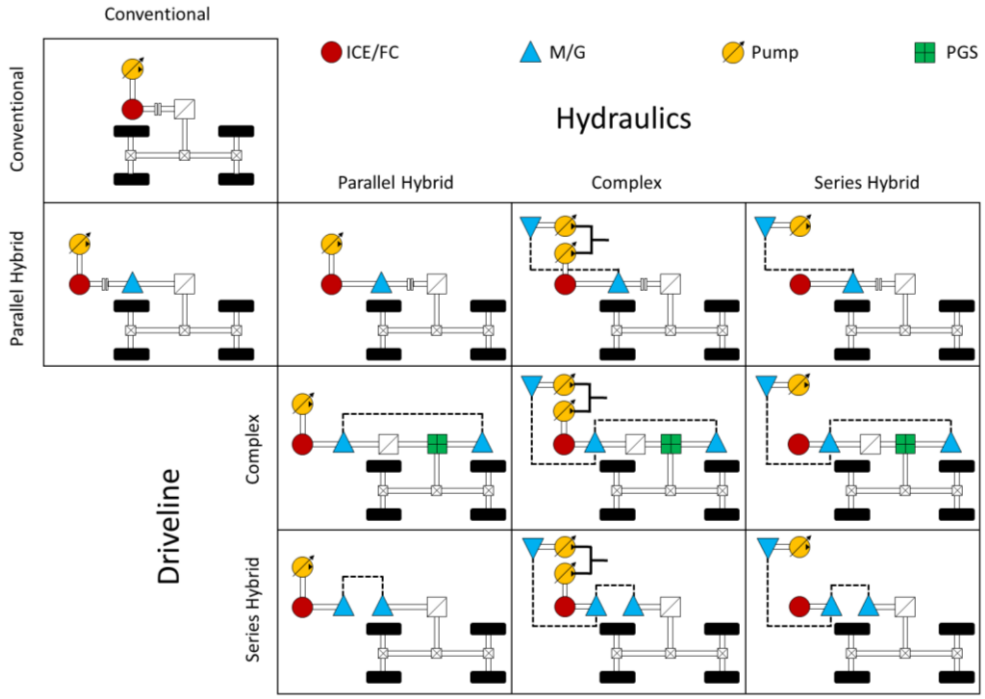

Figure 2.2 Combination of hybrid architectures for mobile machinery. (Adapted from [41])

2.1 Energy Storage Systems

The Energy Storage System ESS is key for any electrified vehicle and machinery. Among the many properties of ESSs, the following are usually considered the most important ones [42], and, in the Table 2.1, there is a comparison between the most common ESSs.

- Specific power $[W/kg]$: It is fundamental to evaluate if the ESS can manage the peak power requests, both while discharging and charging. Hybrid powertrains are usually equipped with ESS with higher specific power.
- Specific energy $[Wh/kg]$ and energy density $[Wh/L]$: It is fundamental to evaluate the working range of the machinery in relation to its weight. It may be the most famous and important parameter for battery electric vehicles and machinery, especially if traction and traveling are important features. However, it is not as fundamental on machinery that works at fixed-point, because they can replace part of the counterweight. Like the specific energy, energy density is still closely related to the working range of the

machinery, but it indicates the occupied volume. Available free space is a very important topic on off-highway machinery, especially on small ones, because it is limited.

- Cycle life [∅]: It represents the number of discharge-charge cycles the battery can experience before it can no longer meet some specific performance requirements. There isn't a standardized ratio of the original and actual capacity of the ESS after which the ESS needs to be replaced, but, in the automotive industry, 80% is usually considered as the rule of thumb for batteries. (It is worth mentioning that it does not represent the number of years the ESS can sustain before maintenance).
- Efficiency [∅]: it is the average of the charging and discharging efficiencies. The more efficient the battery, the less power is wasted in heat.

	Flywheel	Supercapacitor	Hydraulic Accumulator	Lead-Acid Battery	Ni-MH Battery	Li-Ion Battery
Specific Power	40 ÷ 1500	500 ÷ 5000	2000 ÷ 19,000	75 ÷ 300	150 ÷ 200	250 ÷ 340
Specific Energy	10 ÷ 30	2.5 ÷ 5.5	2	30 ÷ 50	60 ÷ 120	75 ÷ 200
Energy Density	20 ÷ 80	35	5	50 ÷ 80	150 ÷ 180	200 ÷ 250
Cycles	20,000	100,000	100,000	500 ÷ 1500	2500	2000 ÷ 10,000
Efficiency	< 96	< 95	< 90	< 80	< 90	95

Table 2.1 Comparison between the main ESSs [42, 43]

Among the ESSs, batteries and, more specifically, lithium batteries are recognized as the current state-of-the-art, as well as the most interesting solution in the medium to long term, both from a technical and cost-effective point of view. Indeed, specific cost per energy unit ($\$/kWh$) dropped significantly in the last decade [44], which is visible in Figure 2.3. Lithium batteries are not all identical, indeed there is more than a single chemistry and each one has its pros and cons. While the automotive industry uses a mix of LiFePO4 (Lithium Iron Phosphate), NCA (Lithium Nickel Cobalt Aluminum Oxide), and NMC (Lithium Nickel Cobalt Oxide) [45], in the off-highway industry LiFePO4 stands out because of its inherent better safety and thermal

stability [46]. NMC batteries are also used by NRMM, but, usually, only if lower weight is a top requirement.

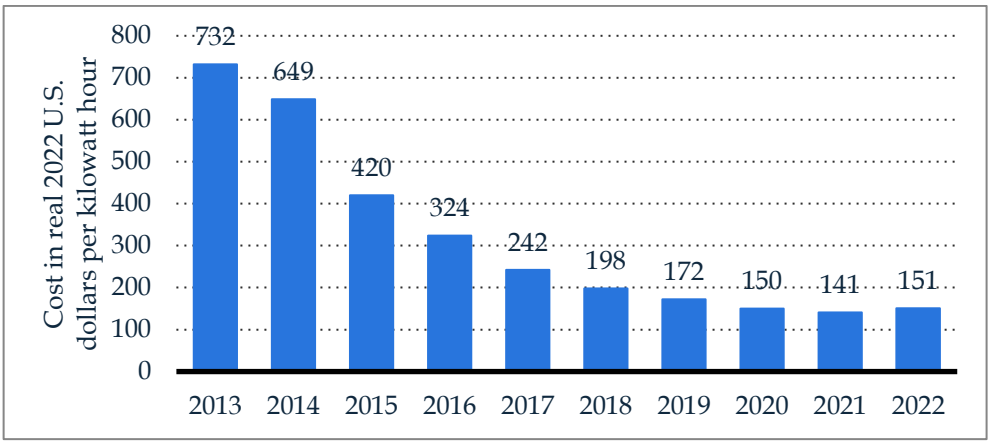

Figure 2.3 Lithium-ion battery pack costs worldwide. (Adapted from [44])

Flywheels, supercapacitors, and hydraulic accumulators have higher power densities than batteries, but they lack energy density. This makes them more suitable for hybrid architectures, where ESSs are used to follow the power peaks without excessively ramping up the main source of energy (ICE or FC) [47], and/or to accumulate energy from the recovery systems. For instance, hydraulic accumulators are by far the most capable ESS concerning specific power, but they also have the worst energy density, making them more difficult to implement in compact vehicles [48].

To improve the overall efficiency, researchers are also focusing on the combination of more than one energy storage system [49, 50], called Hybrid Energy Storage Systems HESSs, to take advantage of both specific power and specific energy.

2.2 Electric Motors

Electric motors are other fundamental components of electrified machinery and vehicles: they convert electrical energy into mechanical energy, and they can also act as generators during regenerative events. Furthermore, their efficiency is much higher than ICEs, and, for limited periods, they can reach much greater peaks of power [51] (in some cases even two or more times higher than continuous power). In addition, thanks to their

inherent characteristics and the use of an inverter, electric motors can supply the maximum available power almost along the entire velocity range [43].

The following characteristics are essential for electric motors used for machinery and vehicles [51]:

- mechanical ruggedness;
- high torque density;
- high energy efficiency;
- wide speed range;
- low noise;
- low to null maintenance;
- simple control;
- low cost.

In Figure 2.4 there is a broad classification of rotary electric motors, but the only ones in use in the automotive and off-highway industries are the following [52]:

- Squirrel Cage Induction Motor SCIM: They are very robust and reliable, and they have reasonable costs due to the absence of permanent magnets. However, they are bulkier and heavier, and control is not as precise as for permanent magnets motors.
- Interior Permanent Magnets Synchronous Motor IPMSM and Surface Permanent Magnets Synchronous Motor SPMSM: they stand out in terms of torque density and controllability, and they are the best choice for high-performance applications (especially for purely tractive efforts). Due to the presence of permanent magnets, the cost is higher than SCIM, and they are not ideal for extreme environmental conditions (very low or very high temperatures).
- Switched Reluctance Motor SRM: the low-cost rotor in place of the more expensive IPMSM and SPMSM, and the higher efficiency in comparison with the SCIM are the great advantages of the SRM machine. However, because of the highly complex control mechanism, they have been implemented on working prototypes only recently. Nonetheless, due to the promising cost/performance

ratio, SRMs have been pointed out as the biggest future improvement in electric motors for both the on-highway and off-highway industries.

The main pros and cons of these three common electric motors are summarized in Table 2.2 [36, 43, 51, 53].

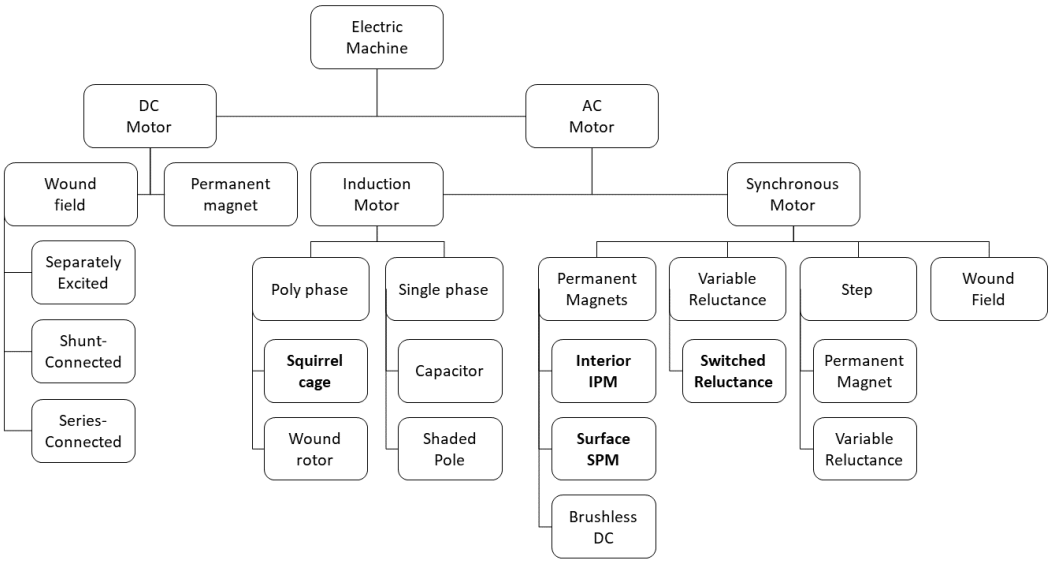

Figure 2.4 Broad scheme of electric machines.

	SCIM	IPMSM | SPMSM	SRM
Advantages	Very robust Low cost Good controllability	High torque density Very high efficiency Great controllability	Good torque density Very robust Low cost
Disadvantages	Low efficiency Narrow speed range	High cost Magnets decay	Complex control Loud noise Torque ripples

Table 2.2 Comparison between most interesting electric machines: Squirrel Cage Induction Motor SCIM, Interior Permanent Magnet Synchronous Motor IPMSM and Surface Permanent Magnet Synchronous Motor SPMSM, Switched Reluctance Motor SRM. [36, 43, 51, 53]

2.3 Hydraulics Systems and Actuators

Off-highway machinery take great advantage of the high power-to-weight ratio and good controllability of the fluid power industry. Hydraulics is so essential for this industry that it has specific products called mobile

hydraulic components and systems, indeed, they are characterized by even higher power density and compactness.

However, using hydraulics has its downsides, among which the low efficiency is the main one: as reported in [54], hydraulic components and systems are indeed the biggest source of inefficiencies in an NRMM, with an efficiency close to 22% [55]. Considering the whole machinery, the efficiency is stated to be around 10% [56].

To increase the overall efficiency of NRMM, both academia and industry have been researching evolutionary and revolutionary hydraulic components and systems, but there is a consensus that fluid power will remain fundamental.

Hydraulics is characterized by a great number of architectures and solutions, but an overview can be found in [57], which is extremely useful for simplifying the understanding of this specific fluid power industry (Figure 2.5).

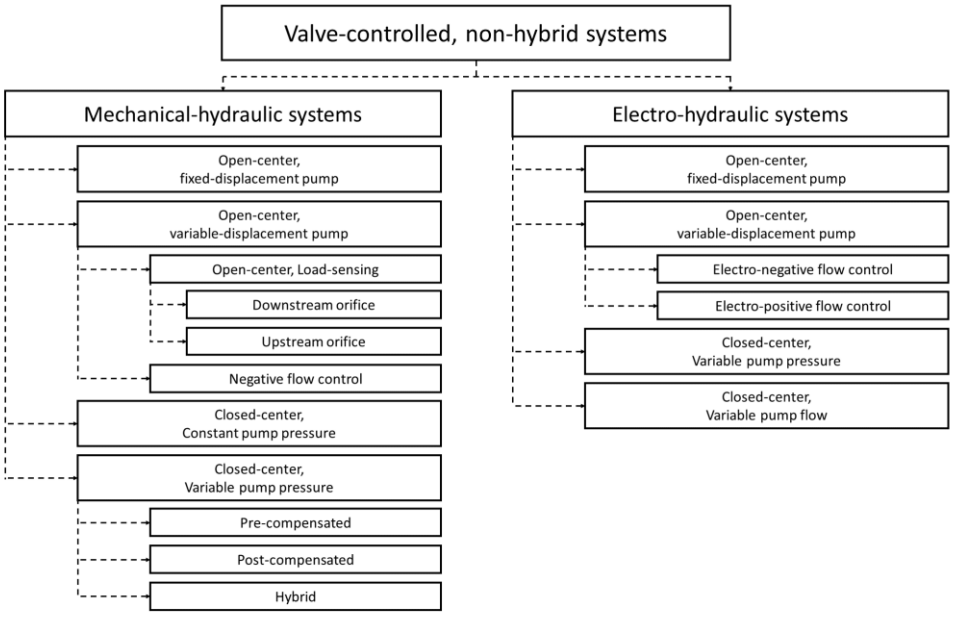

Figure 2.5 Proposed classification of the working hydraulics for non-hybrid, valve-controlled mobile machinery. (Adapted from [57])

Considering that a hydraulic pump must be connected to a motor (ICE or EM) and that the hydraulic system must command at least one actuator, hydraulics basic principles can be summarized as follows:

- Pressure is related to the acceleration/force of the actuator and the acceleration/torque of the pump.
- Flow rate is related to the velocity/displacement of the actuator and the velocity/displacement of the pump.
- The maximum amount of flow in the system is based on the maximum flow rate of the pump. When the required flow exceeds the available one, the phenomenon is called flow saturation.
- The lower the passage area $A_{\mathrm{eq},0}$ of an orifice/valve, the greater the pressure drop across the valve. When a passage area of an orifice is null, the pressure drop Δp is infinite, and the flow rate Q_0 is zero (Eq. 3). The flow discharge coefficient C_d and the oil density ρ can be assumed to be constant.

$$Q_0 = C_\mathrm{d}\, A_{\mathrm{eq},0} \sqrt{\frac{\Delta p}{\rho}} \qquad \text{Eq. 3}$$

- Most of the losses in the system can be considered as pressure drops.
- Some losses in the system can be considered as flow leaks.
- The greater the number of pressure losses, the greater the pressure required at the pump.

Independently of the hydraulic architecture, the three most important downsides of hydraulics are the following [58]:

- High inefficiency: to control the system some pressure drops and flow leaks are intentionally generated.
- Load interference: the pressures required by different actuators influence each other.
- Load dependency: the pressure required by one or multiple actuators influences the flow rate.

2.3.1 Open-Center Systems with Fixed Displacement Pump

Open-center systems are based on open-center valves, hence directional flow control valves in which the neutral position allows the passage of flow only through one single channel, called "open center gallery" (Figure 2.6).

The open center system paired with a fixed-displacement pump is the most basic mobile hydraulic system, and it is still used in small and simple mobile hydraulics, because of the minimal setup effort and cost. Indeed, when in their neutral position (Figure 2.6a), open center valves allow oil to flow directly from the pump to the reservoir, minimizing pressure drops, thus, reducing energy consumption. However, even if simple, cheap, and effective, it brings high energy losses [59].

Multiple actuators are feasible with this scheme as seen in Figure 2.6, but it suffers from load interference and load dependency, especially at flow saturation conditions. Thus, this architecture is not ideal for multiple actuator systems, particularly if precise velocity control is needed.

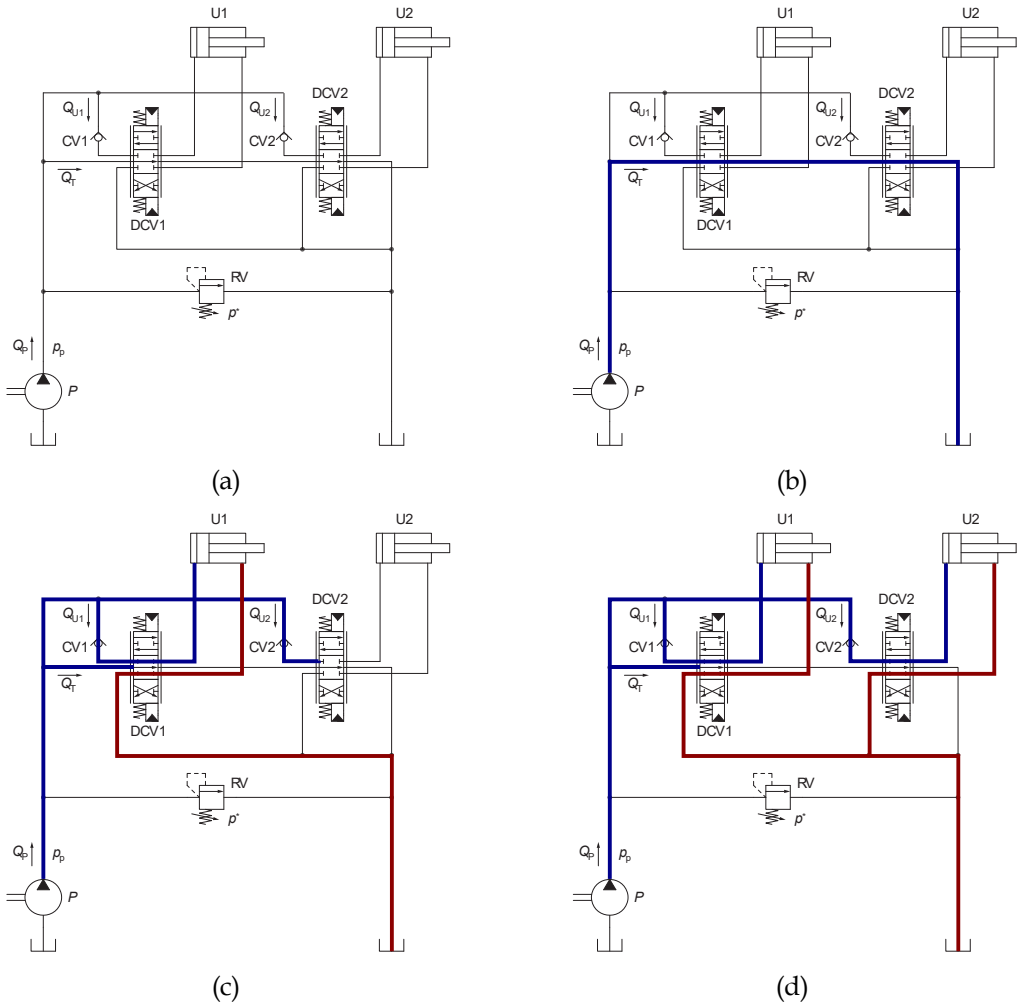

Figure 2.6 Open center with fixed displacement pump: general scheme (a), idle (b), single actuator (c), multiple actuators (d). (Adapted from [60])

2.3.2 Open Center System with Variable Displacement Pump

The application of a variable displacement pump to the open-center system allows the reduction of idle losses. Indeed, the displacement reduction during idle decreases the quantity of flow passing through the center galleries.

The control of the displacement can be achieved by sensing the pressure difference on the by-pass orifice *0* (Figure 2.7) and, based on its position, it is possible to differentiate between the downstream and upstream orifice. In both cases, the aim is to maintain a constant control pressure P_s, so, when a pressure reduction of P_s is detected, the displacement increases to re-establish the initial pressure.

Being an open-center architecture, it still suffers from load dependency and load interference with multiple actuators.

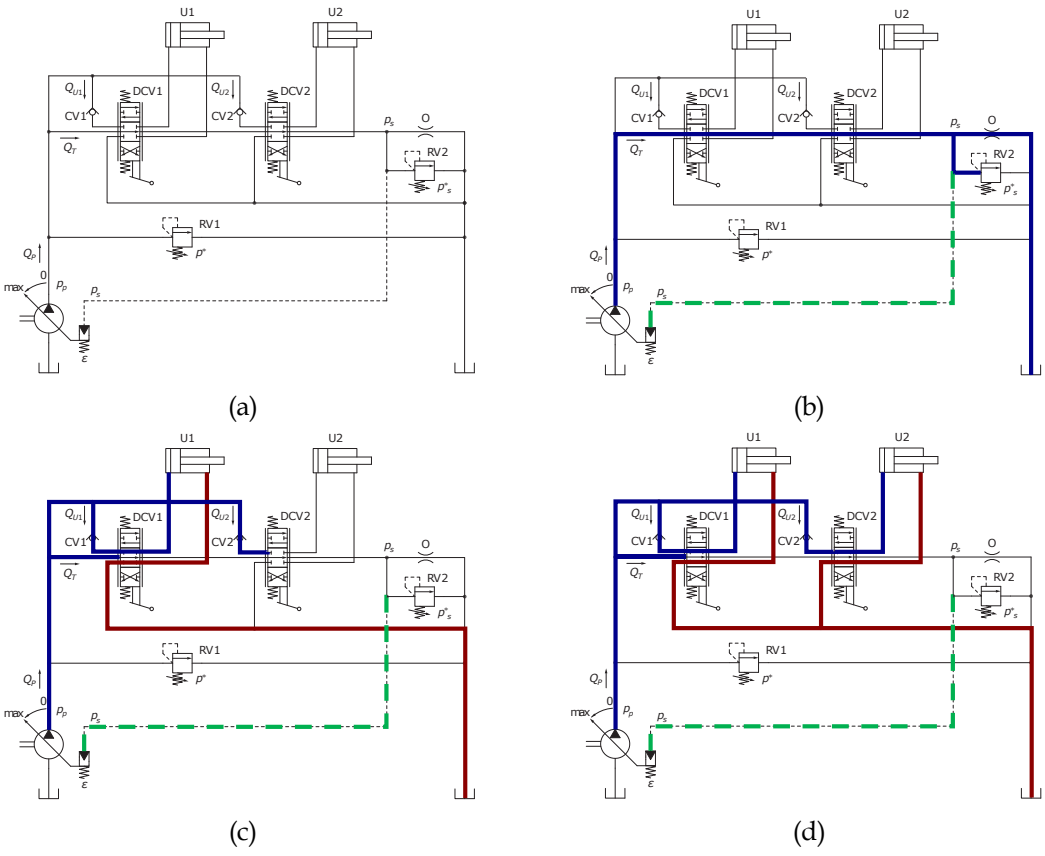

Figure 2.7 Open center with variable displacement pump: general scheme (a), idle (b), single actuator (c), multiple actuators (d). (Adapted from [60])

2.3.3 Closed Center Systems with Constant Pump Pressure

In closed-center systems, the pump displacement control circuit has an absolute pressure limiter to guarantee constant pressure at the outlet of the pump. When the directional control valves are in the neutral position and no function is activated, the inlet ports of the valves are closed, and no flow can pass through (Figure 2.8). On the one hand, this design is simpler than the open-center system, the controllability is increased, there is no load interaction between different functions used in parallel, and the damping of the system is increased. On the other hand, partial loads strongly affect the efficiency of the system.

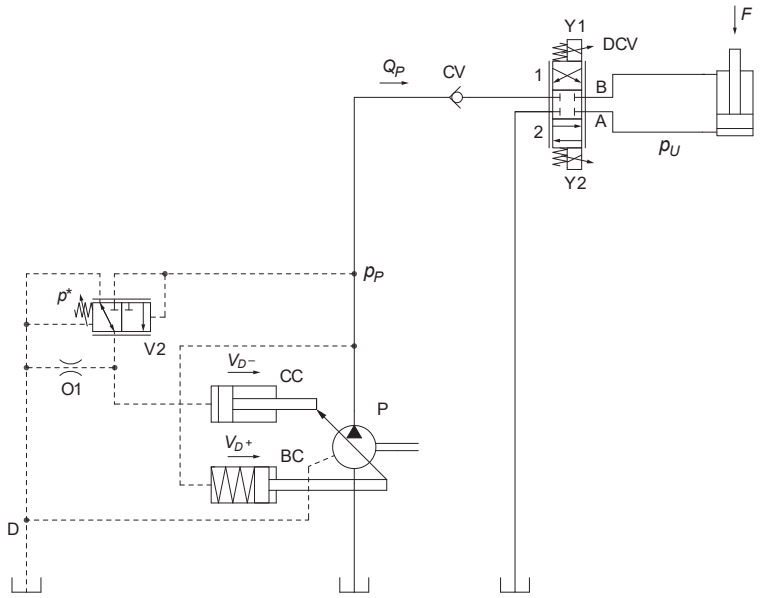

Figure 2.8 Closed center with constant pressure pump. (Adapted from [60])

2.3.4 Closed Center Systems with Variable Pump Pressure

This architecture is the most widespread in the industry, mainly because it allows independent control of actuators without load dependency. This latter important feature is obtained using pressure compensators collocated in each proportional directional valve of the system.

Through a sophisticated metering system, the pressure created by the load is used as feedback to properly control the actuator's velocity. Indeed, the system works on a basic imposed condition: the difference between the pump outlet pressure and the load pressure is equal to a pre-set value s,

which represents the pressure drop of the load-sensing valve. This system is commonly known as the Load Sensing LS system.

Thanks to this LS control mechanism, the following fundamental features are enabled:

- There is no load dependency. The velocity of any actuator is not influenced by the load and depends only on the signals of the joysticks. The higher the offset of the joystick from the neutral position, the higher the pressure signal of the joystick to the directional valve, and the higher the velocity of the actuator.
- Due to the presence of compensators, the architecture does have load interference. However, in this case, load interference is consciously created to avoid load dependency, thus the operator does not experience any dynamic variation while controlling the machinery.
- The pressure provided by the pump is always slightly higher than the load pressure, avoiding high losses in the hydraulic circuit caused by useless high constant pressure.

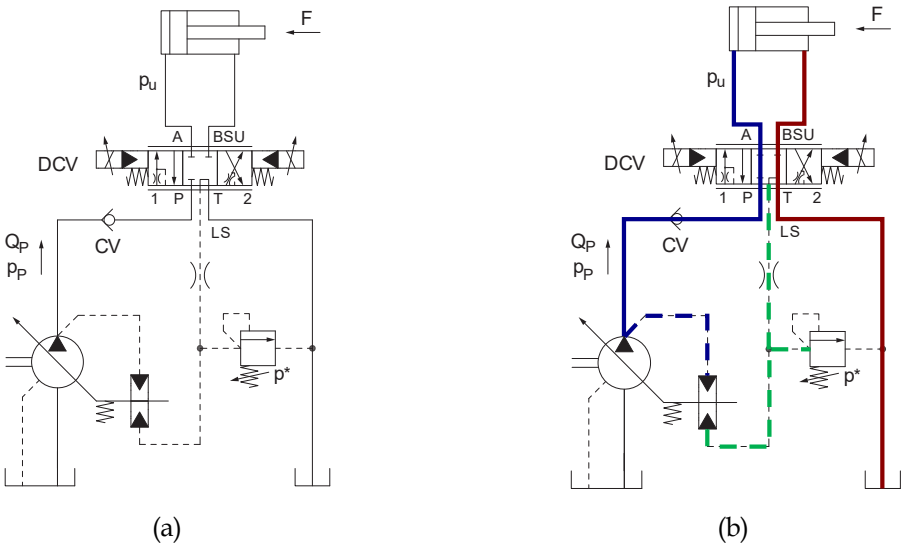

Figure 2.9 Closed center with variable pressure pump. (Adapted from [60])

2.3.5 New Developments in Hydraulics

In ICE-powered machinery, the low hydraulic efficiency is somehow negligible in comparison to the even lower efficiency of the ICE, but in electric

ones, every waste of energy is much more relevant. Indeed, increasing efficiency is key for electrified machinery because every energy waste directly impacts the operational runtime and, accordingly, the battery pack, which is currently the most expensive component. However, due to the very high power-to-weight ratio of hydraulics, it is very difficult for other technologies to stand out as leading technology. So, even if there are examples of NRMM using only electromechanical systems, academia and industry are constantly researching new hydraulic solutions [61].

2.3.5.1 Direct Driven Hydraulics

Among the inefficiencies of hydraulics, idle losses, metering losses, and line losses could be decreased using an electric machine directly connected to the actuator [62].

This type of distributed hydraulics is called Direct Driven Hydraulics (DDH). When there are distributed machines connected to distributed actuators, it is called Zonal Hydraulics [63]. This technology is already used in the aeronautical industry, while only prototypes and research projects exist for the off-highway industry. An example of this application is the compact electric excavator used as a proof of concept in [64, 65] where the overall efficiency can reach up to 73.3% for the performed cycle.

As previously seen, most of the current hydraulic systems require complex valve architecture and hydraulic signal system layout to properly control the pressure and the flow. This means that the flow and pressure control of the system can become very complex. On the opposite, the general idea behind the concept of the DDH is to equip every actuator with individual pumps and closed hydraulic circuits, eliminating the need for long hydraulic connections and/or complex hydraulic valves.

Having a single pump per actuator with a single motor/generator allows the following theoretical advantages:

- The force delivered by the actuator to the load is only dependent on the motor torque because there is almost no pressure drop between the pump and the actuator. Similarly, the velocity of the actuator is

only dependent on the motor speed, because the actuator and pump volume flows are directly connected.
- The efficiency of the system is inherently higher because fewer to no orifices are needed to control the actuator, thus the metering losses are greatly reduced. Furthermore, hydraulics pipes are shorter, so pipe losses are decreased, and almost no flow leaks happen.
- There is no load interference and no load dependency because every actuator has an independent hydraulic circuit.
- It is easier to recover a high amount of energy from braking and overrunning loads. Indeed, hydraulic energy can be directly transformed into electric one by the electric machine.

The first and most intuitive drawback of electro-hydraulics is the space requirement. Indeed, it is necessary to accommodate the motor, the pump, the oil filtering system, the temperature management circuit, and also an oil reservoir to compensate for small leaks [66–68].

The second less intuitive drawback is the need to differentiate the flow based on extension or retraction when using linear actuators. Indeed, traditional linear actuators are characterized by differential cylinder areas, while traditional pumps have symmetrical flow rates [69]. To overcome this issue, there are three possible approaches, coming though with their drawbacks:

- Replacing the traditional actuators with multiple cylinders or more complex multi-chamber cylinders [70, 71]. It usually increases both the volume and the cost.
- Using a combination of hydraulic valves to direct the flow [72]. It reintroduces more hydraulic losses.
- Using a combination of hydraulic pumps to supply asymmetrical flow [73, 74]. It increases volume and cost, and the control is much more sophisticated.

Lastly, it is important to point out that many off-highway machinery are designed to carry out more than a single task employing different attachments. In this scenario, the application of additional tools or different

attachments can be challenging for the design of DDH systems, due to different oil requirements, actuator ratios, etc., while it is one of the major advantages of traditional centralized hydraulics. Indeed, these attachments are usually connected to the far end of the arms of the machinery.

In general, as stated in [75], manufacturers currently seem not to invest great effort in researching and implementing DDH, due to the design effort, the use of new components, and the need for new safety certifications.

2.3.5.2 Independent Metering Control

One interesting innovation in modern hydraulics is the Independent Metering Control (IMC) strategy. This is based on Independent Metering Valves (IMVs), which are composed of a combination of multiple electro-hydraulic poppet valves, and it brings several advantages as reported in [76]. Indeed, by splitting traditional directional valves into several separately controlled valves, IMC can improve the efficiency of the system by switching the IMVs in different configurations, even allowing flow regeneration, as visible in Figure 2.10 and Table 2.3 [77]. For instance, as reported in [78] by using an IMC system instead of the traditional LS the efficiency of the hydraulics increases from 59% to 82%.

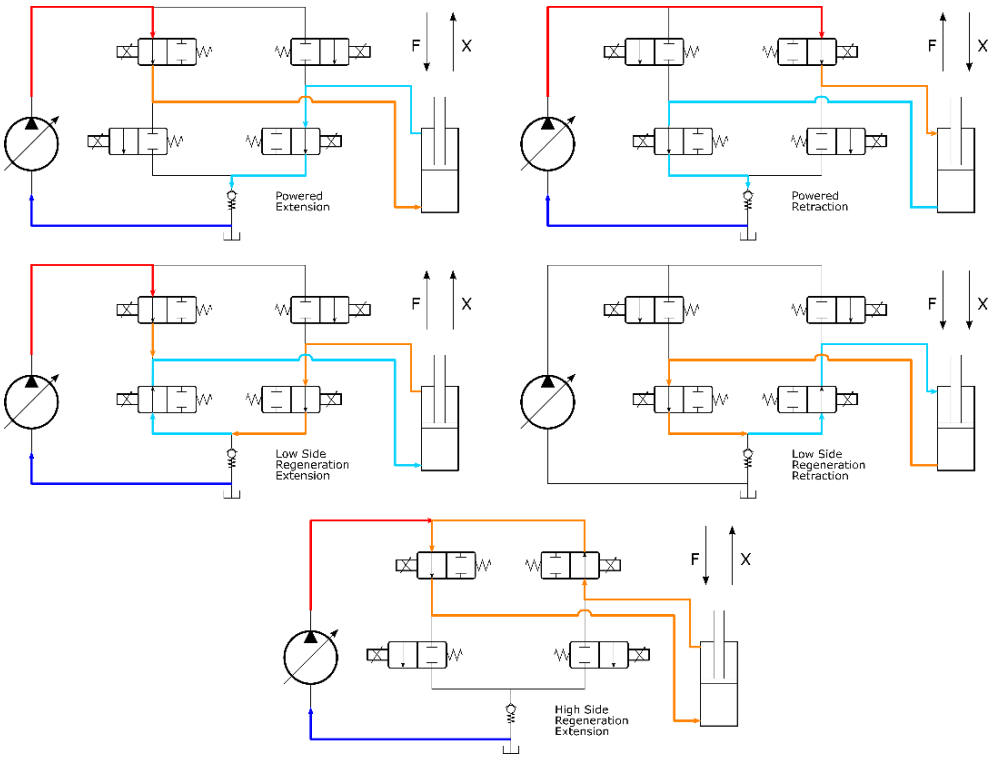

Figure 2.10 Schematization of IMC system. (Adapted from [77])

Metering mode	Ksa	Ksb	Kab	Kbt
Power extension	Open	Closed	Closed	Open
Power retraction	Closed	Open	Open	Closed
High-side regeneration extension	Open	Open	Closed	Closed
Low-side regeneration extension	Open	Closed	Open	Open
Low-side regeneration retraction	Closed	Closed	Open	Open

Table 2.3 Schematization of IMC system. (Adapted from [77])

2.3.5.3 Digital Hydraulic

Another important innovation in hydraulic systems is digital hydraulics. This technology is based on components able to regulate the flow based on discretized control signals [79]: digital control valves, digital pumps, digital transformers, and digital actuators.

In [80], Zhang et al. divide digital control valves into three different types:

- Parallel digital valves. Also known as Digital Flow Control Unit DFCU, they are composed of multiple two-way switching valves connected in parallel.
- High-speed digital switching valves. A high-frequency signal dynamically controls the opening and closing of these valves, and thus the flow rate [81].
- Stepping digital valves. They are based on stepping motors, that allow an intelligent positioning of the spool, using though a mechanical transmission to convert rotational movement into linear ones.

One of the fields in which digital technology is achieving good results is the pump and motor design. Artemisia Intelligent Power (currently part of the Danfoss Group) has been developing this type of machine since 1994 [82], and the project DEXTER represents the first functional off-highway machinery equipped with a Digital Displacement Pump (DDP). A digital displacement tandem pump is mounted indeed on a 16-ton excavator. The pump is a radial piston machine, where the overall displacement is varied modifying the volume of each single cylinder at every cycle. This displacement variation is obtained using solenoids that control the inlet valves. The DDP can change its displacement very rapidly, going from zero displacement to full displacement in half a shaft revolution. Green et al. [83] have demonstrated that, by only changing the tandem axial swash plate pump with a tandem radial digital displacement pump, the fuel consumption decreases by around 21%.

Digital hydraulics is useful also for developing new actuators, as done in [71] with the NorrDigiTM produced by NorrHydro. This system consists of a multi-chamber hydraulic cylinder, with integrated digital hydraulics, and electronics. Using this system, which enables great control over the energy flow, in [84] a 45-60% fuel saving is declared[1].

- [1] Some of the main results of this analysis have been published in the journal article: Beltrami, D.; Iora, P.; Tribioli, L.; Uberti, S. Electrification of Compact Off-Highway Vehicles—Overview of the Current State of the Art and Trends. Energies 2021, 14, 5565. https://doi.org/10.3390/en14175565 [85]

3 State of the Art and Trends

As previously seen, construction and agricultural machinery are the two most developed categories of NRMM. Therefore, as already published by the author in [85], it is possible to evaluate the current market by analyzing these two.

Starting from construction, the most common machinery is the excavator [48].

In Figure 3.1 the ratio between the operative weight and ICE maximum power is shown, along with their electric counterparts, where EM continuous power is considered. The linear regressions of the scattered values of the two are also reported, and it is visible that the power-to-weight ratio is almost identical.

It is different though if the EM peak power is considered. Indeed, as visible in Figure 3.2, the power-to-weight ratio of electric excavators is constantly higher than ICE-powered ones. The combination of these two analyses is significant. It shows indeed that most of the electric excavators are developed simply by replacing the original ICE with an equal power EM (continuous power), not capitalizing, for instance, the peak power capabilities of electric machines. Being retrofitted machinery, the design effort is limited to the integration of the electric motor, battery pack, and charging system in place of the ICE and the fuel tank, with additional effort to implement the control system of the new powertrain.

Another key aspect visible in the plot is that most of the machinery belongs to the compact segment, characterized by a weight below 5000 kg and a maximum power of 30 kW. This is due to two key reasons: on the one hand, the electrification of compact machinery is less expensive for manufacturers, providing the opportunity to have cost-efficient running vehicles, from which useful operating data can be collected for scaling up toward bigger and more remunerative vehicles [86]. On the other hand, the emission regulation policies and the increasing number of "zero-emission"

city centers [14] make electrification necessary for the compact class of excavators.

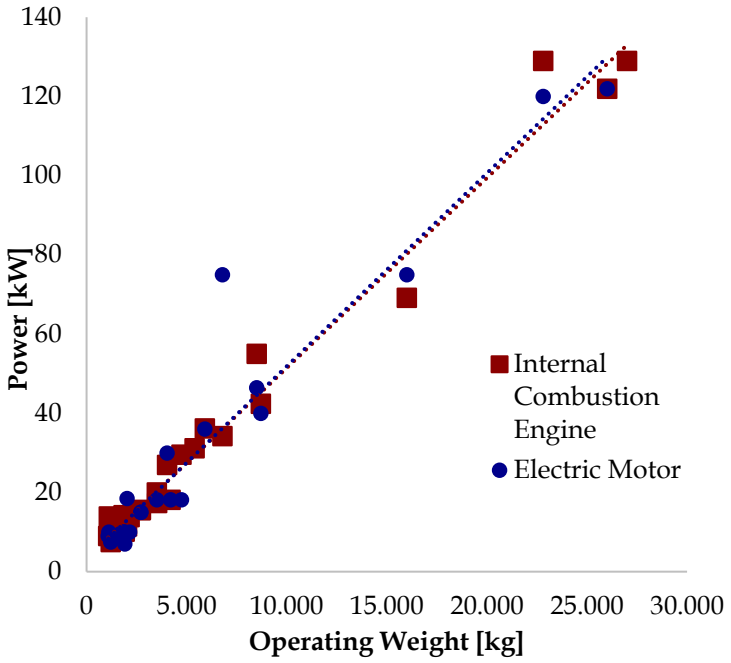

Figure 3.1 Power-to-weight ratio of ICE-powered excavators and EM-powered excavators (continuous power) with linear regressions. [85]

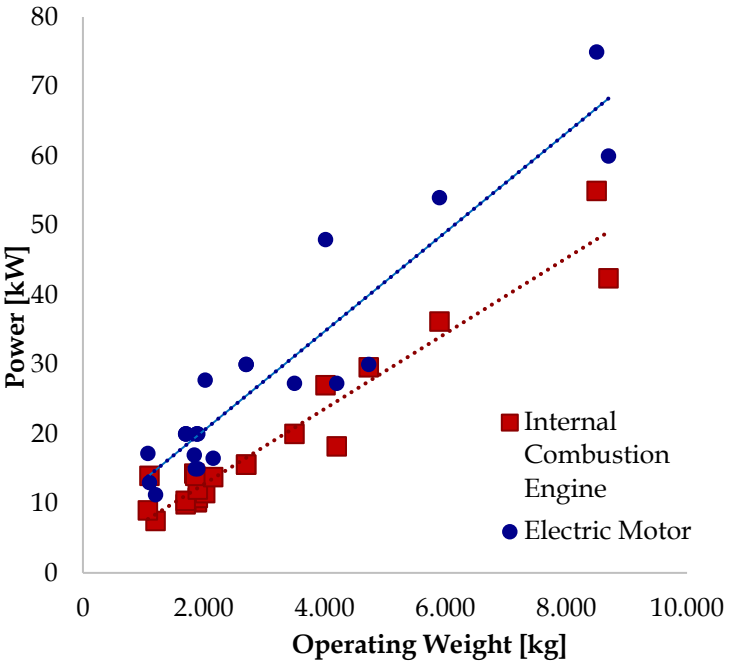

Figure 3.2 Power-to-weight ratio of ICE-powered excavators and EM-powered excavators (peak power) with linear regressions (only small excavators). [85]

In Figure 3.3, it is shown how common it is to keep the voltage below the high-voltage automotive limit of 60 V DC [87], providing an advantage in terms of cost reduction. Indeed, electric forklifts with 60 V electric systems have been produced for more than a decade, thus creating a standardized 60 V components market [88]. Higher voltage systems are inherently more efficient, but they require much more sophisticated, protective, and reliable systems for preventing short circuits [89]. Taking advantage of the economy of scale, the automotive industry already moved toward high-voltage systems, and the same does the off-highway industry for bigger machinery [89].

Regarding efficiency and energy consumption, it can be seen from Figure 3.4 that the operational runtimes of electric excavators are extremely scattered. As previously discussed (Introductory Chapter), the main reason for this confusion is the lack of a standard duty cycle commonly recognized by manufacturers. Therefore, many of the available data regarding running times are neither accurate nor validated. Unfortunately, even if there are scientific papers and manufacturers' reports in which the operational runtimes are calculated through published duty cycles, like the one by the Swiss manufacturer Suncar HK AG [29], these are barely comparable with each other.

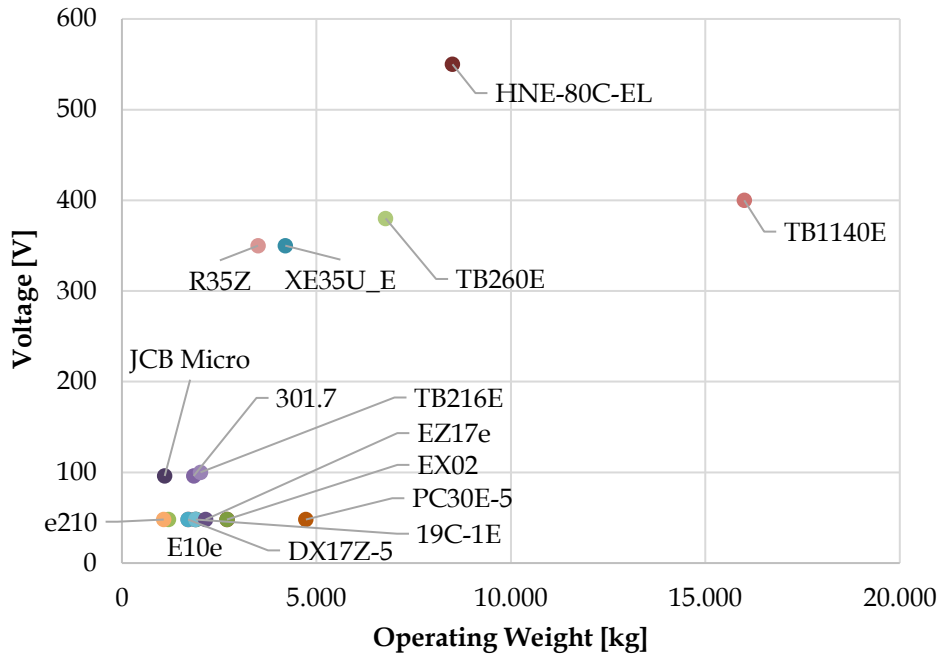

Figure 3.3 System voltage in relation to operating weight. Labels refer to different excavator models according to manufacturers' datasheets. [85]

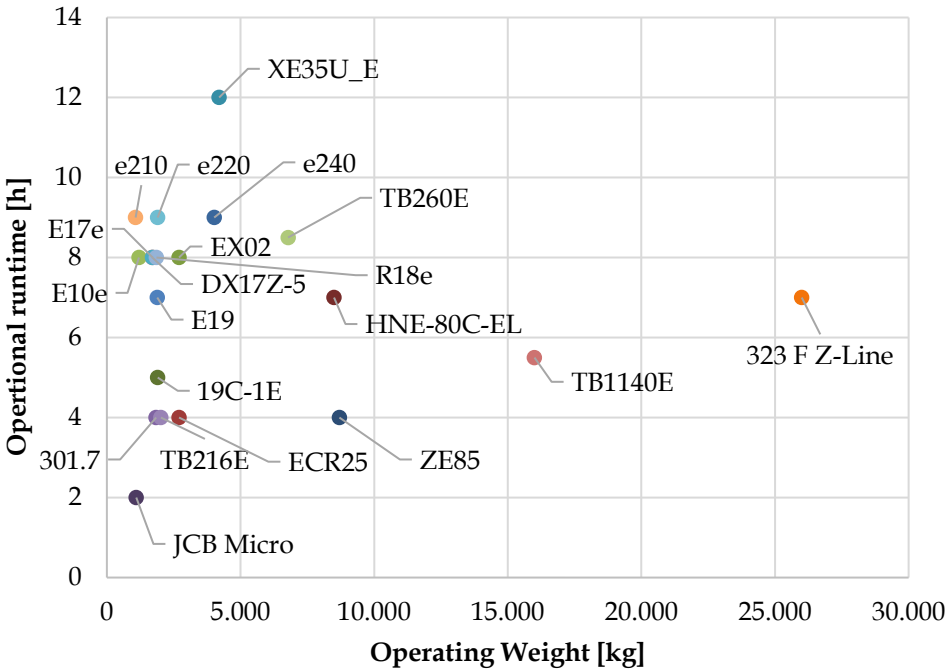

Figure 3.4 Operational runtime in relation to operating weight. Labels refer to different excavator models according to manufacturers' datasheets. [85]

The situation is similar for front-end loaders, as can be seen in Figure 3.5, even if the number of electric vehicles is much lower and data are much more

scattered. Another relevant difference is related to the powertrain architecture. For instance, in most front-end loaders, manufacturers prefer to differentiate the power flow requested by traction from the power flow requested by hydraulic actuators and ancillaries. Indeed, front-end loaders require great tractive effort, while excavators usually work at fixed-point. The results are visible in Figure 3.5, where it is shown that the continuous power of electric loaders is usually lower than the corresponding ICE-powered original versions.

The lower number of electric front-end loaders can be justified by higher development costs, but, like the excavators, most of the electric applications are within the compact segment, characterized, once again, by weight under 5000 kg and power below 30 kW.

The common and most important aspect of the current electrification process is the attempt to maintain reasonable costs by limiting disruptive innovations, developing retrofitted electric machinery from existing ICE-based ones, and/or outsourcing much of the design process to more specialized and agile companies, such as Green Machine, who have played an extensive role in the electrification of many pieces of construction equipment from different manufacturers such as Case CE, Takeuchi Mfg and Bobcat [86].

In this scenario, forecasts from Frost and Sullivan [90] foresee an increase of the battery electric compact excavator market share from the current 1% to 4% in 2030, as well as an increase in compact battery electric front-end loaders to 6% before 2030.

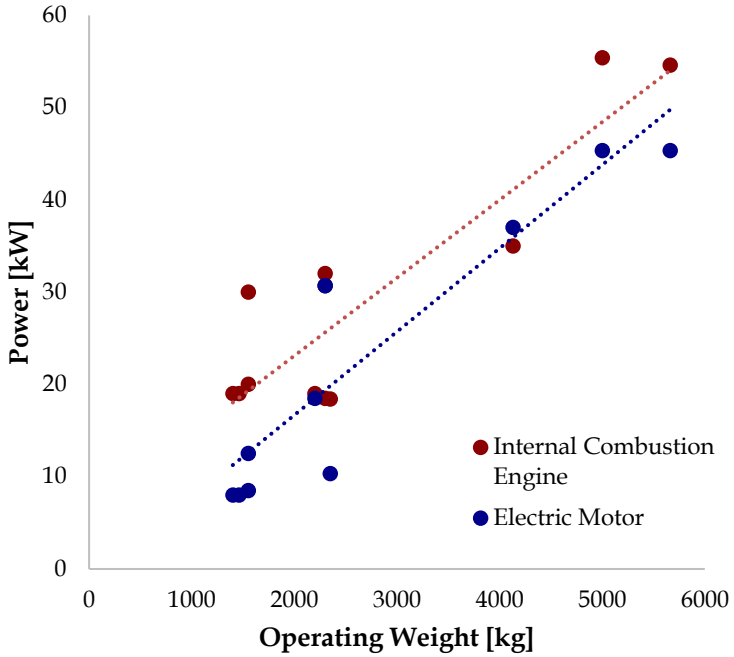

Figure 3.5 Power-to-weight ratio of ICE-powered loaders and EM-powered loaders (continuous power) with linear regressions. [85]

Talking about agricultural machinery, in Figure 3.6 there is the power-to-ratio analysis of agricultural tractors, which are by far the most known machinery of the category. Once again, it is visible how the power-to-weight ratio remains similar. Furthermore, as seen for excavators and front-end loaders, most of the electrified tractors are in the compact segment of the industry. This can be seen also in Figure 3.7, where the number of tractors is divided by power class. In this regard, the most interesting partition is based on power output, which divides the tractors into three main categories: below 49 HP, between 50 HP and 79 HP, and above 80 HP [91]. Here this categorization is split based on kW only to emphasize the categories.

Differently from the construction industry, in agriculture robots and unmanned machinery are more common, thus electrified agricultural robots AGBot are displayed too.

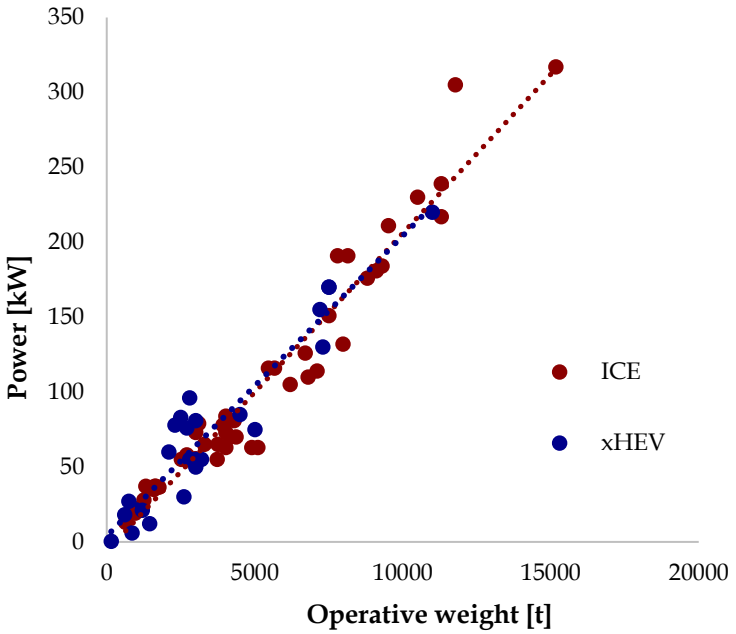

Figure 3.6 Power-to-weight ratio of ICE-powered agricultural tractors and electrified ones with linear regressions. [85]

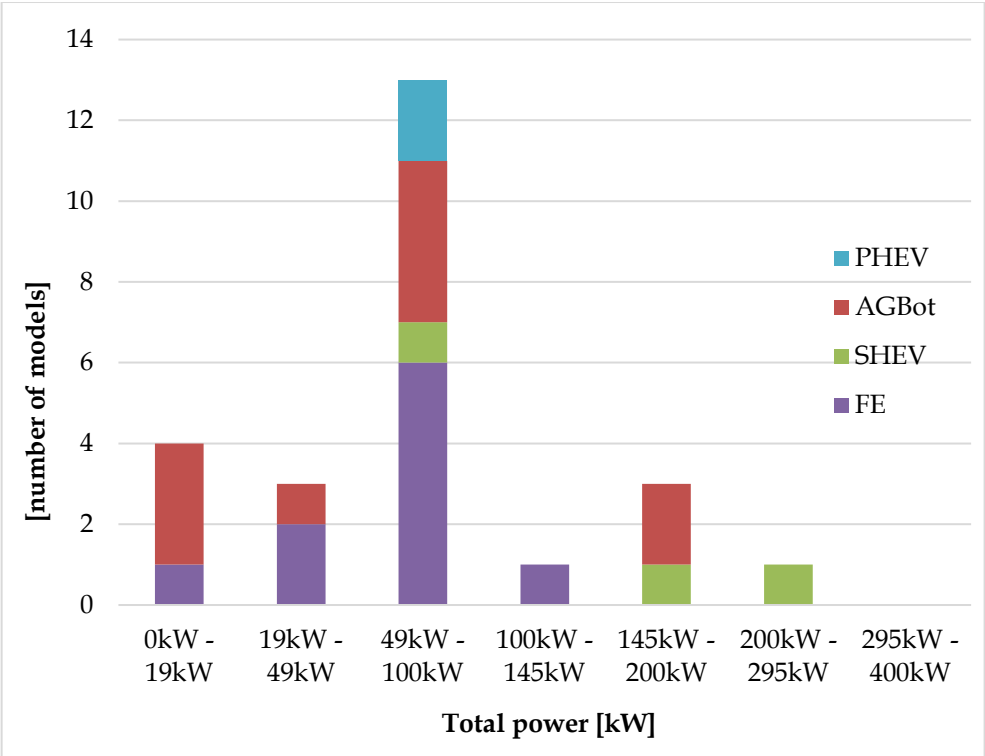

Figure 3.7 Number of electrified agricultural tractors divided by power class.

Regarding other categories of NRMM, the number of electric products is much more limited. Thus, it is impossible to statistically verify the trends

identified above. Nevertheless, picking some machinery for any category confirms the trends. For instance, the electric telehandler 525-60E by JCB [92], which is within both the construction and agricultural categories, has two electric motors (17 kW and 22 kW), and it follows the trend of the front-end loaders. Indeed, due to relatively better efficiency, its power-to-weight ratio is slightly lower than the ICE-based one. In the mining industry, the biggest battery electric vehicle is the Swiss e-dumper, retrofitted from a Komatsu HD-605 [93]. The original version has a diesel engine of 578 kW, while the electric one has a 673-kW motor. However, the operating weight of the electric version is higher, thus the power-to-weight ratio remains similar.

It is worth mentioning that the trends cited above agree with the electrification roadmap of some of the major Tier 1 companies, such as ZF Friedrichshafen AG [94], Bosch Rexroth AG [95], and Deutz AG [96].

3.1 Relevant Electrified Off-Highway Machinery

As done in [85], in this paragraph, relevant electrified off-highway machinery are presented to give practical instances of existing electric and hybrid vehicles; while some of them are purely research projects or experimental prototypes, others are already available on the market.

3.1.1 Tractor and Agricultural Machinery

Within the category of tractors and agricultural machinery, electrification has been pointed out as the next important milestone [97]. Technology has almost reached its optimization limit, but the need for agricultural equipment is increasing due to global population growth. However, based on the market research reported in [98], current electrified solutions are feasible only for a small niche of greenhouses and orchards. As previously said, most of the projects are related to compact machinery, so they usually are below 79 HP.

One of the most interesting compact electric projects is the Fendt e100 Vario (Figure 3.8a) which is equipped with a 50-kW electric motor and a 100-kWh lithium battery at 400 V, with a stated working autonomy of 5 h and the possibility to restore the battery SOC up to 80% in 40 min. Implements can be

attached via traditional PTOs or hydraulic, but there is also a 150-kW electric plug [99].

Other fascinating projects are the Rigitrac SK-50 and SK-40 (Figure 3.8b). These are market products for alpine farming, and they use five electric motors: two traction motors, one motor for each of the two power take-offs, and one motor for the hydraulic system. The operational runtime is stated to be about 5 hours, with the possibility to fast charge the battery to 80% SOC in 2 hours [100].

The Monarch MK4 (Figure 3.8c) has also some unique characteristics. It is the first orchard and vineyard tractor of the Californian start-up company Monarch, and it is also the first automated tractor available on the market. It has two 30-kW electric motors, one for traction and one for the PTO, and the company claims an operational runtime longer than 4 hours. To use it for longer or more intense duty cycles, it is possible to swap the entire battery pack after depletion [101].

Lastly, the Farmtrac 25G is a 15-kW electric tractor [102]. It is commercially available, and, thanks to its 22-kWh NMC lithium battery, the operational runtime is stated to be about 8 hours, with the charging time estimated to be close to 5 hours.

(a) (b) (c)

Figure 3.8 Electrified tractor: Fendt e100 Vario (a); Rigitrac SKE 40 (b); Monarch MK4 (c).

Among the electric agricultural vehicles that cannot be considered compact, the concept machinery and working prototypes of John Deere are surely worth mentioning. Indeed, the John Deere SESAM (Sustainable Energy Supply for Agricultural Machinery) and the John Deere GridCON are a testament to the interest of the company in researching novel approaches to face similar problems. The SESAM tractor is equipped with a 150-kWh

battery pack for 1 hour of intense work before recharging [103], while the GridCON is a tethered, fully autonomous, and unmanned tractor equipped with a 100-kW electric motor for traction, and 200-kW electric motor directly connected to the PTO to transfer mechanical power to implements [104].

The E-OX 175 is a unique piece of machinery [105], and it is the most recent development of the innovative Multi Tool Tractor. It probably represents one of the most groundbreaking examples of how much electrification can transform common mechanical and powertrain architectures. Indeed, not only traction is guaranteed by four-wheel-drive electric motors, but it can also change its wheelbase and turning radius to optimize its use on fields without damaging the crop.

Talking about hybrid machinery, the main focus is different based on size. Indeed, on compact machinery hybridization is useful to add functionalities or avoid advanced exhaust gas treatment systems, while better productivity and return on investments are essential for bigger tractors.

For instance, the REX4 by Landini uses a hybrid architecture to allow more precise all-wheel drive mode and to enhance steering capabilities by implementing torque vectoring [106]. Another example is the Rigitrac EWD120, which is a series hybrid prototype tractor for alpine agriculture, where off-road climbing is enhanced by in-wheel electric motors [107].

3.1.2 Municipal and Property Maintenance

The most important municipal and property maintenance machinery are municipal vehicles and street sweepers. They are among the most interesting vehicles for the electrification process due to their urban use, their highly fluctuating duty cycle, and the use of many different types of equipment for sweeping, cleaning, and vacuuming. Furthermore, these machinery usually work at night, meaning that noise level reduction is a very attractive feature, and these are also interesting applications for futuristic autonomous processes.

In [108], a feasibility study is performed for an electric street sweeper, including the definition of a representative duty cycle, modeling of the machinery, and the selection of suitable components for the powertrain and driveline. The simulated duty cycle results in an operational runtime below 5

hours, where the cleaning equipment requires more than half of the gross power of the electric motor.

Dulevo International S.p.A., one of the leading companies in street sweeping vehicles and equipment, already offers an electric vehicle called Dulevo D.Zero2 (Figure 3.9a), equipped with a lithium battery pack and capable of working for an entire work shift [109]. Another example is the Swiss Boschung Holding AG, which has an electric street sweeper called the Urban-Sweeper S2 (Figure 3.9b), equipped with a 54.4-kWh battery capable of providing up to 10 hours of autonomy, with the possibility to fully charge the battery in 100 min thanks to the rapid charger [110].

In [111], an electric municipal vehicle by Esagono Energia S.r.l. (Figure 3.9c) is used to validate a mathematical model able to predict the working range of an L-7 vehicle with sufficient accuracy, while taking into consideration the effect of slopes. The tested vehicle is equipped with a 15-kW induction motor, LiFePO4 battery of 15.3 kWh and it is available with many different types of equipment. Because of the vehicle equipment, the duty cycle is a simple drive cycle registered via an experimental campaign. The working autonomy results are adequate for a complete work shift, but further investigations would be useful to predict the impact of different equipment on the same base model.

Examples of non-compact vehicles are electric refuse trucks. For instance, the City Council of Nottingham has declared that electric refuse trucks are outperforming their ICE-powered counterparts, with lower fuel consumption and greater speed in completing the shift route [112]. This result highly depends on the duty cycle, where there are many stop-and-go. For the same reason, there are different studies regarding hybrid refuse trucks, like the one studied in [113, 114], where the focus is on the modeling, simulation, and control strategies of the hybrid powertrain.

(a) (b) (c)

Figure 3.9 Electric maintain property vehicle: Dulevo D.Zero2 (a), Boschung Urban-Sweeper S2 (b), Esagono Energia Gastone (c).

3.1.3 Transportation of Goods and Material Handling

There are specific applications in which electrified machinery and vehicles already represent suitable and highly appreciated solutions, such as in the case of forklifts, which are also the most widely known goods transportation machinery. Indeed, forklifts were the first NRMM to be converted into electric ones and, as a consequence, they are currently very popular for use inside warehouses. In this kind of working environment, the absence of exhaust gas emissions and lower noise levels are great advantages. Furthermore, the charging infrastructure is already in place and ready to use. The technology is mature and competitive to such an extent that, according to Toyota Material Handling [115], even electric forklifts up to 9000 kg are gaining acceptance among consumers, and their upfront cost is only 10-15% higher than ICE-based counterparts. Consequently, all the major forklift manufacturers, such as Toyota Material Handling, Hyster-Yale Materials Handling Inc., KION Group AG, and Jungheinrich AG have large portfolios of electric forklifts with lead acid or lithium batteries (Figure 3.10a).

It is worth mentioning that much of the current 48-V technology for the electrification of compact NRMM descends directly from research on forklifts.

Currently, forklifts remain among the most interesting NRMM for research and testing purposes, since their duty cycles can be easily monitored, and the available movements of their actuators are limited. For instance, in [116], the researchers investigate the application of two hydraulic motors to recover energy.

Other important compact material handling machinery are towing tractors, for which there is already a great number of electrified products due to their use in warehouses, production plants, ports, and airports (Figure 3.10b). In all these cases, routes are well defined, as well as timetables, consequently, their use can be carefully planned to optimize energy consumption and recharge times. Furthermore, electric powertrains fit perfectly these types of machinery due to their typical high torque and low-speed demands, with multiple speed variations that can be exploited to recover energy.

The last interesting machinery in this category are material handlers (Figure 3.10c). In this regard, tethered electric machines are used for very intensive use applications, while more compact battery electric ones are slowly entering the market. They are already suitable for less demanding applications and for use in cases where the cable connection is a great obstacle to the machinery. However, one of the most advanced material handlers is the prototype built by Dolomitech S.r.l. and Moog Inc. [117]: it is a 50-ton battery electric machinery with direct-driven hydraulics, which makes it capable of optimizing energy consumption while guaranteeing the performance of equivalent ICE-based counterpart. It currently represents the state of the art of electric material handlers, and its innovative hydraulic system is very interesting also for other off-highway machinery.

Material handling machinery are also extremely used to experiment with hydrogen hybrid systems, like the forklifts studied in [118, 119]. Indeed, ports and big warehouses are good environments for the implementation of PEM electrolyzers and fuel cell machinery. The 24-hour continuous working shift needs machinery to go on without interruption, and the installation of PEM electrolyzers is not as complicated as in other cases [120].

(a) (b) (c)

Figure 3.10 Goods transportation and material handling vehicles: Hyster-Yale forklift (a), Simai towing tractor (b), Sennebogen material handler (c).

3.1.4 Construction and Mining

The construction equipment industry is the biggest category of off-highway machinery and it is very promising for the electrification process. Indeed, compact machinery can be used in urban construction sites or indoor environments, matching the increasingly strict emission policies. Indeed, both the market and the scientific literature have been experiencing a remarkable increase in retrofitted electrified machinery in recent years, particularly concerning compact excavators.

For instance, JCB Ltd. was one of the first manufacturers to enter the market with an electric construction vehicle, and now it has many electric products for zero-emission construction sites under the JCB E-Tech brand. The most known example is the compact excavator 19C-1E (Figure 3.11a), which is equipped with a 19.8-kWh lithium battery and a 7-kW continuous power PMSM motor. This solution can exceed 4 hours of continuous use and includes also a proprietary rapid charge system able to reach 100% SOC in 2 hours [121].

The second most common construction machinery type is the front-end loader. A typical example of an electric loader is the TobrocoGiant G2200E (Figure 3.11b), which is a four-wheel drive machinery with two different motors: a 6.5-kW (continuous power) motor for traction and a 12-kW motor for the hydraulics. Two lithium battery sizes are available, and the biggest one can store 24.9 kWh for an operational runtime of up to 8 hours [122].

Undoubtedly, one of the leading companies in the electrification process is Volvo, and within its very large portfolio of NRMM, there is the Volvo EX02

(Figure 3.11c), which is a full electric excavator equipped with electromechanical linear actuators and a 38-kWh lithium battery pack [123]. Being a testing prototype and a proof of concept, many technical details are unpublished, but Volvo claims a 10-fold fuel reduction for its ICE-powered counterpart and a considerable decrease in the total cost of ownership.

There are many other examples in the literature. For instance, in [28], a 2-ton electric excavator was modeled using Matlab/Simulink. The research aimed to create a model able to predict the operational runtime of the machinery, and consequently, much attention was given to the modeling of the overall system, including hydraulics. The second purpose of the article was to develop a validated model to safely simulate new control strategies. Thanks to a 9.6-kW (continuous power) electric motor and a 15-kWh LiFePO4 battery pack, the electric excavator retrofitted from a Bobcat E19 can reach up to 7 h of real working performance, and the power consumption is differentiated between excavation, relocation, and travel. Another case that is worth mentioning is the compact excavator studied in [31], which has been used for multiple studies focused on electrification and hydraulics [64, 65].

Regarding the mining sector, there are already many electric loaders that are very useful for reducing air pollution in underground sites, but these are usually tethered machinery. One innovative project is the HX-02 load carrier studied by Volvo and tested in the Swedish mining site Skanska: it is a battery-electric, completely autonomous machinery with continuous power of 200 kW. Thanks to its implementation in more digitalized and automated mining sites, Volvo and Skanska state a reduction in total cost of operation of about 25%, with a CO2 emission reduction of 95% [124].

(a) (b) (c)

Figure 3.11 Electric construction vehicles: JCB 19C-1E (a), Tobroco-Giant E2200 (b), Volvo EX02 (c).

Hybrid construction machinery have been in the market for several years and prototypes came out almost two decades ago, but their acceptance has been limited due to their higher upfront costs and only marginal decrease in energy consumption. Furthermore, different types of energy storage systems have been experimented on these machinery, like supercapacitors, hydraulic accumulators, and batteries. For instance, both the hybrid excavators from Komatsu [125] and Hitachi [126] use supercapacitors, while lithium batteries are selected by Kobelco for their excavator [127]. Hybrid powertrains fit also the high acceleration ratio of front-end loaders and alike [128, 129][2].

- [2] Some of the main results of this analysis have been published in the journal article: Beltrami, D.; Iora, P.; Tribioli, L.; Uberti, S. Electrification of Compact Off-Highway Vehicles—Overview of the Current State of the Art and Trends. Energies 2021, 14, 5565. https://doi.org/10.3390/en14175565 [85]

4 Modeling the Machinery

In the following, the machinery is presented along with all its subsystems and models. Because of the multidisciplinary nature of the model, even considering the splitting into subsystems, some components could be considered within different parts.

4.1 Officine Minelli M15e Hydraulic Material Handler

The modeled machinery is an electric 14-ton material handler called M15e and it is produced by Officine Minelli s.r.l., which is an off-highway SME specialized in material handlers. The original machinery is ICE-powered and the electric version is a retrofit of the latter, meaning that the ICE and fuel tank are substituted respectively with an electric machine and an energy storage system, but most of the components remain the same between the two versions of the machinery.

As visible in Figure 4.1, where the machinery is shown with its main components, the mechanical structure of the M15e is extremely similar to an excavator, and so it is also its duty cycle. Indeed, the main duty cycle of a hydraulic material handler is based on the movements of the boom, stick, and rotation of the upper carriage, while driving and longitudinal movements of the undercarriage are negligible. As mentioned in the previous chapters, such a cycle can also be identified as a fixed-point duty cycle.

Being commonly employed to move scrap metal and paper waste, the orange peel grab is the most common end-effector for this machinery, but different end-effectors can be mounted upon request. Similarly, based on customer needs, a lifting system can be mounted for the cab, as well as additional stabilizers coming out from the undercarriage, and the extendable arm.

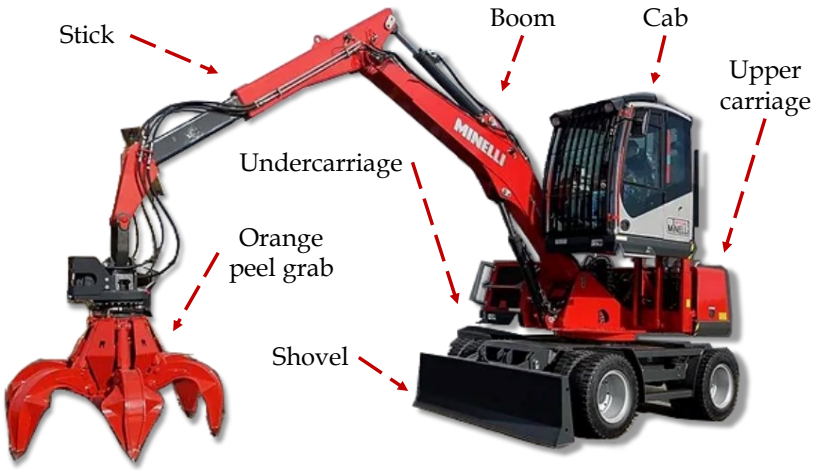

Figure 4.1 Substructures names of the Minelli M15 hydraulic material handler.

In the ICE version of the machinery, the engine, the fuel tank, and the hydraulic pump are mounted in the upper carriage, while hydraulics is appointed to transmit power throughout the machinery. Likewise, the electric version has the energy storage system and the electric machine in place of the engine and tank collocated in the upper carriage.

As visible from the hydraulic scheme of the machinery in Figure 4.2, the hydraulic pump is mechanically connected to the electric machine using a shaft, thus the two rotational speeds are identical. Then, the hydraulic system has a DCV to control every actuator. If the actuators (linear and/or rotational) are positioned in the undercarriage, the flow passes through the hydraulic swing joint. The DCV is controlled using hydraulic pilot signals coming from the joysticks and pedals installed in the cab, and these pressure/flow signals are supplied from an auxiliary fixed displacement hydraulic pump.

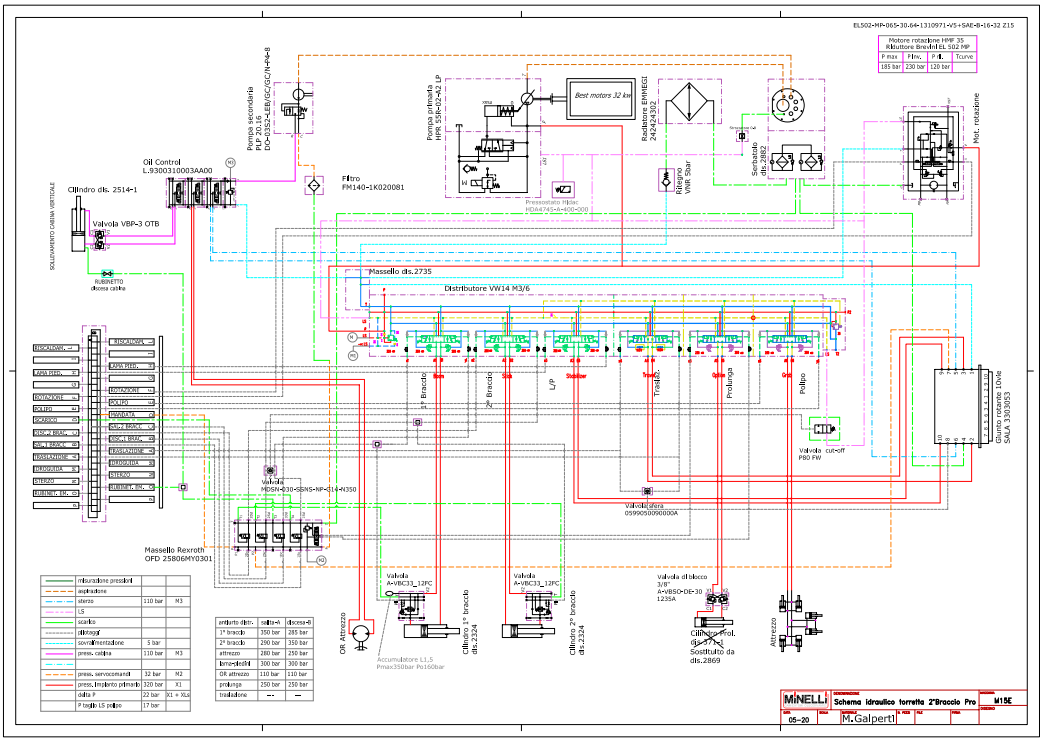

Figure 4.2 Hydraulic scheme of the electric Minelli M15e.

4.2 Mechanical Structures

The simplified 3D model of the M15 mechanical structure is completely drawn in SolidWorks, such as to decrease the complexity of the assembly, as visible in Figure 4.3. Indeed, instead of designing all the welded structures, these are simply drawn as extrusion components.

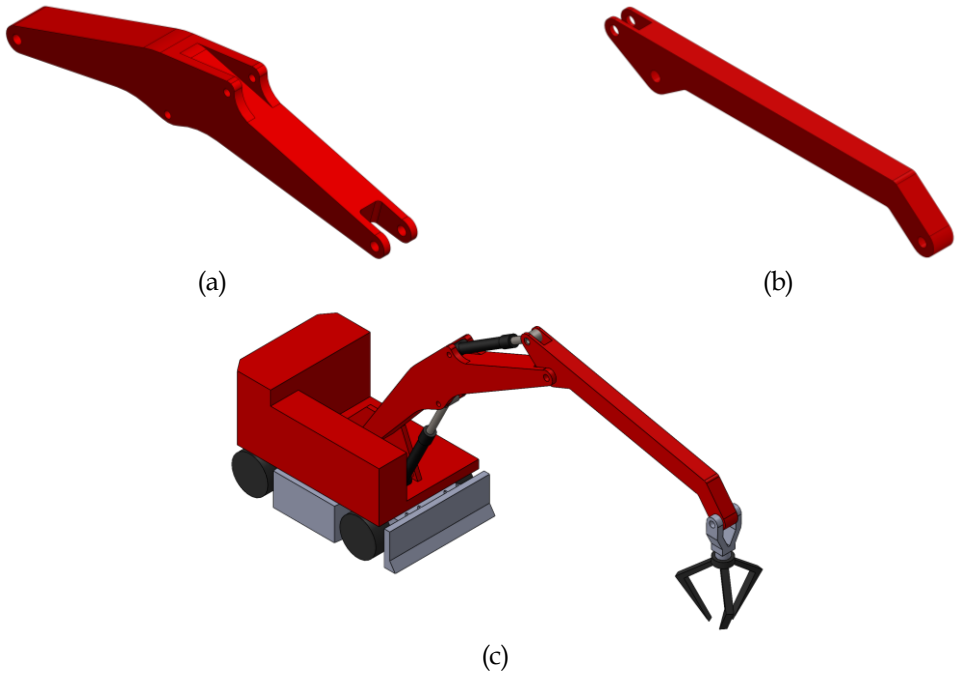

Figure 4.3 Simplified CAD of the Minelli M15: boom (a), stick (b), assembly (c).

For the sake of the modeling and simulation, the CAD assembly must be imported into Simscape, which can be used as a multibody simulation environment. In this regard, SolidWorks offers the possibility to export CAD assembly to MATLAB Simscape. However, because of the simplifications, the mass and, most importantly, the moments of inertia of the components are different. For instance, in Table 4.1 it is visible the difference between the simplified SolidWorks data of the boom and the manufacturer data of the same component. For this reason, all the correct data of the mechanical structures (undercarriage, upper carriage, boom, arm, orange peel grab, and actuators) are imported from an original assembly of the machinery and superimposed using a MATLAB script.

Thanks to Simscape Multibody, it is then possible to visualize the movements of the machinery using the Open Mechanics Explorer.

		Simplified	Original
Mass	$[kg]$	610	494
Center of Mass $[x \quad y \quad z]$	$[m]$	[1.90 0.28 0]	[1.94 0.24 0]
Moment of Inertia $[xx \quad yy \quad zz]$	$[kgm^2]$	[28.6 654.5 667.5]	[26.6 733.0 751.3]
Product of Inertia $[yz \quad xz \quad xy]$	$[kgm^2]$	[0 0 1.7]	[0 0 4.9]

Table 4.1 Difference value for the boom arm between the simplified CAD and the original CAD.

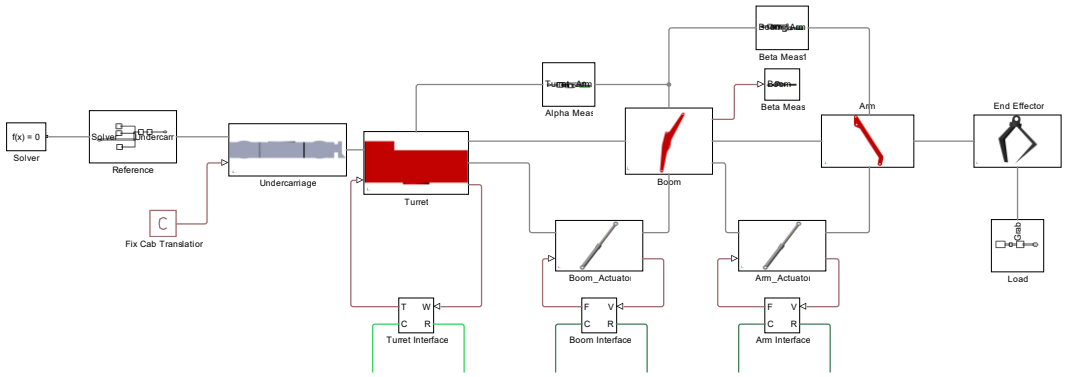

Figure 4.4 Screenshot of the Simscape multibody model.

The 3D model is imported into Simscape using the following three basic components:

- Mechanical joint [130] – It is fundamental to kinematically connect the mechanical components of the system. Friction, damping, and internal limits can be modified. Sensors can be added to a single component to measure important data such as position, velocity, and acceleration. Inputs can be modified to apply force or position to the system. For instance, the hydraulic cylinder mechanics is replaced by a prismatic joint, and the hydraulic forces applied on the two sides are translated into force input inside the joint.
- Solid [131] – It contains the mass and inertia of a single mechanical component. The correct mass and inertia matrices are imported into the model through these component variables.

- Rigid Transform [132] – It applies a time-invariant transformation between two frames, computing the position and orientation of each connected component.

4.3 Energy Storage System

The energy storage system of the M15e is composed of 504 Vented Regulated Lead-Acid (VLRA) modules, each one of them with a capacity of 155 Ah and Open Circuit Voltage (OCV) of 2.14 V. The connection between the modules is such to guarantee a capacity of 1240 Ah and an OCV of 128 V, so it has 8 modules in parallel and 60 modules in series. This configuration is commonly referred to as 60s8p.

While the battery capacity was calculated by Officine Minelli s.r.l. to accomplish a minimum of four hours of continuous work, the voltage of the machinery was selected based on industrial and commercial reasons, as well as on the analysis of the typical working environment and related safety measures. Indeed, higher voltage would have guaranteed higher efficiency, but these components come at a higher price over 120 V. Furthermore, as previously said, this machinery is currently used to move scrap metal, thus the air in which it operates is filled with an incredibly high amount of metal particles, highly increasing the possibility of short circuits. Therefore, instead of increasing the cost for high voltage functional and safety components, Officine Minelli s.r.l. prefers to work with lower voltage.

Thanks to the broad distribution of electric vehicles, more and more people are getting used to energy storage capacity, which is commonly shared as kWh instead of Ah. This capacity can be easily computed using the equation in Eq. 4 and considering nominal capacity and nominal voltage. The capacity in kWh is then equal to 156 kWh.

$$Q_{kWh} = V_{\text{nom}} \cdot Q_{Ah} \qquad \text{Eq. 4}$$

To model batteries there are two main possibilities, and, in both cases, it is possible to include electro and thermal analysis of the battery:

- First-Principle Models: they are based on the physiochemical interactions that happen inside the cells, thus they rely on coupled Partial Differential Equations (PDE). These models can be extremely complex and are more suited for in-depth analysis of single cells.

- Empirical Models: they are lumped-parameter models built on low-order Ordinary Differential Equations (ODE). Usually, they consist of Equivalent Circuit Models (ECM). They are simpler to build and use, as well as more suited for control and estimation.

For the model of the M15e, a 0th-order ECM like the one visible in Figure 4.5 is derived from the datasheet released by the supplier [133]. Interpolating the supplier data, it is possible to identify the relation between the DoD, the OCV, and the voltage drop at C-Rate $C10$ (Figure 4.6a), as well as the internal resistance R_0 of the equivalent circuit model (Figure 4.6b).

The computed internal resistance R_0 is close to the average values found in the literature [134, 135], therefore it is considered feasible.

Voltage and internal resistance are implemented in the model as Look-Up Tables LUTs, such as to properly simulate the power required for the energy storage system.

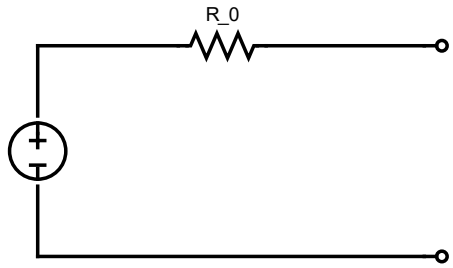

Figure 4.5 Scheme of the 0th Order Equivalent Circuit Model.

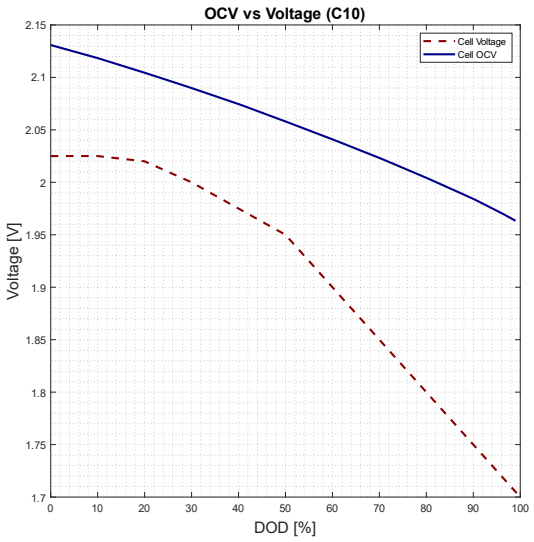

(a)

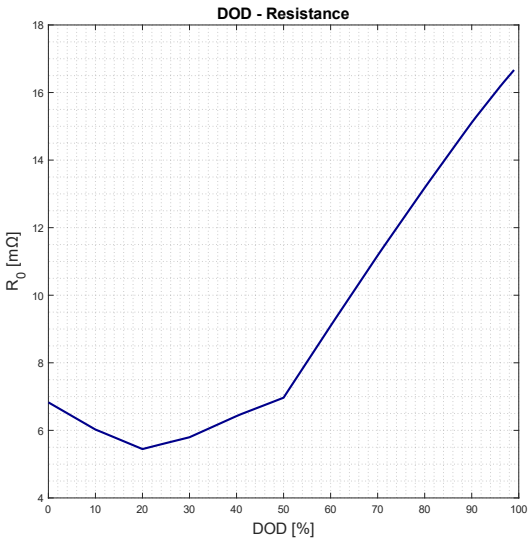

(b)

Figure 4.6 Fundamental relation for the 0th order ECM of the lead-acid battery: $E(DoD)$ (a), $R_0(DoD)$ (b).

The use of the 0th-order ECM greatly simplifies the dynamics of the battery, indeed, at every time step, it considers the battery as a steady-state system. However, this model is sufficient to compute the required current. Then, the SoC is calculated using the equation in (Eq. 5), known also as "Coulomb Counting".

$$\mathrm{SoC}(t) = \mathrm{SoC}_{t_0} - \frac{1}{3600\ C_{nom}} \int_{t_0}^{t} I(t)dt \qquad \text{Eq. 5}$$

Considering the scope and simplicity of the battery model, it is completely designed using MATLAB scripts and Simulink. No Simscape component is used. The Simulink model is visible in Figure 4.7.

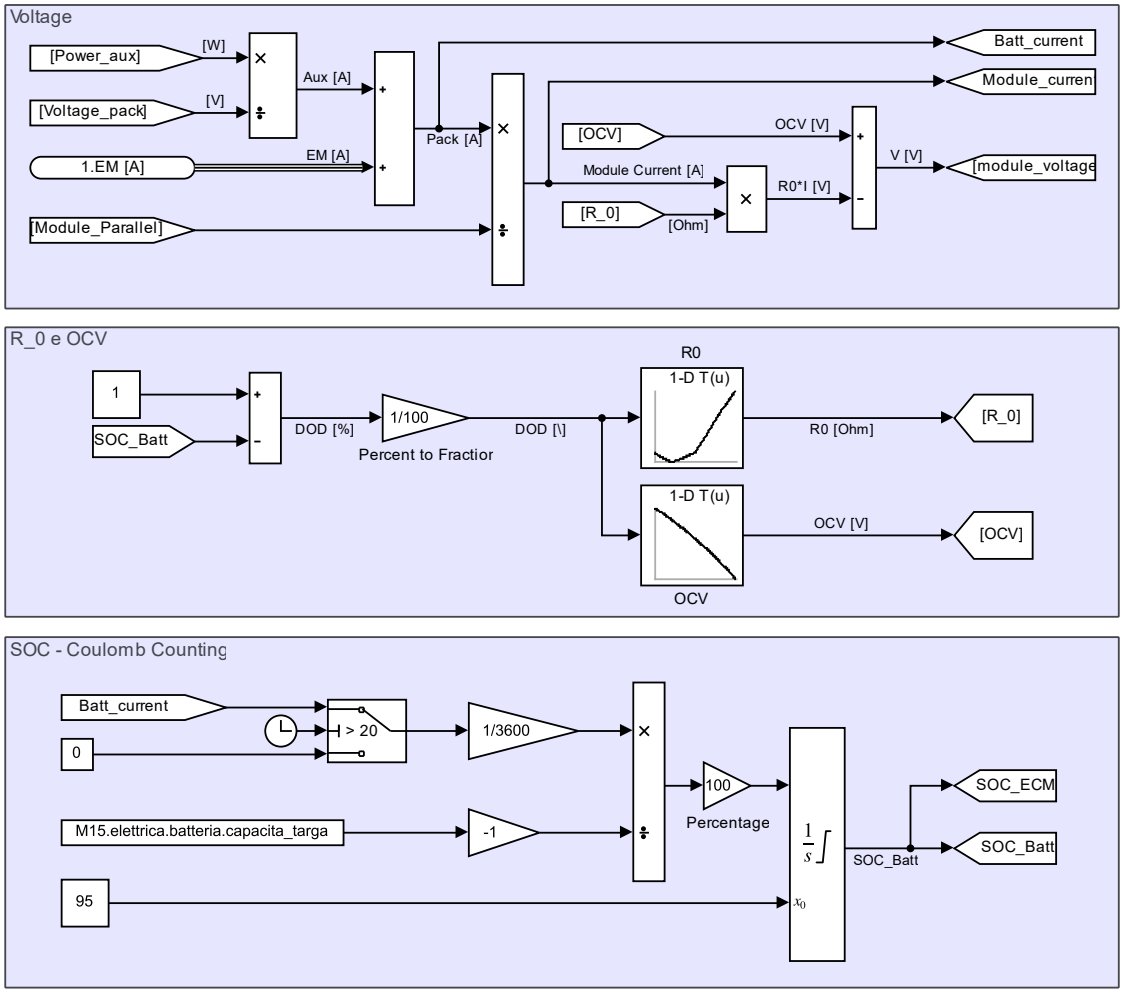

Figure 4.7 Screenshot of the battery model in Simulink.

4.4 Electric Motor

The electric motor of the M15e is an AC SCIM produced by Best Motor and its datasheet is visible in Table 4.2. Furthermore, the electric machine is supplied to Officine Minelli s.r.l. as a smart actuator, meaning that the inverter to control the motor is already included, and it is a ZAPI AC3 [136]. From the mechanical point of view, it means that there is a single assembly/component, while for the electric one, it means that the combined efficiencies of the motor and its inverter are given in the same testing report.

Producer	**Best Motor s.r.l.**	
Name	G1Z04706	
Number of pole-pairs	$[\emptyset]$	2
Rated Power	$[kW]$	32
Nominal Voltage	$[V]$	120
S2 Service[3]	$[min]$	60
S3 Service[4]	[%]	70

Table 4.2 Electric motor "Best Motor G1Z0406" datasheet.

However, due to the absence of the electrical and mechanical internal data of the electric machine (inertia of the rotor, characteristic of the stator's windings, etc.), it is not possible to model the whole machine using Simscape. Thus, to get to a functional model of the motor, the model is split into two parts:

- A Simscape model to supply mechanical power to the hydraulic system;

- [3] It represents the "short-time duty". The motor works at a constant load for a limited period during which thermal equilibrium is not reached. The motor can start again when its temperature decreases to room temperature.
- [4] It represents the "intermittent periodic duty". This involves a sequence of identical duty cycles, each consisting of a time of operation at constant load and a time at rest. When at rest, the motor is not fed.

- A Simulink LUT of the motor-inverter efficiency to compute the electric power required by the battery.

As visible in Figure 4.8, to supply mechanical power to the hydraulic pump, the electric motor is modeled as an ideal torque source. However, to avoid the unrealistic response of the motor, such as to match the requested torque and velocity perfectly and instantly, a transfer function and a PI controller are added into Simscape to simulate the dynamics of the motor. The transfer function is used to add a little lag, while the PI controller tries to reduce the error between the reference and measured velocities.

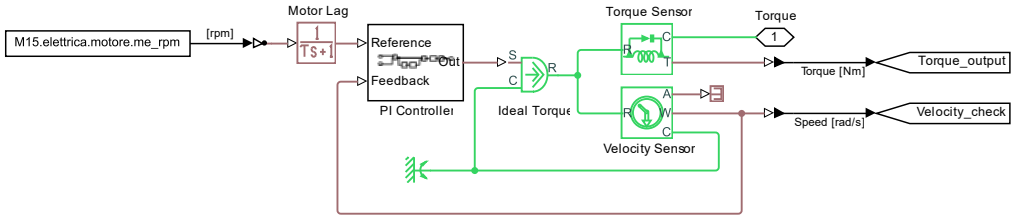

Figure 4.8 Simscape model of the "Best Motor G1Z0406" electric motor.

The efficiency points given by the supplier are visible in Figure 4.9, and by looking at them it is clear that these points are not enough to create a complete efficiency LUT. Consequently, interpolation and filtering are needed to get to a feasible LUT. The result of the interpolation is visible in Figure 4.10a, while the final efficiency map visible in Figure 4.10b is implemented in the model using the Mapped Motor component of the Simulink Powertrain Blockset [137], which computes how much current is needed to match the torque and velocity of the requested working point.

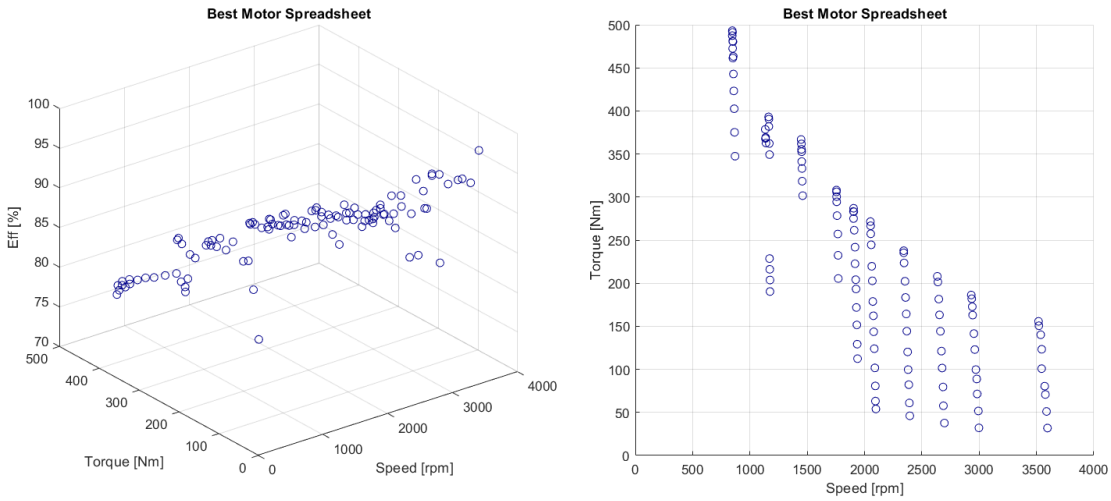

(a) (b)

Figure 4.9 Efficiency points from the original spreadsheet of the "Best Motor G1Z0406".

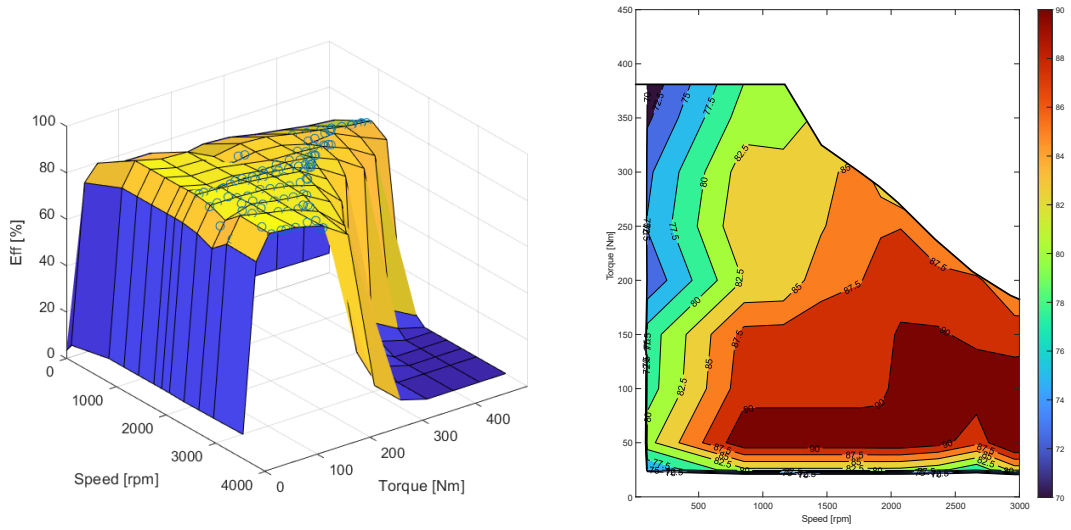

(a) (b)

Figure 4.10 Efficiency points after interpolation and filtering of the "Best Motor G1Z0406".

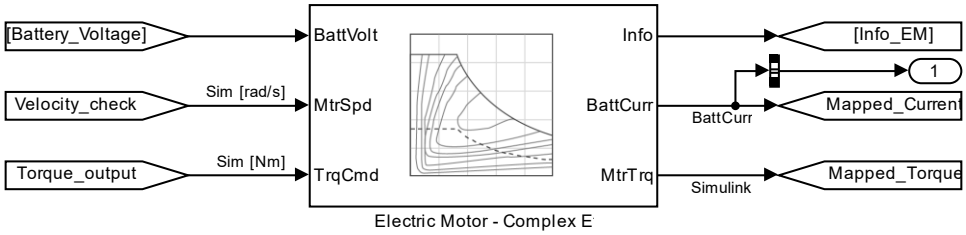

Figure 4.11 Mapped Motor component of the Simulink Powertrain Blockset.

4.5 Hydraulics

As previously discussed, the hydraulic system of the M15e relies on two hydraulic pumps:

- The main hydraulic pump is a variable displacement pump, and it supplies all the actuators of both the upper carriage and undercarriage. This pump is included in the Simulink/Simscape model of the machinery.
- The secondary hydraulic pump is a fixed displacement pump, and it supplies the joystick control circuit. It is not included in the Simulink/Simscape model of the machinery.

As in every hydraulic circuit, the main hydraulic pump is characterized by two main outputs, pressure p_{pump} and flow Q_{pump}, which derive respectively from the torque and velocity of the motor, and then define the hydraulic power consumption based on the known following equation (Eq. 4):

$$P_{\text{pump}} = p_{\text{pump}} \cdot Q_{\text{pump}} \qquad \text{Eq. 6}$$

Idealizing and simplifying the system to a single linear actuator, it is possible to state that:

- the pump pressure matches the system pressure, which is set by the load on the actuator. The higher the force on the actuator, the higher the pressure.
- the hydraulic flow sets the velocity of the actuator, which is decided by the operator and transmitted to the system using the joysticks inside the cab, thus, the higher the flow, the higher the velocity.

However, as already discussed in previous chapters (Hydraulics Systems and Actuators), real hydraulics systems are not ideal, and using multiple actuators complicates the relation between force/torque/pressure and velocity/flow, and phenomena like load interference and load dependency can occur.

To avoid these issues and to improve the overall efficiency of the machinery, the M15e relies on a Closed Center System with Variable Pump Pressure (Closed Center Systems with Variable Pump Pressure), which is identical to the one installed in the ICE-powered version. Consequently, the pump outlet pressure is always set slightly higher than the load pressure by a pre-set value *s*, and hydraulic feedback is used to control the actuator's velocity. Furthermore, to allow the movement of multiple actuators without load dependency, multiple pressure compensators are positioned after the DCV[5].

So, the M15e hydraulic system can be addressed as a Post-Compensated Load Sensing System. In particular, thanks to the LS applied to a variable displacement pump, much less power is wasted during partial loads in comparison to a fixed displacement pump, as visible in Figure 4.12.

To allow multiple actuator movements without any load dependency, post compensators are used and the simplified representation of how they work is visible in Figure 4.13, while in Figure 4.14 it is shown its energy analysis. The main concept of post-compensators is to intentionally create extra pressure drops on lower-pressure demanding loads, limiting the natural tendency of the oil to flow where the resistance is lower. However, it is worth noticing that the application of such controlled pressure drops adds power waste to the system.

- [5] An excepetion exist on the M15e for the swing movement of the upper carriage, and it is presented in the chapter Upper Carriage.

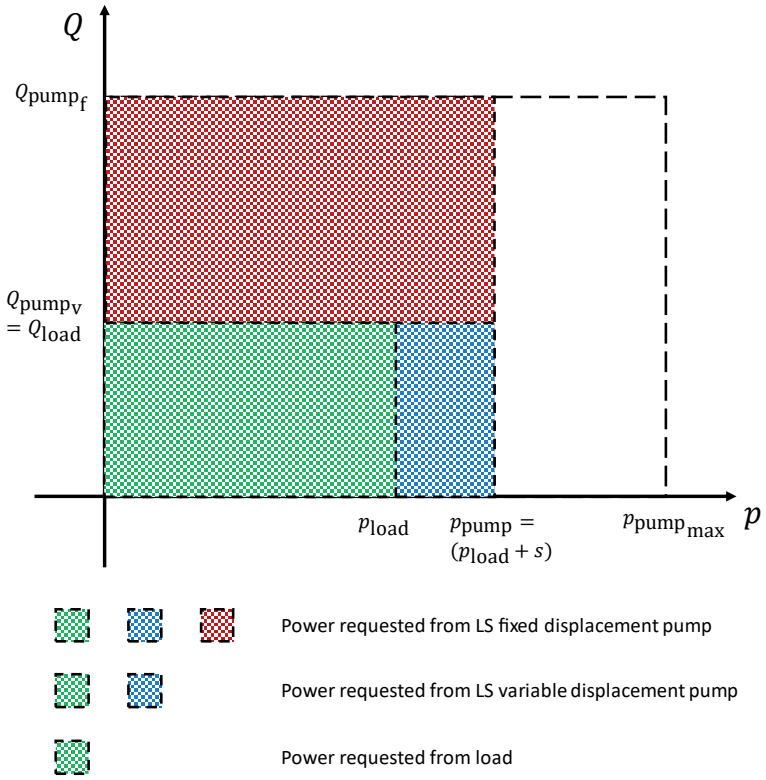

Figure 4.12 Energy plot of the LS hydraulic system.

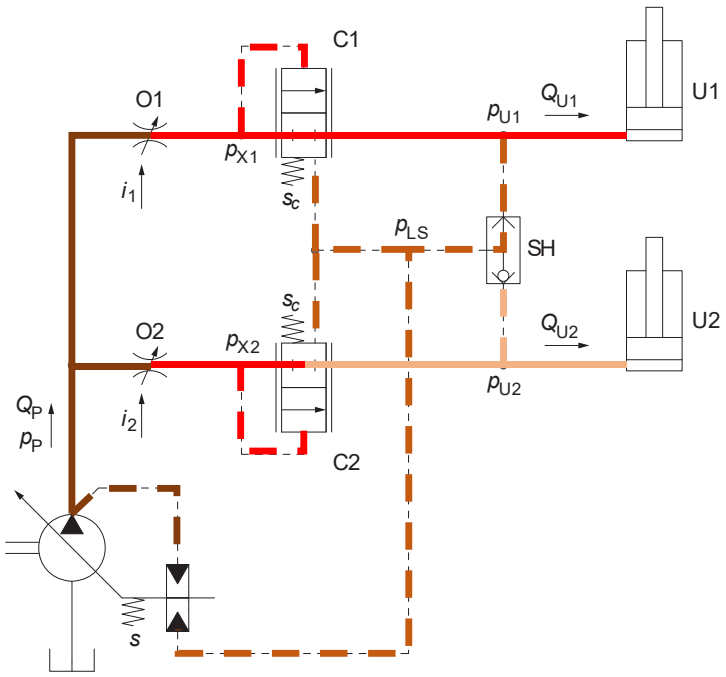

Figure 4.13 Simplified scheme of an LS Post-Compensated hydraulic system.

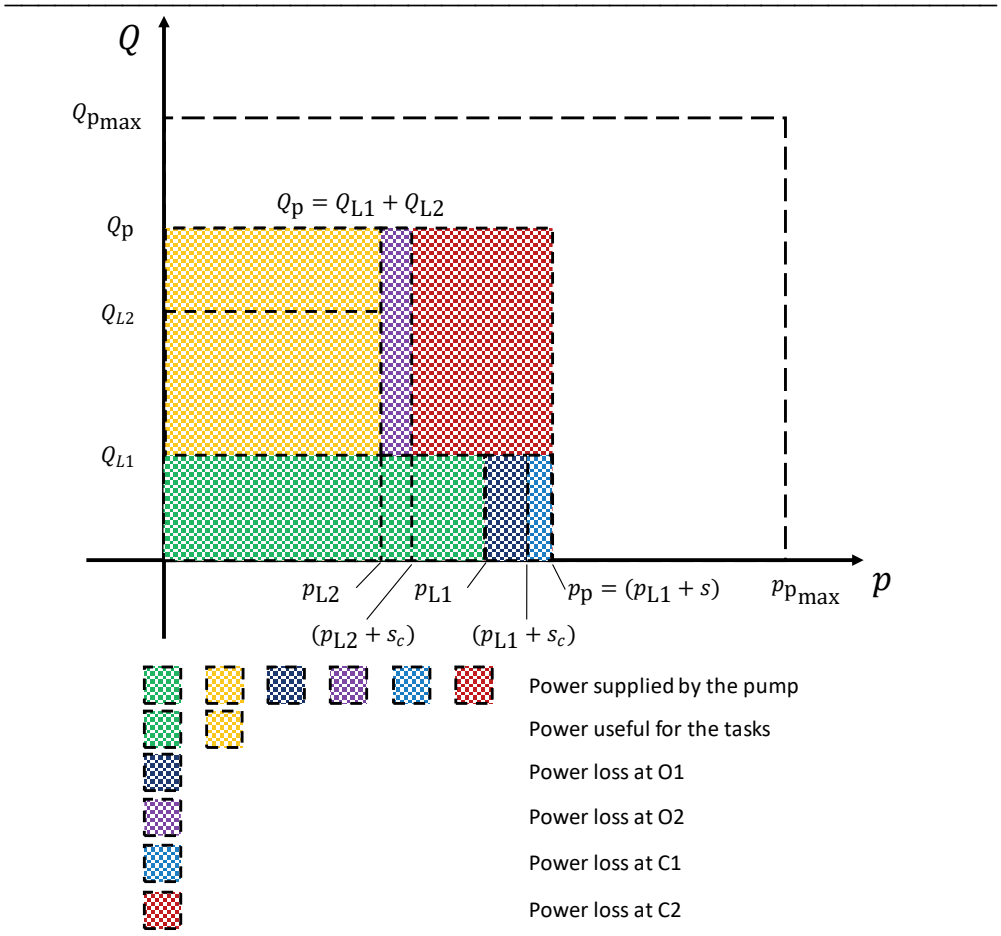

Figure 4.14 Energy plot of the Post-Compensated LS hydraulic system.

To function, both the hydraulic pump and DCV must have integrated LS functionalities because the LS requires specific hydraulics. For this reason, the LS system is divided also in the model: the part incorporated in the hydraulic pump is included in the general screenshot of the model visible in Figure 4.15, while the DCV implementation is split into the boom, stick, and turret subsystems.

Other basic values and valves must be added to the hydraulic system, like the fluid used by the hydraulics, the pump relief valve, and the hydraulic pipes resistance.

Thanks to the "*hydraulic fluid*" Simscape component (Figure 4.16) [138], implementing the oil parameters is extremely simple, especially considering that there is a list of precompiled fluids. The hydraulic fluid used by the M15e is supplied by Q8, and its characteristics are extremely close to the one of a 10W Oil [139].

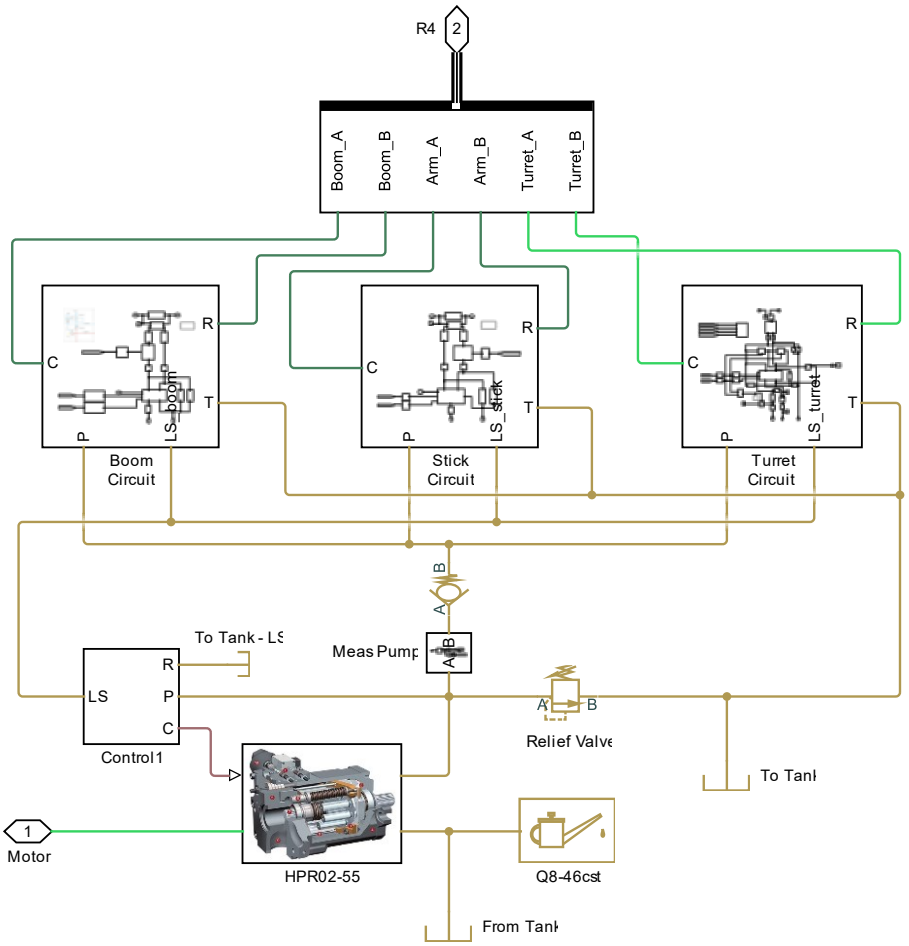

Figure 4.15 General overview of the M15e Simscape model of the hydraulics.

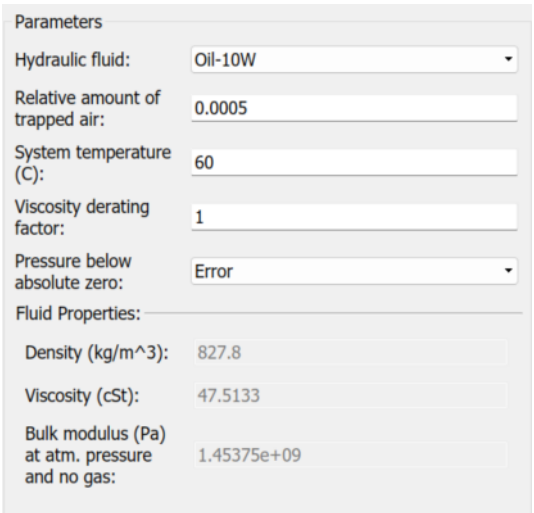

Figure 4.16 Hydraulic fluid working parameters. [138, 139]

The relief valve component visible in Figure 4.15 represents the nominal maximum pressure of the hydraulic pump, and it is set at $420\,bar$ as requested by Linde in the hydraulic pump's datasheet [140].

Lastly, the resistance due to hydraulic pipes is implemented in the subsystems of the three main functions. Indeed, the DCV and pump are extremely close to each other, while most of the pipe length is between the DCV and the actuators. Considering that most of the pressure drops are due to load intensity, valves, and actuators, the pipe resistance is considered entirely caused by their length, and not by fittings and curves. The hydraulic pipes are supplied by Alfagomma S.p.A., they have an internal diameter of 19 mm [141] and they are implemented in the model using "*hydraulic pipeline*" components [142].

4.5.1 Hydraulic Pump

The axial piston LS variable displacement pump is supplied by Linde Hydraulics Gmbh, it has a maximum displacement of $55\,cm^3/rev$, and its technical details are visible in the Table 4.3 [140].

HPR-02-55		
Max. displacement	$[cm^3/rev]$	55
Max. operating speed	$[rpm]$	2700
Max. oil flow	$[l/min]$	148.5
Max. nominal pressure	$[bar]$	420
Perm. housing pressure	$[bar]$	2.5
Max. input torque	$[Nm]$	368
Max. moment of inertia	$[kgm^2]$	7.9×10^{-3}

Table 4.3 Technical datasheet of the Linde HPR-02-55 hydraulic pump. [140]

The simplified scheme of the internal circuit of the pump is visible in Figure 4.17, and it shows how the LS influences the displacement. Indeed, the displacement actuator is balanced by the outlet pressure pump on its piston side, while the LS pushes on the cap side.

For the implementation inside the model, the "*Variable-Displacement Bidirectional Hydraulic Pump*" Simscape component is used [143], because it mechanically (and mathematically) links the mechanical rotation of the electric motor with the hydraulic system. Indeed, as visible in Figure 4.18, it extracts mechanical power from the Simscape mechanical rotational

dimension, delivering it to the hydraulic one, while the inertia of the pump is implemented as a mechanical rotational component.

One great advantage of the "*Variable-Displacement Bidirectional Hydraulic Pump*" Simscape component is that it analytically and automatically computes the efficiency of the pump (based on the implemented parameters). In particular, every hydraulic pump is defined by two different efficiencies [60]:

- Volumetric efficiency η_v: it is the ratio between the actual output flow and the ideal one, and it is caused by compressibility losses and leakages.
- Hydromechanical efficiency η_{hm}: it is the ratio between the ideal shaft torque and the actual one, and it is caused by frictional losses of the mechanics as well as fluid shear inside the pump.

The overall efficiency of the pump is then computed as in Eq. 7:

$$\eta_{tot} = \eta_v \cdot \eta_{hm} \qquad \text{Eq. 7}$$

In this regard, a Simscape model is built to evaluate how close these analytical efficiencies are to the ones of the pump installed in the machinery.

The Simscape component internally computes both the hydraulic and hydromechanical efficiency, and varying the parameters of the component allows engineers to slightly change its behavior. However, not having the efficiency map of the Linde HPR-02-55, nor any of its internal mechanism dimensions and characteristics, the efficiency maps of a similar pump (Figure 4.19) are derived from the paper in [144] and implemented with a LUT into Simulink.

A Matlab script and model are designed to sweep different combinations of pressure and flow, computing for each combination how much difference exists between the analytical solution integrated into the Simscape component and the LUT. The following speed, pump velocity, displacement, and pressure loads are tested:

- $\text{velocity} = [1000, 1200, 1400, 1600, 1800, 2000]$
- $\text{displacement} = [5, 15, 25, 35, 45, 55]$

- $\text{pressure} = [50, 100, 150, 200, 250, 300, 350]$

The entire simulated testing campaign shows an average error of 2.37 %, which means that the analytical efficiencies computed automatically by the Simscape component are in line with a real component.

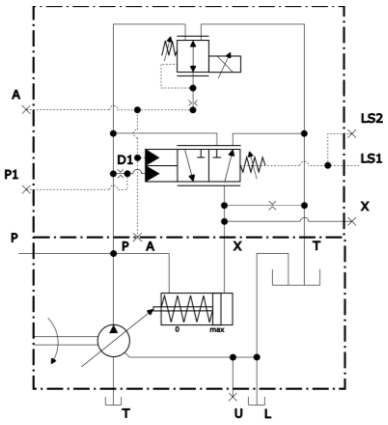

Figure 4.17 Hydraulic pump simplified internal scheme. [140]

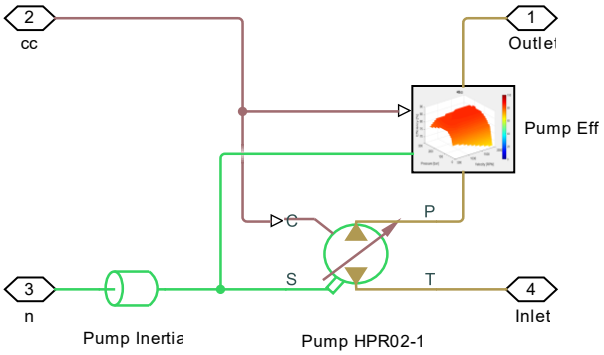

Figure 4.18 Overview of the hydraulic pump in Simscape.

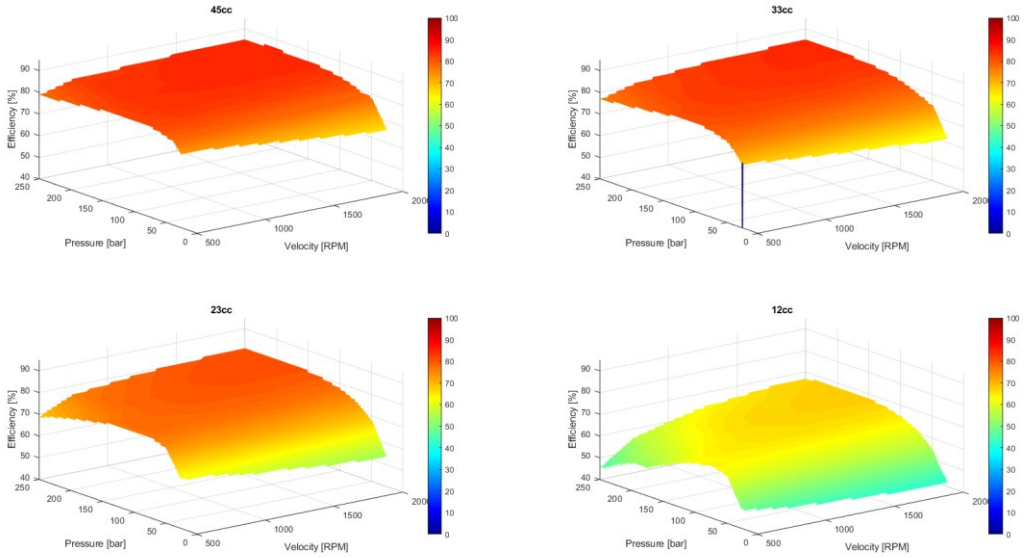

Figure 4.19 Efficiency map of a 45cc hydraulic pump. Results derived from [144].

4.5.2 Linear Actuator

The three most important functions of the machinery are the movements of the first and second arms and the swing of the upper carriage. Regarding the first two, one pair of identical hydraulic linear actuators is used to move the arms. Because the operator must be able to control both the extension and retraction of the cylinders independently of resistive or overrunning loads, these are double-acting cylinders, and their characteristics are summarized in Table 4.4, while the mechanical assembly is visible in Figure 4.20.

Hydraulic cylinders		
Retracted length	$[mm]$	1400
Extended length	$[mm]$	2250
Stroke	$[mm]$	850
Operating pressure	$[bar]$	350
Peak pressure	$[bar]$	420

Table 4.4 General characteristics of the hydraulic cylinder for boom and arm.

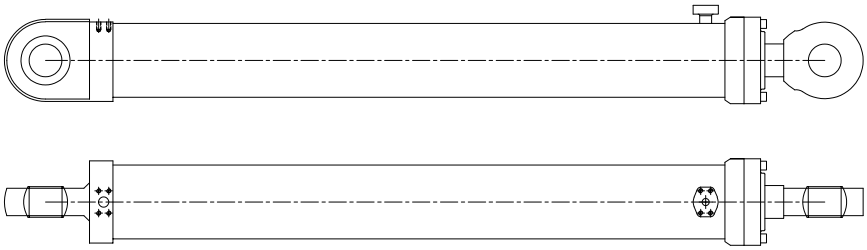

Figure 4.20 Mechanical assembly of the hydraulic cylinder for boom and arm.

The hydraulic cylinders are fundamental components of the machinery, indeed they allow the fundamental transformation from hydraulic to mechanical energy. Consequently, their implementation into the model is very important. In this regard, each cylinder is modeled both in the hydraulic and mechanical dimensions (Figure 4.21), while a third subsystem is needed to go from the former to the latter (Figure 4.22). Indeed, as visible from Figure 4.21a, the Simscape component "*Double-acting Hydraulic Cylinder*" [145] transforms the Simscape hydraulic signal into the Simscape linear mechanical signal, but the "*Prismatic Joint*" of Simscape multibody requires a force signal as input, giving back the velocity as output (Figure 4.21b) [146].

It is worth noticing that the mechanical dimensions of the cylinder are requested as inputs into the "*Double-acting Hydraulic Cylinder*" (Figure 4.23), while the damping overall coefficient must be implemented into the "*Prismatic Joint*". In addition, the mass and inertia of the cylinder are imported in Simscape multibody as done for the rest of the mechanics, meaning that they are drawn in SolidWorks, and mass and inertia are properly overwritten using a MATLAB script.

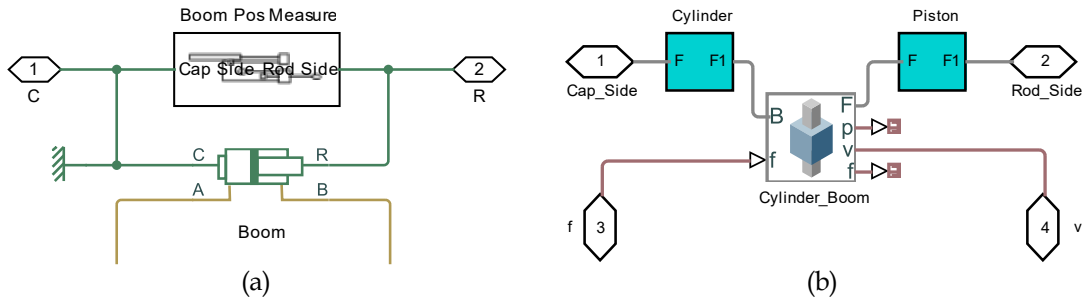

Figure 4.21 Hydraulic and mechanical sub-models of the hydraulic cylinder.

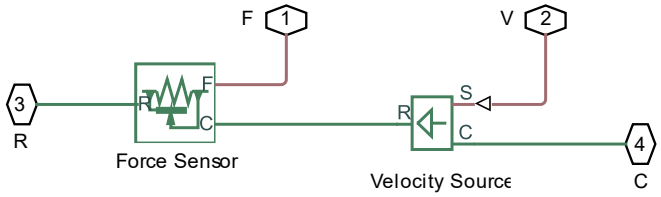

Figure 4.22 Modeling interface needed for the implementation of the hydraulic actuator.

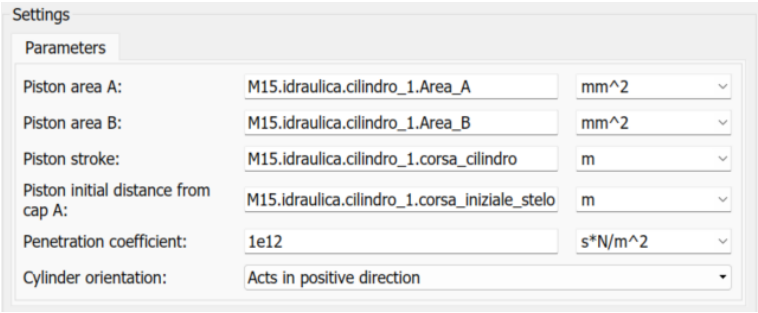

Figure 4.23 Input parameters of the Double-acting Hydraulic Cylinder. [145]

Each line to and from the actuators has a relief valve, which is easily modeled using the "*Pressure Relief Valve*" Simscape component [147]. For instance, on the boom A line the pressure relief valve is set to 350 bar, while on the B line is set to 285 bar.

4.5.3 Directional Control Valve

As previously mentioned, to be compatible with the LS, the DCV must include LS capabilities within its structure, otherwise it would be impossible to generate proper hydraulic feedback.

As for the hydraulic pump, the DCV is supplied by Linde Hydraulics Gmbh. In particular, the DCV mounted on the M15e is the Linde VW14 [148], which is composed of multiple spools, each one of them with the general characteristics and scheme visible in Table 4.5 and Figure 4.24.

	Description	**VW 14**
Flow	Maximum Flow $[l/min]$	140
	Working port pressure $[bar]$	350
Pressure	Max. work port pressure $[bar]$	420
	Max. pilot port pressure $[bar]$	45

Table 4.5 Main characteristics of the DCV WM 14 by Linde. [148]

Each valve is a pilot-actuated, closed center, 5/3 valve, with two additional LS channels, which are integrated inside the main spool, as clearly visible in the mechanical assembly in Figure 4.24b, along with the pressure compensators.

Taking into consideration the spool of a single linear actuator, its joystick's pressure moves the spool toward the A or B port, deciding to address the flow toward the cap-side or piston-side of the actuator. From the mechanical point of view, the hydraulic spool is a complex machined component, with multiple internal orifices carefully designed in parallel and series. However, from a more functional and simplified point of view, the spool controls the direction of the flow and, thus, the velocity of the actuator by varying an equivalent passage area based on the following equation[6]:

$$Q_0 = C_\mathrm{d}\, A_{\mathrm{eq},\,0} \sqrt{\frac{2\Delta p}{\rho}} \qquad \text{Eq. 8}$$

- [6] The orifice basic equation is based on the known Bernoulli's equation.

Where:

- C_d is the flow coefficient of the orifice.
- $A_{eq,\,0}$ is the equivalent passage area of the orifice.
- Δp is the pressure drop across the orifice.
- ρ is the density of the fluid.

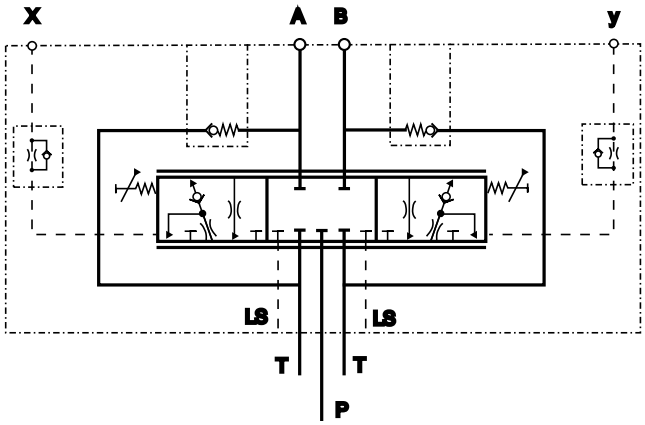

(a)

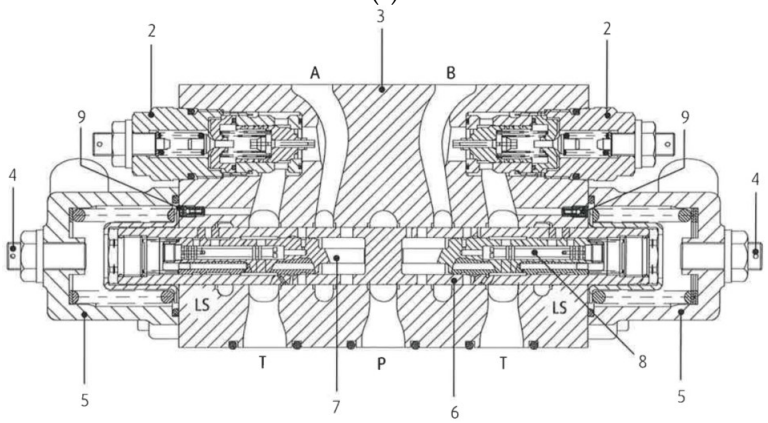

2 – Relief and make-up valve
3 – Housing
4 – Mechanical stroke limitation
5 – Control spool
7 – Pressure compensator
8 – Shuttle spool
9 – Ventilation valve

(b)

Figure 4.24 Pilot actuated closed center LS valve by Linde: (a) simplified internal scheme; (b) mechanical assembly.

Because each function/actuator has slightly different needs, Linde offers different control spools to be mounted in the DCV. Regarding the M15e, the DCV is formed by six different spools, each one controlling a different function. In this regard, the inlet and return experimental curves of M15e spools are visible in Figure 4.25 [149–151]. These curves are generated by

Linde on a hydraulic bench test equipped with an LS system, allowing the emulation of the spool behavior on the machinery, with the flow passing through the DCV to the actuator (e.g. $P \rightarrow A$), and then coming back from the actuator to the DCV (e.g. $B \rightarrow T$).

- The inlet curve relates the movement of the spool with the flow.
- The return curve relates the movement of the spool with the resistance pressure.

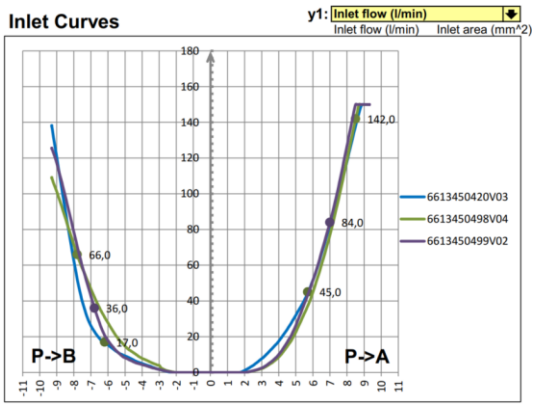

(a)

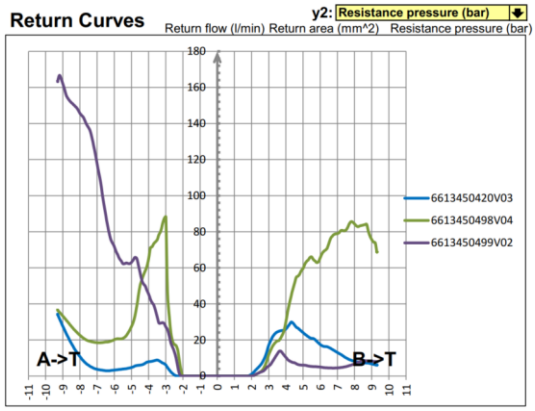

(b)

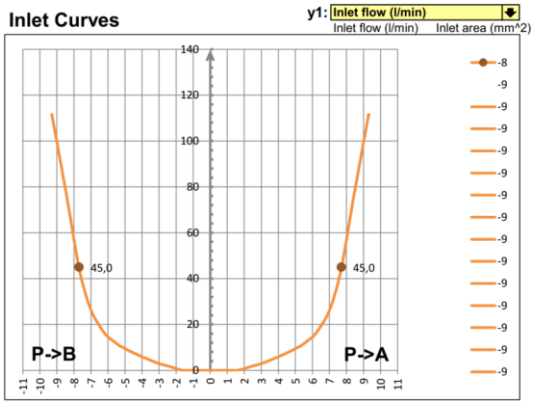

(c)

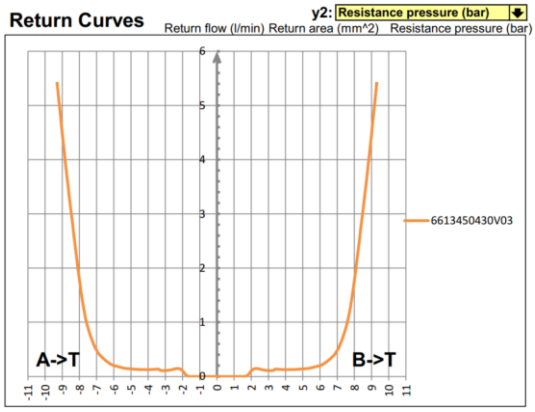

(d)

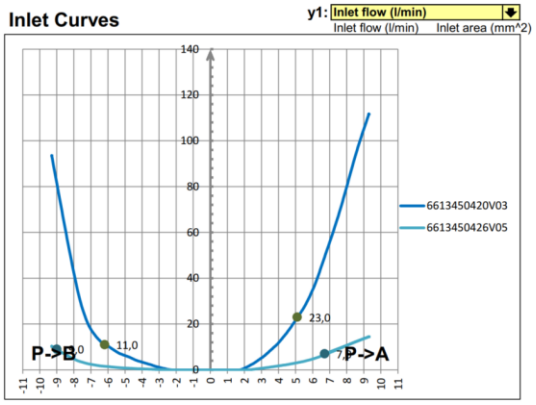

(e)

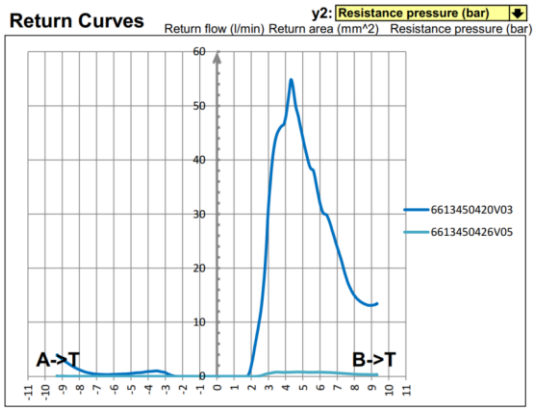

(f)

Figure 4.25 Spools installed on the M15e DCV VW14. [149–151]

Besides behaving differently from each other, it is worth noticing that most of the spools have asymmetrical behavior. First of all, this is due to the cylinder ratio of the actuator (piston-side and cap-side are not symmetrical for most actuators, especially for linear ones), and secondly, the spool can be specifically designed to better address a specific function. The exception is the spool visible in Figure 4.25c and Figure 4.25d, which is related to the swing of the upper carriage. Indeed, the swing motor is a symmetrical rotational actuator and doesn't need any asymmetrical behavior to better accomplish its task.

Simscape does not have any components with the same characteristic as the Linde VW 14, thus a new subsystem needs to be created using more simple components. How the VW is reproduced in the model is visible in Figure 4.26. First of all, the single main spool is divided into four different "*Variable Orifices*" [152], splitting so the related channels P-A, P-B, A-T, B-T. Then, the function of the Post Compensator is addressed by two additional subsystems, as well as the LS, which is implemented in the model using two variable orifices.

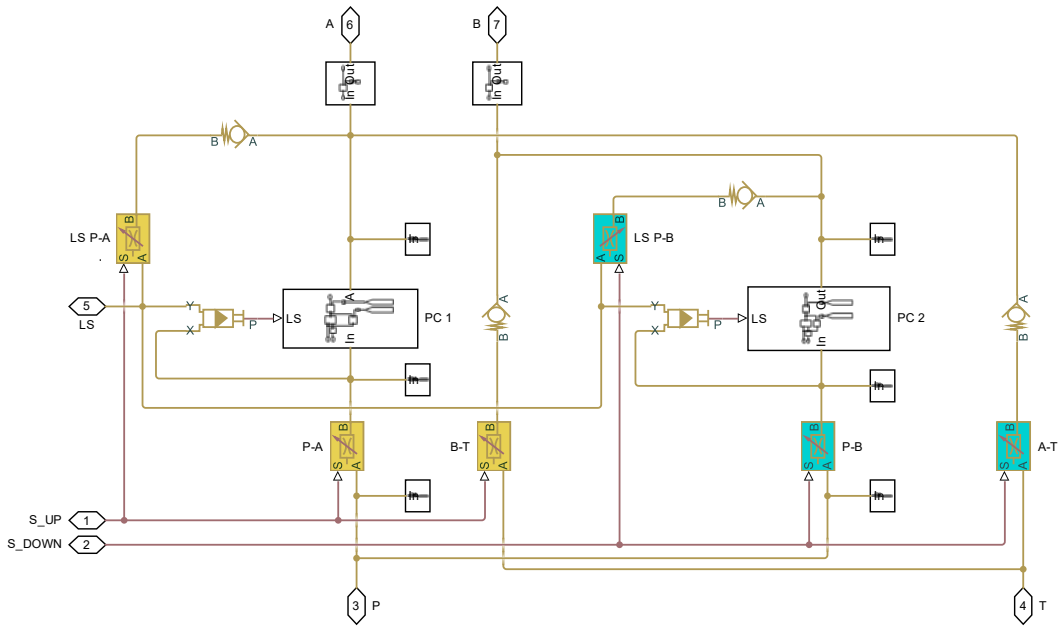

Figure 4.26 Simscape subsystem of a spool inside the DCV.

The main equation on which the component is based is visible in Eq. 9 [152], which is very similar to Eq. 8.

$$Q = C_{\mathrm{d}}\, A(h) \sqrt{\frac{2}{\rho}} \frac{\Delta p}{(\Delta p^2 + p_{Cr}^2)^{\frac{1}{4}}} \qquad \text{Eq. 9}$$

As clearly visible, the only input in this equation is the passage area $A(h)$, because the density ρ is a given data, the flow Q is the final output, p_{cr} is related to the type of flow (laminar or turbulent) and the pressure drop Δp depends on the load. Thus, to model the single channel of the spool it is necessary to know its area, which in turn depends on the physical signal h that identifies the shifting of the spool.

However, as visible from the curve in Figure 4.25, the relation between the movement of the spool and its area is not given by the supplier, thus it must be computed from the spool curves. To do so, a Matlab script, a Simscape model, and a graphic interface are created, and the related final Graphical User Interface (GUI) is visible in Figure 4.27.

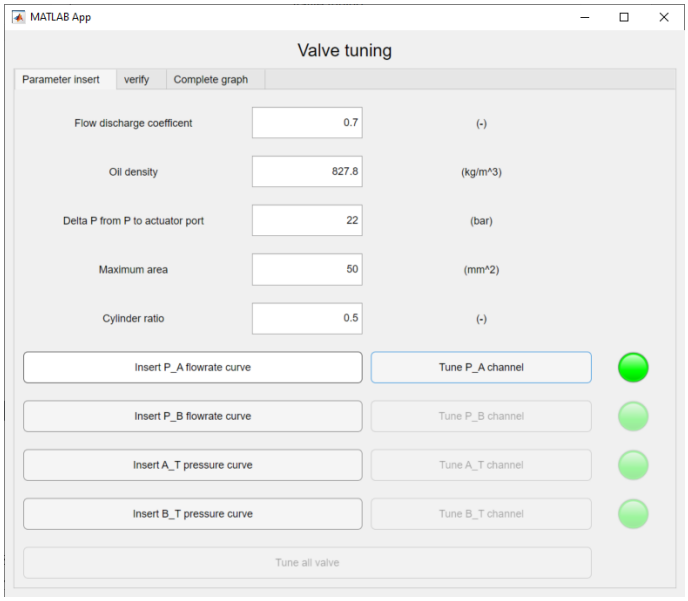

Figure 4.27 GUI for the computation of the area–spool relation of each valve.

Due to the difference between the inlet curve $Q(h)$ and return curve $p(h)$ the computation of the area–spool relation is different, but it is always based on Eq. 8:

- $P \rightarrow A, B$: firstly, the curve is extracted from the .pdf using the *GRABIT* GUI [153]. Then, using the modeled GUI, spool movement and flow vectors are interpolated and resampled, while a vector of increasingly bigger areas is created. For each value of the spool and setting the pressure drop at $22\ bar$, a vector of computed flows is generated using Eq. 8. This vector is compared with the interpolated flows, generating a vector of normalized errors. Finding the index of the minimum errors allows the selection of the best area for each spool movement, generating step-by-step the vector of the orifice's area. Finally, a Simscape model is used to check the match between the spool curve of the datasheet and the one generated using the computed orifice area.
- $A, B \rightarrow T$: once again, the curve is extracted using the *GRABIT* GUI [153]. Overall, the process is similar to the previous one, in this case however the input flow depends on the inlet flow curve and cylinder ratio, while the vector of increasingly bigger areas and Eq. 8 are used to compute the pressure drop. Thus, the vector of normalized errors is based on the difference between the pressure drop of the curve and the computed pressure drop. After generating the vector of the areas, a Simscape model is used once again to check the results.

Using the GUI, the inlet and outlet curves of each spool are well recreated. However, each curve must be filtered and interpolated, as visible in details in Figure 4.28. Indeed, the "*Variable Orifice*" [152] component requires not only the orifice area to be an increasing function, but, to avoid numerical errors at lower spool movements, it is also helpful to interpolate the curve to obtain a strictly increasing function.

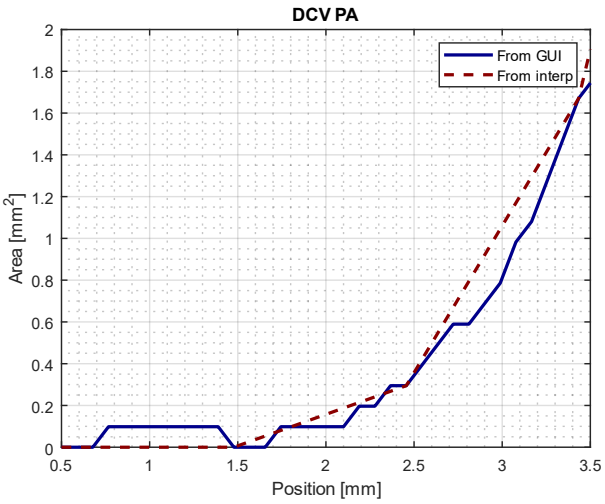

Figure 4.28 Detail at low movement of the DCV PA spool.

4.5.4 Load Sensing Controller

As previously discussed, the LS system is a fundamental characteristic of the hydraulic system installed on the machinery.

Indeed, thanks to the control of the pump displacement, it avoids unnecessary overflow and energy waste. To do so, the pressure drop across the DCV Δp_{DCV} is taken as feedback, while the LS controller compares this parameter with the pump outlet pressure p_p (Figure 4.29). Simultaneously, the LS system allows the velocity of the actuator to be independent of the load.

Thus, the objective of the LS controller is to keep the pressure drop across the DCV at a constant value s, which is usually around 20 bar and is called "LS margin". In Figure 4.29a, there is the scheme of a didactical LS controller, while the flowchart visible in Figure 4.29b is useful to understand how it works. This flow diagram is valid independently of the number of actuators used simultaneously. However, in the case of multiple actuators, a combination of shuttle valves allows the selection of the highest P_{LS} among the utilities.

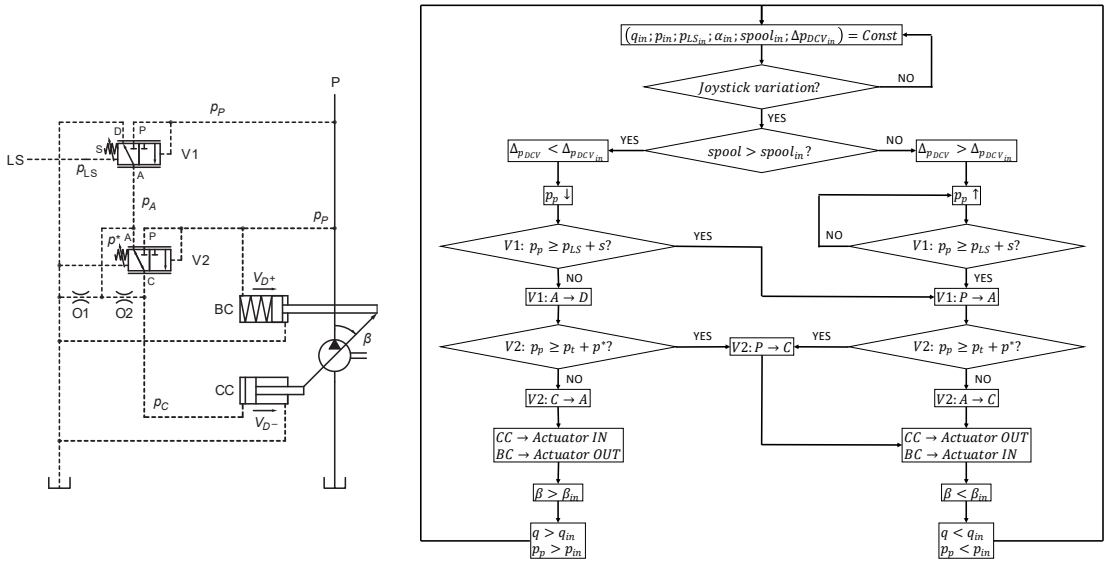

(a) (b)

Figure 4.29 Scheme of the LS system: didactic scheme (a) [60], flow diagram of the didactic scheme (b).

Technically speaking, the LS system can be implemented relying only on hydraulics, and this is what allowed the LS to gain so much relevance in mobile hydraulic systems. However, more advanced LS systems use servo-actuated valves to improve and add functionalities. This is the case for the LSC system by Linde (Figure 4.30a) [140], where a servoactuated valve is used both as the anti-stall and to electronically vary the LS margin from 8 to 23 bar [140].

Unfortunately, a prebuilt LS Simscape component does not exist, and the internal mechanical data of the LS controller are not provided by the supplier due to intellectual property. Thus, it is necessary to rely on more simple Simscape components and to design a similarly behaving model. The comparison between the simplified LS controller scheme published by the supplier and the Simscape model is visible in Figure 4.30.

The first thing to notice in Figure 4.30, is how the LS Simscape subsystem is not entirely modeled within the hydraulic domain, on the contrary, also physical signals are used. Indeed, not knowing the mechanical characteristics of the internal valves, it would be impossible to model the interaction between the valves. However, using physical signals instead of hydraulic connections precludes some hydraulic dynamics, meaning that extremely

steep variations can occur, causing so numerical errors. For this reason, lag transfer functions are added to physical signals.

An example of this variation of domains is the double-acting linear cylinder controlling the displacement pump, for which a "*Hydraulic Double-Acting Valve*" is used [154], while its output is subtracted from the constant maximum displacement value.

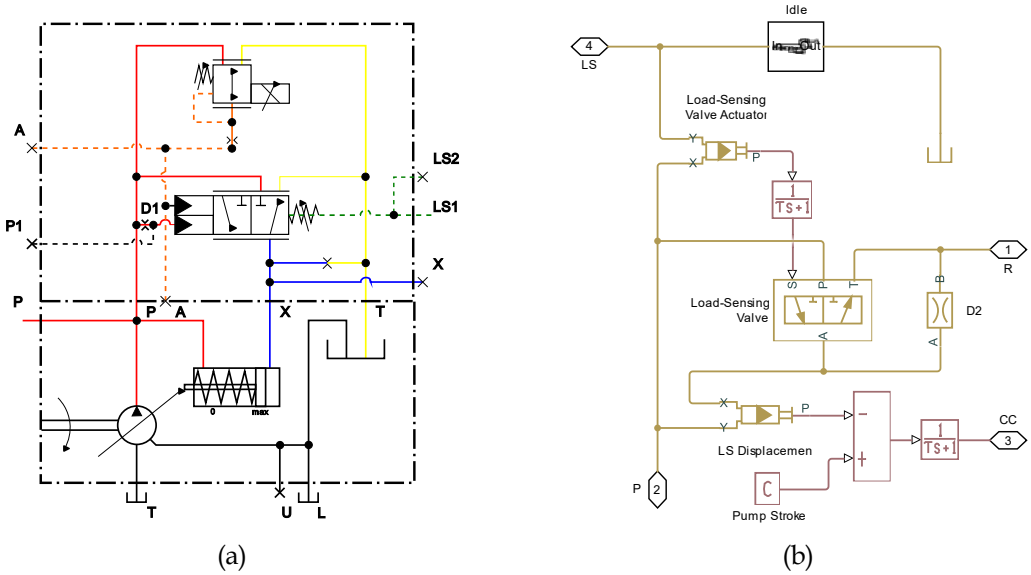

Figure 4.30 LS controller: simplified scheme from the supplier (a), model in Simscape (b).

The basic equation of this Simscape component is the following:

$$F = p_x \cdot A_x - p_y \cdot A_y \qquad \text{Eq. 10}$$

Where:

- p_x, p_y are the pressure at the two sides of the valve.
- A_x, A_y are the cylinder area of the two sides of the valve.

Because the desired output is a linear movement, the next equations must be taken into account:

$$L_x = \frac{s_x}{F_{\max_x} - F_{\mathrm{pr}_x}} \qquad \text{Eq. 11}$$

$$L_y = \frac{s_y}{F_{\max_y} - F_{\mathrm{pr}_y}} \qquad \text{Eq. 12}$$

$$s = \begin{cases} 0 \rightarrow 0 \leq F \leq F_{\mathrm{pr}_y} \\ L_y \cdot \left(F - F_{\mathrm{pr}_y}\right) \rightarrow F_{\mathrm{pr}_y} < F < F_{\max_y} \\ s_y \rightarrow F \geq F_{\max_y} \end{cases} \qquad \text{Eq. 13}$$

Where:

- s is the final linear displacement of the valve.
- s_x, s_y are the strokes of the two sides of the valve.
- $F_{\max_x}, F_{\max_y}$ are the maximum spring force at the two sides of the valve.
- $F_{\mathrm{pr}_x}, F_{\mathrm{pr}_y}$ are the preload spring force at the two sides of the valve.

The values inside the component are selected by knowing the maximum linear displacement, how much the pressure values can change at its side, and that the movement must be limited to a single side of the actuator.

The modeling of the valve named "LS Valve Actuator" visible in the same Figure 4.30b follows the same logic. In this case, the main variable to set the component is the LS pressure margin of 20 bar.

As already mentioned, the LS is not completely concentrated in the LS controller, but it must be implemented also in the DCV (as visible in Figure 4.31). In a real hydraulic system, the LS connections in the DCV are completely based on hydraulic relations (see Figure 4.24 for the simplified scheme of the DCV and its mechanical section view), and these rely on some extremely complex set of orifices, internal leakages, and so on. However, these sets of internal micro-hydraulic components cannot be modeled, thus, the completely hydraulic LS system inside a spool of the DCV is once again composed of hydraulic and physical signals with some adaptation from the general scheme. In particular, as visible in Figure 4.31, two variable orifices are added to the LS system to select the pressure signals, and, instead of relying on hydraulic relations inside the main spool, they are opened or closed by the joystick signals. It is worth noticing that these pressure signals are used not only by the LS system but also by the pressure compensators.

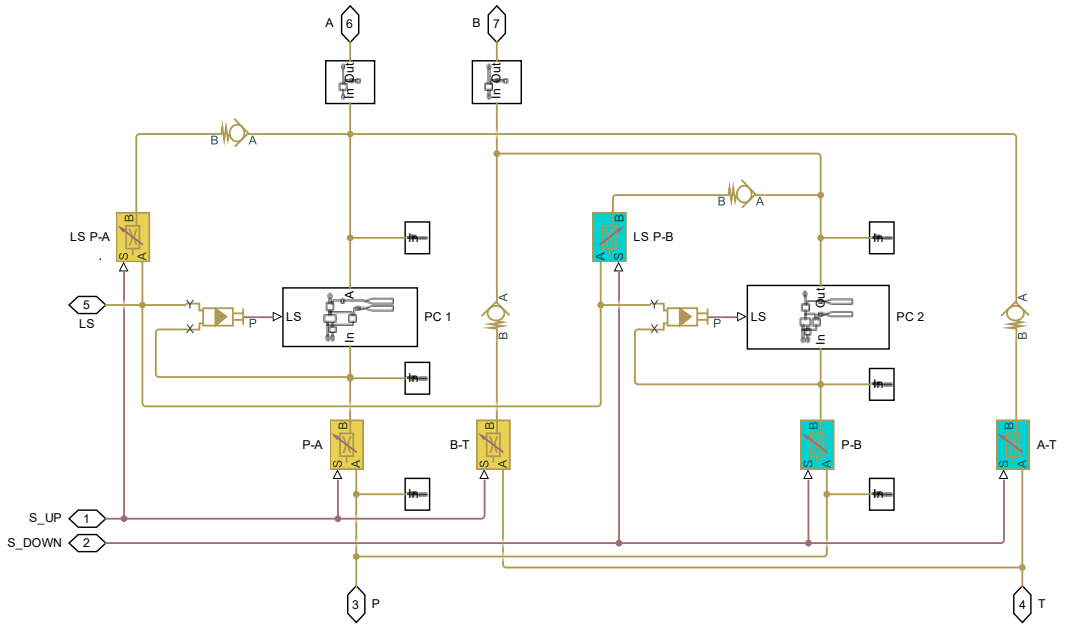

Figure 4.31 Detail of the LS connection inside the DCV.

4.5.5 Pressure Compensator

Pressure compensators are essential to allow the flow distribution to multiple actuators proportionally to their requested velocity, without being influenced by the load.

As previously explained (Hydraulics Systems and Actuators), without these valves, the flow tends to follow the channel with the least amount of resistance. For this reason, as the name suggests, the pressure compensator of this least resistant channel creates additional resistance by adding a restriction, limiting the natural tendency of the flow to run toward this function.

Let's assume a scheme with two different utilities U_1 and U_2, where $p_1 > p_2$. The flow for U_1 is based on Eq. 8, where Δp is replaced by s:

$$Q_1 = C_\mathrm{d}\, A_{\mathrm{eq},\,01} \sqrt{\frac{2s}{\rho}} \qquad \text{Eq. 14}$$

However, for the second utility U_2, the pressure across the valve cannot be s, indeed:

$$Q_2 = C_\mathrm{d}\, A_{\mathrm{eq},\,02} \sqrt{\frac{2s + (\mathrm{p}_1 - \mathrm{p}_2)}{\rho}} \qquad \text{Eq. 15}$$

From this latter equation, it is clear how the load dependency occurs also from the mathematical point of view. Indeed, Q_2 is higher than the theoretical flow rate without interaction.

The scheme that implements the Load Sensing Pressure Compensation (LSPC) can be divided into two different categories: pre-compensated systems (known also as upstream compensators) (Figure 4.32a) and post-compensated systems (known also as downstream compensators) (Figure 4.32b). In the case of the M15e, the upper carriage is moved by a pre-compensated hydraulic motor, while the boom and stick hydraulic circuits are post-compensated.

As previously seen, the post-compensators for the Linde VW14 DCV are mechanically included in the main spools, and they are selected directly by the supplier, thus, there is no data about their characteristics.

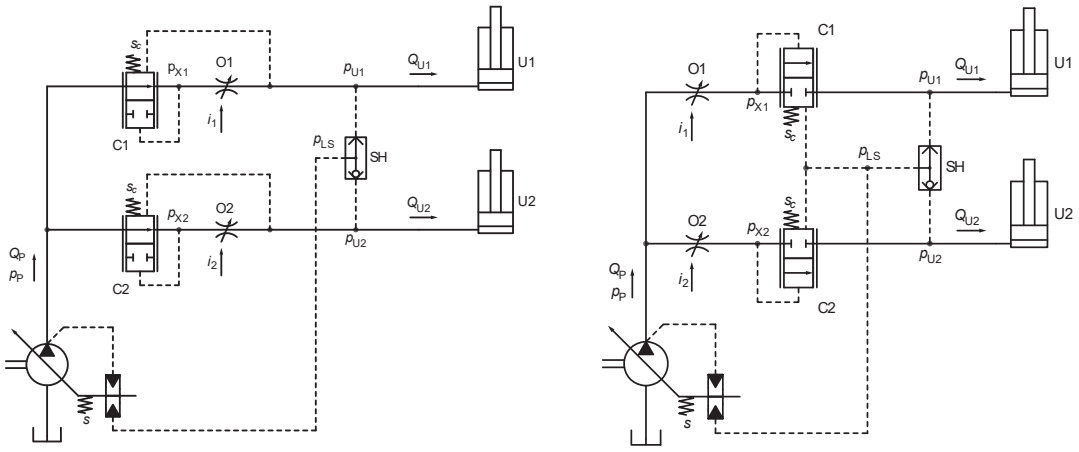

Figure 4.32 Simplified schemes of LSPC: pre-compensated system (a); post-compensated system (b). [60]

As visible in Figure 4.32b, the post-compensator can be seen as a normally closed 2/2 infinite positioning valve. This valve is held in place by a spring, and its preload force is set to equalize the pressure s_c. The upstream pressure P_x is used to pilot the opening of the valve, while its closing is controlled by the actuator pressure. The equilibrium equation is then:

$$p_x = p_{LS} + s_c \qquad \text{Eq. 16}$$

Considering again p_1 as the highest required pressure, the LS pump must deliver a pressure p_P equal to Eq. 17.

$$p_p = p_1 + s \qquad \text{Eq. 17}$$

Knowing by the literature that the minimum pressure drop caused by the pressure compensator can vary between $0.5 \div 3\ bar$ [60], the pressure compensators are modeled as two sequential valves after the $P \rightarrow A$ and $P \rightarrow B$ orifices of the DCV. As visible from Figure 4.33, similarly to what is done for the LS controller, a "*Hydraulic Double-Acting Valve*" [154] is used to compare the pressure p_x with the pressure p_{LS}, and to transmit hydraulic power to a "*2-Way Directional Valve*" [155], while a lag transfer function is added to include dynamics and avoid numerical errors.

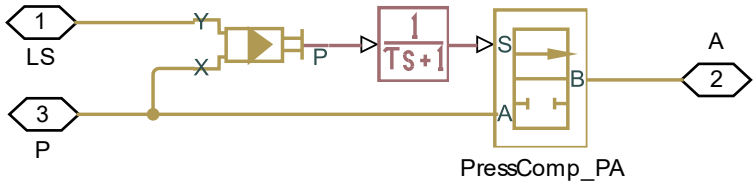

Figure 4.33 Detail of the Simscape model of the post-pressure compensator.

Due to the absence of any other technical data, a different Simscape model is designed to test and tune these two components. In this case, a hydraulic test bench with the same DCV architecture is modeled, but the actuators and loads are completely independent. With this supplementary model, it is possible to sweep different combinations of loads and velocities, with synchronous and asynchronous movements, thus it is easier to validate the behavior of the pressure compensators.

The plots in Figure 4.34 show one example of the synchronous movement of the two actuators. Firstly, it is important to notice that the pump pressure is the same (slightly over 60 bar). Then, because the maximum load is on the first actuator (Figure 4.34a), its compensator remains completely open causing a minimal pressure drop. On the contrary, the compensator of

the second actuator (Figure 4.34b) applies a bigger restriction, causing a pressure drop of about 18 bar.

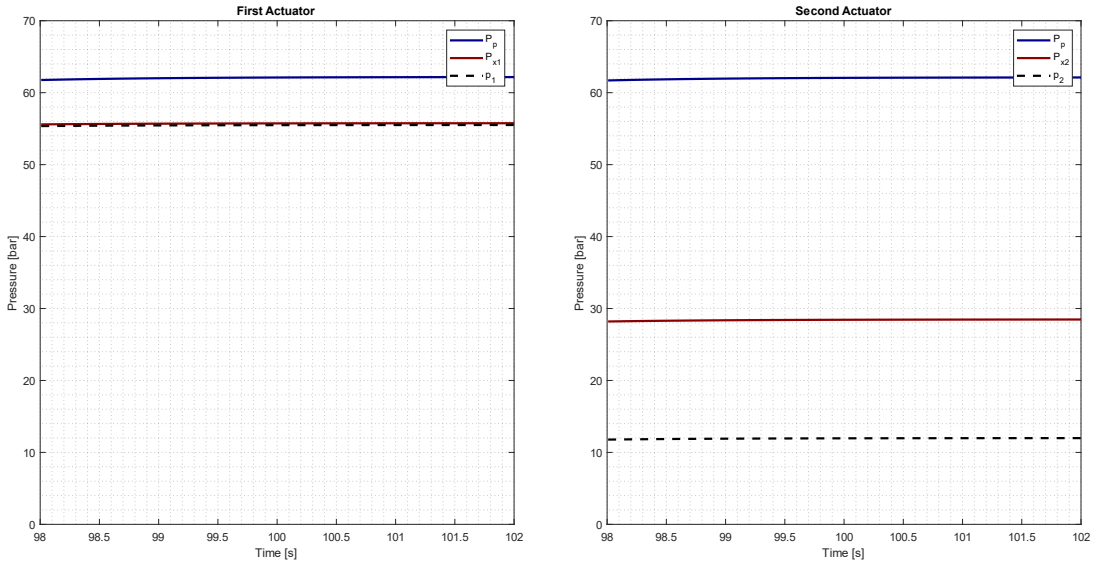

(a) (b)

Figure 4.34 Testing of the post compensators in a synchronous movement: first actuator (a); second actuator (b).

4.5.6 Upper Carriage

While the undercarriage of the machinery is barely used, the upper carriage is essential. Indeed, removing the swing degree of freedom would greatly handicap the use of the machinery.

As for most of the hydraulics, also the swing motor is supplied by Linde. It is a motor of the HMF series, with a fixed displacement of 75 cm^3 [156]. The main characteristics are visible in the Table 4.6:

HMF-75-02-P		
Max. displacement	$[cm^3/rev]$	75
Nominal pressure	$[bar]$	280
Max. peak pressure	$[bar]$	300

Table 4.6 Available data of the Linde HMF-75-02 hydraulic motor. [156]

As anticipated, also the swing motor is controlled by the LS system, but it is a pre-compensated LSPC and not post-compensated. This choice allows the swing motor to have the top priority among all the functions. Indeed, in case of flow saturation, all the functions are slowed down, while the upper

carriage motor can be still used at its full capacity. In particular, the priority function is made possible by the combination of the valve "2", and the shuttle valve "7" visible in Figure 4.35. The former is the actual pre-compensator, and it sets a maximum constant pressure margin of $s_c = 15\ bar$ for this function. As visible from Eq. 18, if a pre-compensator is installed, the flow depends only on the movement of the spool and is independent of the load.

$$Q_{\text{turret}} = C_{\text{d}}\, A_{\text{eq, 0}_{\text{turret}}} \sqrt{\frac{2s_{\text{c}}}{\rho}} \qquad \text{Eq. 18}$$

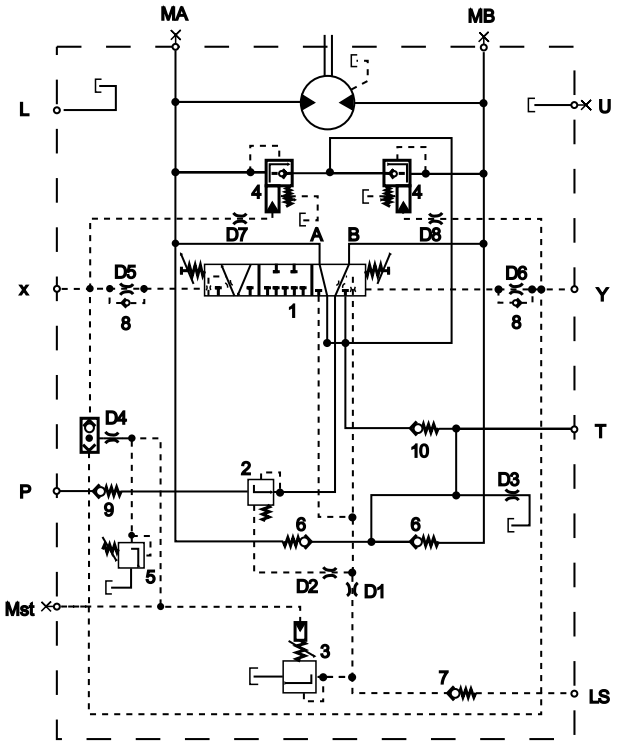

Figure 4.35 Simplified hydraulic scheme of the HMF hydraulic motor.

Thanks to the combination of the pilot-actuated pressure relief valve "3", pressure relief valve "4" and pressure relief valve "5", another key feature is enabled: the swing torque control. This feature is based on the curve visible in Figure 4.36, and it transforms the swing joystick from a velocity controller to an acceleration controller:

- Low acceleration – the joystick controls the spool, and the valve "3" is slightly opened by the LS signal, meaning that the LS margin is

lower than $s_c = 15\ bar$, resulting in a more accurate but slower movement.

- High acceleration – the joystick controls the spool, the valve "3" is completely closed by the joystick signal, the LS margin is at $s_c = 15\ bar$, thus the movement is faster but less accurate.
- High deceleration – the joystick controls the spool, the valve "3" is completely closed by the joystick signal, the LS margin is at $s_c = 15\ bar$, furthermore, the opening pressure of the relief valve "4" is increased to generate a higher counter pressure to slow/stop the swing motor.

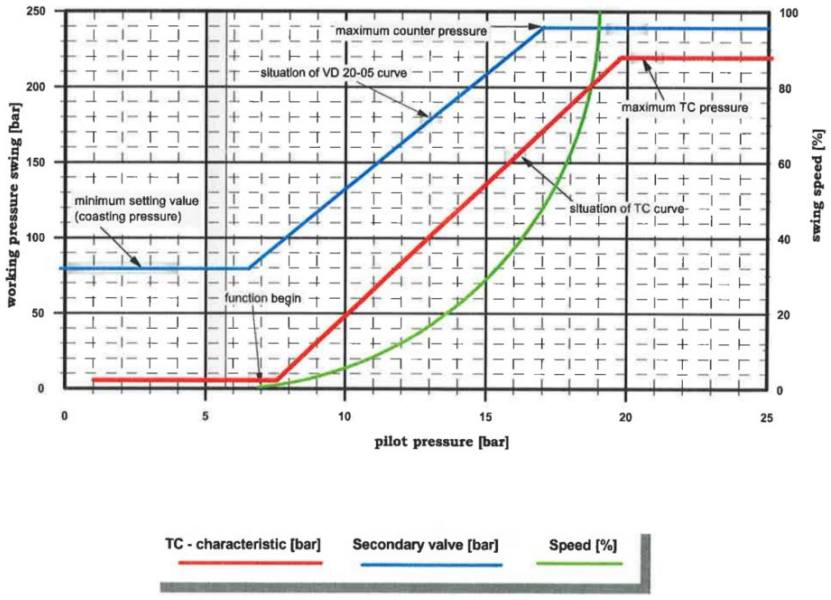

Figure 4.36 Torque control characteristic curve for the Linde HMF-02.

As visible from the overview of the upper carriage Simscape model in Figure 4.37, the component for the pre-compensator already exists in Simscape [157], thus it is easily modeled, while the relief valves are modeled to include the torque control effect. The pressures coming from the joystick's signals are indeed transformed into physical and Simulink signals to apply the characteristics curve of Figure 4.36, and then they are transformed once again into pressure signals to control the equivalent pressure relief valve (Figure 4.38).

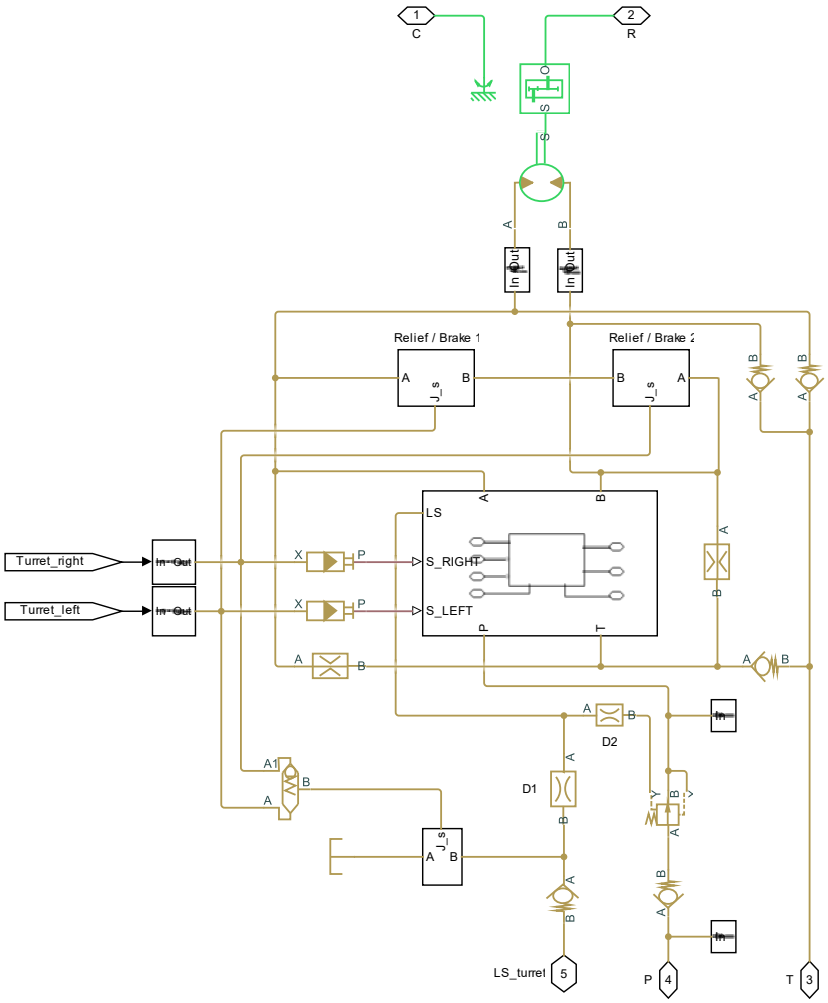

Figure 4.37 Simscape model of the upper carriage.

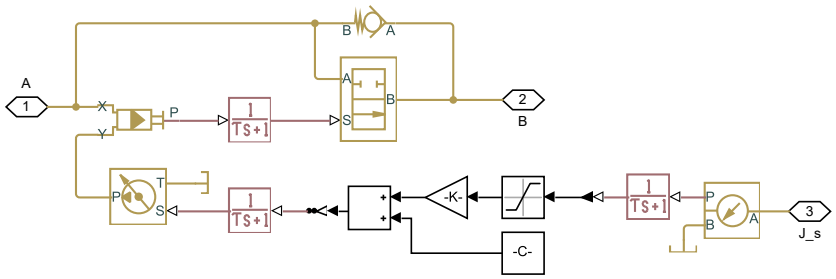

Figure 4.38 Simscape model of the relief valve of the upper carriage.

4.5.7 Load-Holding Valve and Joysticks

The load load-holding valve is another important part of the hydraulic system of machinery like the M15e. Indeed, being positioned on both the first and second arm, this valve guarantees that the load remains in position even when the machinery is turned off.

The valve installed on M15e is the Rexroth VBC33 [158], whose internal scheme and characteristic curves are visible in Figure 4.39.

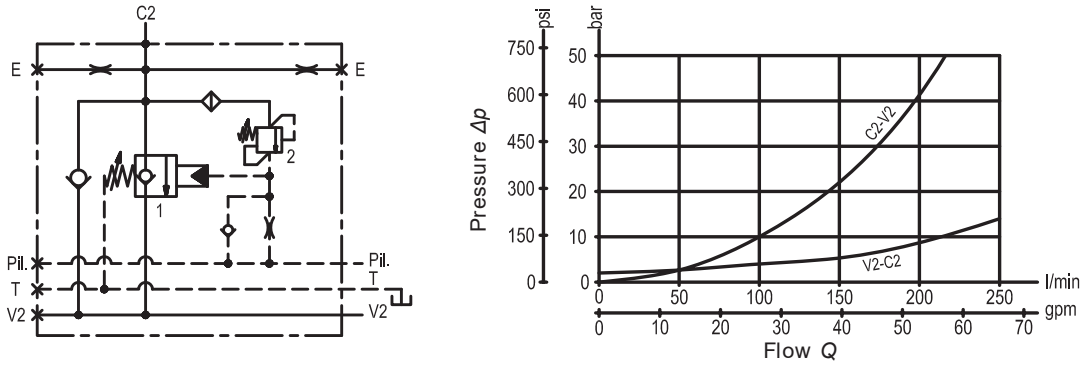

(a) (b)

Figure 4.39 Load holding valve: simplified scheme (a); characteristic curves (b). [158]

The main difference between the real valve and the Simscape model (Figure 4.40) is the absence of valve "2", indeed the whole Simscape subsystem is modeled to follow the curves of Figure 4.39b. As done for other components (e.g., spools of the DCV), a supplementary MATLAB script and Simscape model are designed to calculate the relation between spool movement and the area of the valve, replicating the characteristic curves.

However, their behavior is controlled not only by the single modeled valve but also by its interaction with the hydraulic joysticks.

These are other hydraulic components that need to be modeled[7]. However, the hydraulic joysticks are mostly modeled as physical signals, and their dynamics is almost completely simulated by lag transfer functions, neglecting all their hydraulic piloting circuit (Figure 4.41).

- [7] Officine Minelli s.r.l. has decided to replace the hydraulic joysticks with electric ones for its entire portfolio of machinery, thus these components will be modeled differently only in future releases of the model.

The control joystick hydraulic circuit of the M15e has a maximum pressure of 35 bar, thus the pressure of the joysticks varies in the range of $0 \div 35\ bar$. However, based on the related DCV and load holding valve, a maximum pressure and minimum preload exist. Indeed, the opening pressures of each combination of joysticks and holding valves are set based on Officine Minelli's indications.

For instance, the load-holding valve of the boom is set to open over 5 bar, while the DCV does not move under 6 bar. Consequently, there is a small fraction of time/pressure where the arm starts its descending even if the DCV is still closed[8].

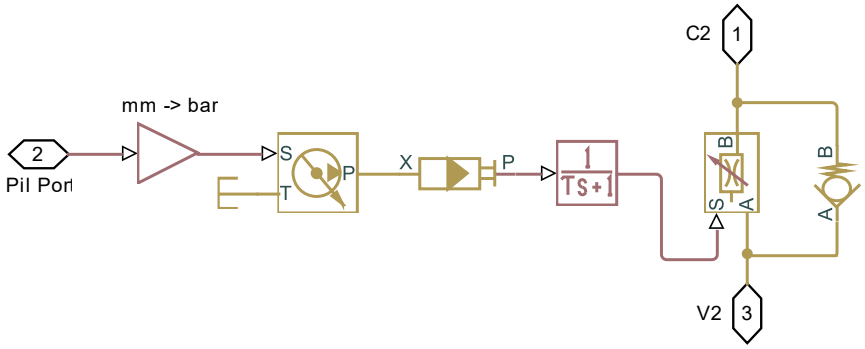

Figure 4.40 Simscape model of the load holding valve.

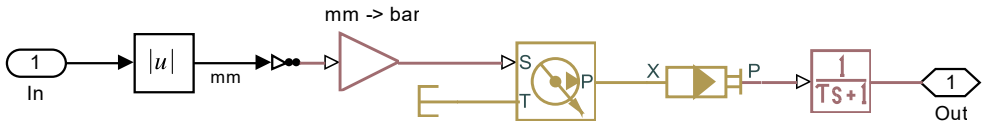

Figure 4.41 Simscape model of the hydraulic joystick.

- [8] Some of the main results of this analysis have been published as conference proceedings. Beltrami, D., Ferrari, M., Iora, P.G., Uberti, S. (2024). Application of Physics-Based Modeling Techniques as a Tool to Help the Development of More Electrified Off-Highway Machinery. In: Carfagni, M., Furferi, R., Di Stefano, P., Governi, L., Gherardini, F. (eds) Design Tools and Methods in Industrial Engineering III. ADM 2023. Lecture Notes in Mechanical Engineering. Springer, Cham. https://doi.org/10.1007/978-3-031-52075-4_56 [163]

5 Testing

Even if model-based design has been gaining acceptance as a cornerstone of engineering, testing remains fundamental.

As seen in the previous chapters (Modeling the Machinery), the model of the M15e, and in general any model-based design, relies on certain assumptions about the system's behavior. Thus, these assumptions need to be verified by comparing model predictions with actual test results. Furthermore, in most model-based designs some various modeled components or subsystems need to work together. This is especially true for multi-domain systems, like electric hydraulic material handlers such as the M15e. Thus, testing helps verify that the integration of these components is successful and that the overall system functions as intended.

In academia and companies with high heritage and expertise in research and development, there are multiple and somewhat subsequential approaches to verify the behavior of a model in comparison to its real-world counterparts, like:

- Model-In-the-Loop (MIL) testing: it relies on the comparison of different simulations and mathematical models to ensure that the integration of different domains is accurate.
- Software-In-the-Loop (SIL) testing: it integrates the model-based design with the actual control software that runs the real-world system. It is important to verify that the control strategies can be executed effectively.
- Hardware-In-the-Loop (HIL) testing: it is based on the connection between the model-base design and the real hardware components (sensors, actuators, controllers, etc.). It is useful to check that the design works seamlessly with physical components and not only in a simulation.
- Co-simulation: it controls the accuracy of models by comparing different simulation tools and/or languages, more or less as it

happens with MIL. Indeed, even if the languages can vary between different software, the output should be at least similar.

- Real-world testing: it relies on prototypes and field tests to compare model-based design and real-world systems in a real-world environment.

These multiple testing approaches are useful to ensure that each modeled component and/or subsystem behaves properly. There are instances where models and real-world systems are so similar that it is possible to address the model to be a "digital twin". However, to achieve this level of accuracy, almost every component must be validated separately.

It often happens that the time, resources, expertise, etc., required to assess all the aforementioned steps do not suit the workflow and workforce of SMEs. This is the case also for the testing of the M15e, for which the only used approach is the real-world testing of the entire machinery, for which the overall system acquisition scheme is visible in Figure 5.1.

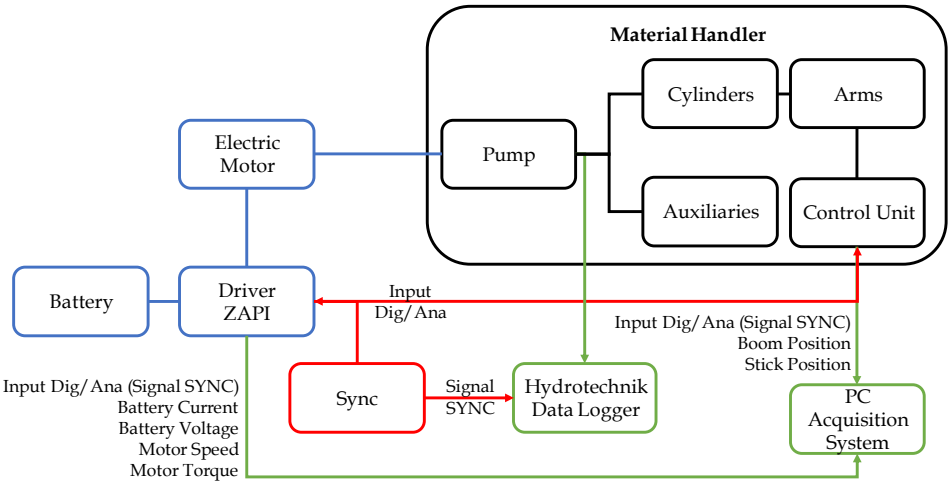

Figure 5.1 Simplified scheme of the acquisition system.

As previously seen, two of the most important variables in a hydraulic system are flow and pressure: starting with the former, one flow sensor (Hydrotechnik QT-400 [159]) is positioned at the outlet of the pump (Figure 5.2). Regarding the latter, two pressure sensors (Hydrotechnik PR 100 [160]) are installed at the outlet port of the main pump and on the LS signal connection from the DCV to the pump. Both flow and pressure

measurements are managed by the Hydrotechnik data logger which allows data exportation.

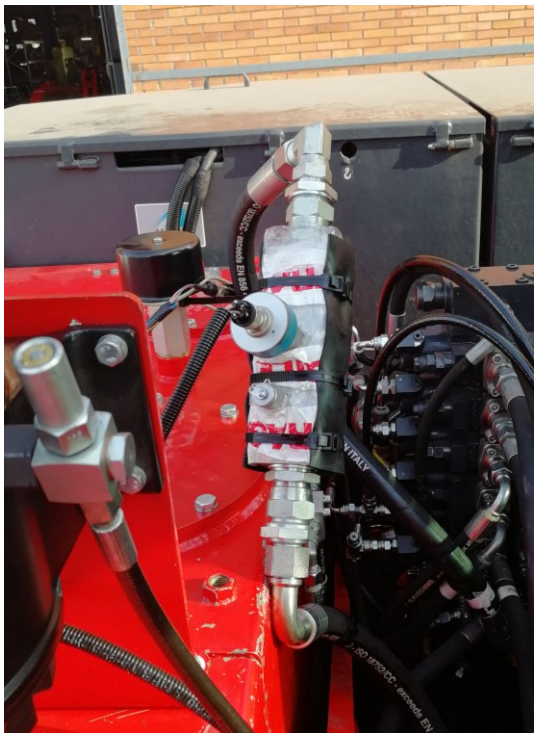

Figure 5.2 Hydrotechnik QT-400 flow sensor installation on the M15e.

Thanks to the presence of a smart actuator as the Induction Motor, which comes with its controller/inverter, the following data are read directly from its driver (ZAPI ZTP AC3 [136]). Indeed, by using its proprietary digital console in the "tester function" and a personal computer, it is possible to read and save:

- Battery voltage;
- Battery current;
- Motor voltage;
- Motor input frequency;
- Motor output frequency;
- Motor slip value;
- Motor torque.

Lastly, the angles of the first and second arms of the machinery are read by connecting the CAN bus of the machinery to a PEAK-System CAN interface for USB [161], which also allows the exportation of the data[9].

Due to the presence of multiple unrelated measurement systems, a sync signal is used to align data in post-processing.

Post-processing and data visualization are done using MATLAB after having exported all the data as CSV files.

To increase the variability of the measurement, the machinery is tested under different known load configurations (mass attached to the orange peel grab at the end of the second arm) and different motor speeds:

- Unloaded machinery;
- Low-loaded machinery: $200\ kg$;
- High-loaded machinery: $1500\ kg$;
- Low motor speed: $1500\ rpm$;
- High motor speed: $2000\ rpm$.

For instance, in Figure 5.3, there are the measurements of pressure and flow during a high-loaded and high motor speed test, with simultaneous movements of arms and upper carriage.

For what concerns the pressure, it is worth noticing how the LS pressure, which is taken after the DCV, is always lower than the pump pressure. In particular, when the flow is almost constant, the pressure difference is about $20\ bar$, which is indeed the LS margin. At the same time, it is important to see how difficult it is for the flow running in the machinery to remain constant.

In Figure 5.4 there are the measured angles:

- Alpha is the angle between the first arm and the ground;
- Beta is the angle between the first and second arm.

- [9] The swing angle of the upper carriage is not included in the measurements. Indeed, the installation of an angular sensor on the swing hydraulic was not possible.

Comparing Figure 5.3 and Figure 5.4 some oscillations are visible for the angle sensors and not for pressure and flow, and vice versa.

The battery current and voltage are visible in Figure 5.5. The first thing to notice is that the sample time is completely different from other measurements, and this is due to the preset "tester function" values of the ZAPI controller. The second important thing to notice is that the battery voltage does not remain constant during usage, but it varies based on the requested current. Nonetheless, while current varies from 100 A to 600 A, the voltage remains close to its nominal value of 120 V.

The same sample time based on the ZAPI preset visible in Figure 5.5 can be seen also in Figure 5.6, where the motor speed and motor torque are reported. Even if the operator inside the cab selects a single speed, it is visible in Figure 5.6 that this speed cannot be held constant. Indeed, the speed selected by the operator is a reference speed, and the controller of the electric motor follows it while supplying the torque requested by the hydraulic pump. In this regard, comparing Figure 5.3, Figure 5.5, and Figure 5.6 it is clear the relationship between the pressure, the current, and the torque, especially focusing on the time frame between $t = 43\ s$ and $t = 48\ s$.

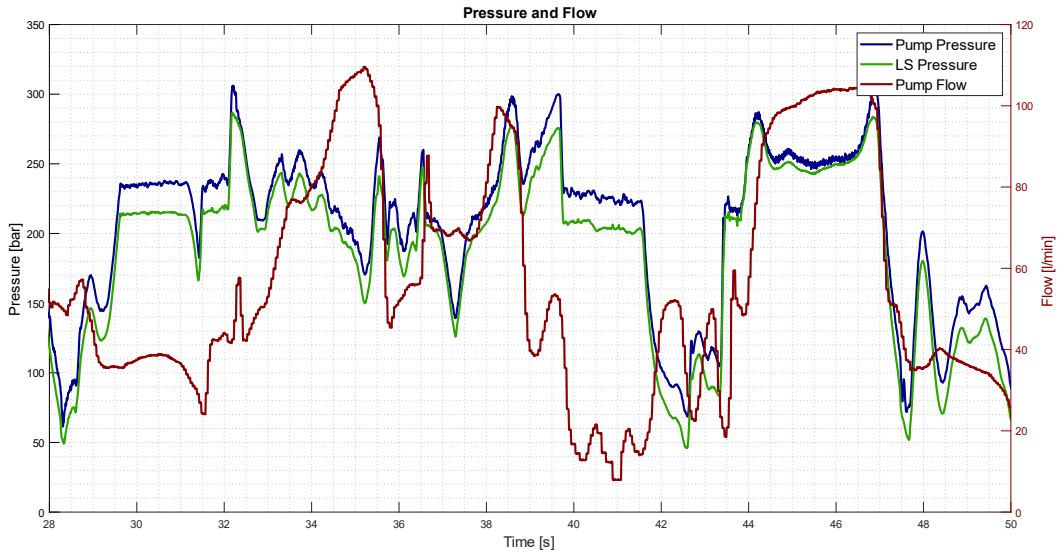

Figure 5.3 Example of experimental data: high load, high speed, synchronous movements. Pump pressure, LS pressure, and pump flow.

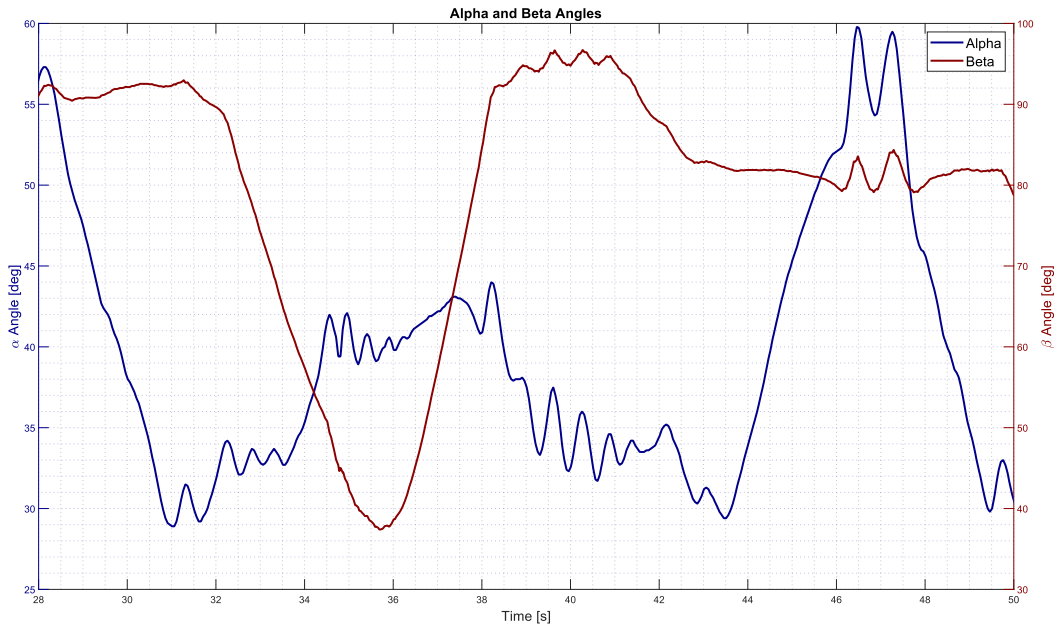

Figure 5.4 Example of experimental data: high load, high speed, synchronous movements. Alpha and beta angle.

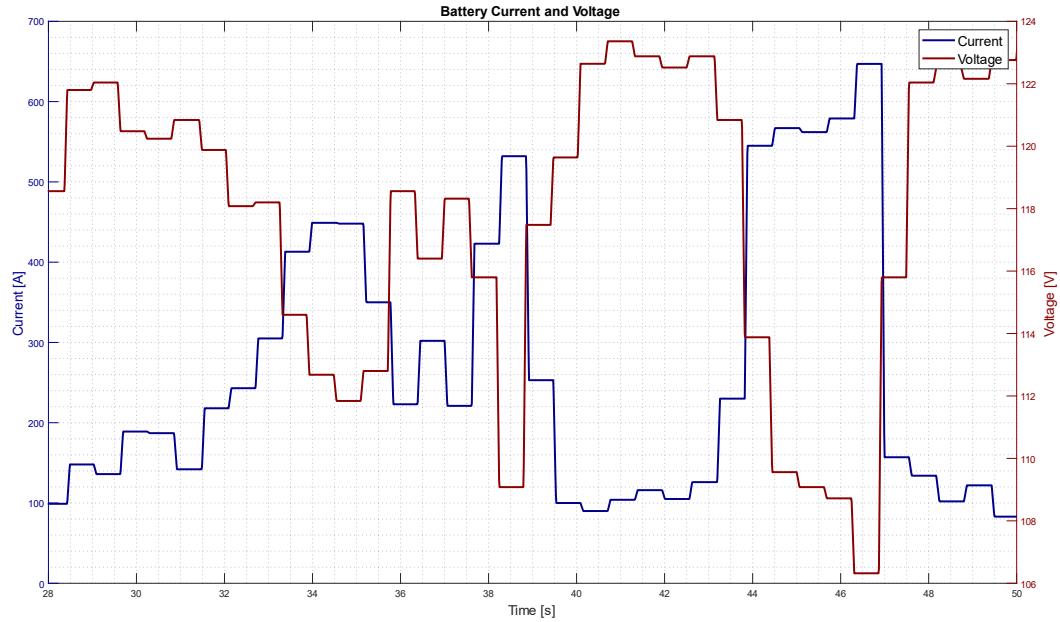

Figure 5.5 Example of experimental data: high load, high speed, synchronous movements. Current and voltage of the battery.

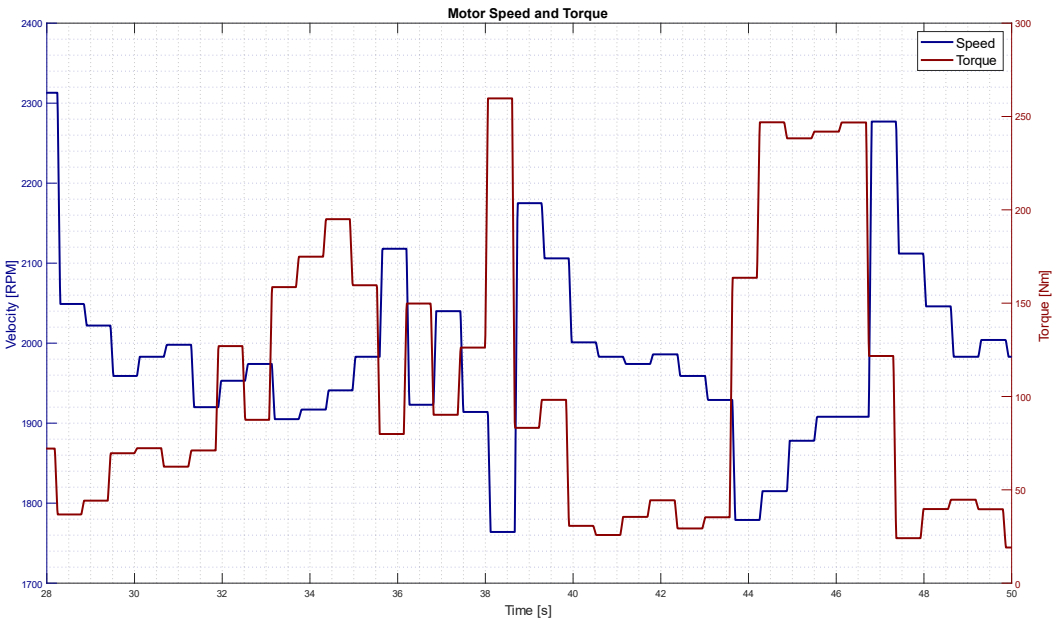

Figure 5.6 Example of experimental data: high load, high speed, synchronous movements. Speed and torque of the electric motor.

6 Results and Discussion

In the following, there is a comparison of the model with the experimental results, and it is divided into subchapters based on the movement. However, before going into details, it is essential to recall the goal of this model.

Because this model is almost completely built using Simscape, which is an industry-oriented software, what's most important to achieve is a general harmony of the trends between experimental results and simulations. Thus, a perfect match between the two is preferred, but not requested. The goal is indeed the transition from a spreadsheets-based steady-design to dynamic or transient-state design, and not the design of a digital twin, for which a different approach should be carried out. If such a model is accurate enough, then using it allows the investigation of new control strategies, working modes, etc., building the framework to truly take advantage of electrification for off-highway machinery: less energy consumption, and/or better productivity, and/or better comfort, and/or new services, etc.

For each movement, there is an evaluation and discussion of the four subsystems of the model:

- Mechanics: are the experimental and simulated angles alike? Does the model carry out the same movements as the real machinery?
- Hydraulics: can the model simulate the same behavior of the pressure and flow? Does the LS function properly?
- Electric motor: is the simplified model of the electric motor enough to properly transform hydraulic power into electric one? Does it behave similarly to the electric motor of the real machinery?
- Energy storage: considering the simple 0^{th} ECM, is it able to simulate how current and voltage vary during usage? Can it compute the energy consumption of the machinery?

Finally, there is a conclusive discussion, highlighting the challenges that are overcome and the ones that need to be addressed.

However, it is worth specifying the following:

- As seen in the previous chapter (Results and Discussion), some of the experimental values derive from the controller-inverter already installed on the machinery, on which the sampling time is fixed by default and cannot be varied. Thus, there are unmeasured/unknown phenomena, while others may be imprecise due to aliasing.
- Differently from the movements of the boom and stick, the value of the mechanical angle is not measured for the upper carriage. This is due to the impossibility of installing an angle sensor on the machinery under testing, thus the simulation and its movement are set up based on visual evaluations.

6.1 Boom

The first movement to investigate is the lowering of the boom, starting with the angle between the boom and the ground, called "alpha" and visible in Figure 6.1. In the same Figure 6.1 the "beta" angle is reported, which is the angle between the boom and the stick.

While the initial position of the simulation is manually set, the final position depends entirely on Simscape computation. The movement is well simulated, even if some oscillations are completely filtered out by the model. The same type of oscillation is visible for the "beta" angle, and they are probably caused by the oscillating mass of the orange peel grab. Looking at the scale of the y-axis is clear that these oscillations are very little, thus they can be neglected from further investigations.

A bigger difference is related to hydraulics and it is visible in Figure 6.2. Indeed, bigger pressure variations are visible in both the simulated and experimental curves. Overall, the simulated pressure curve recalls the real one, but it lacks accuracy. The big oscillation at the beginning of the movement is due to the combination of the load-holding valve, the preload pressure of the joystick, and the make-up valves, which are not modeled. This combination of factors at the start also influences the central part of the movement, making the match between the curves difficult. In the last part,

the experimental curve shows a counterpressure to control the lowering of the boom, but this is not reported in the model. The curves related to the flow are more precise, even if there is both a lag at the beginning and an early reduction of the flow towards the end of the movement.

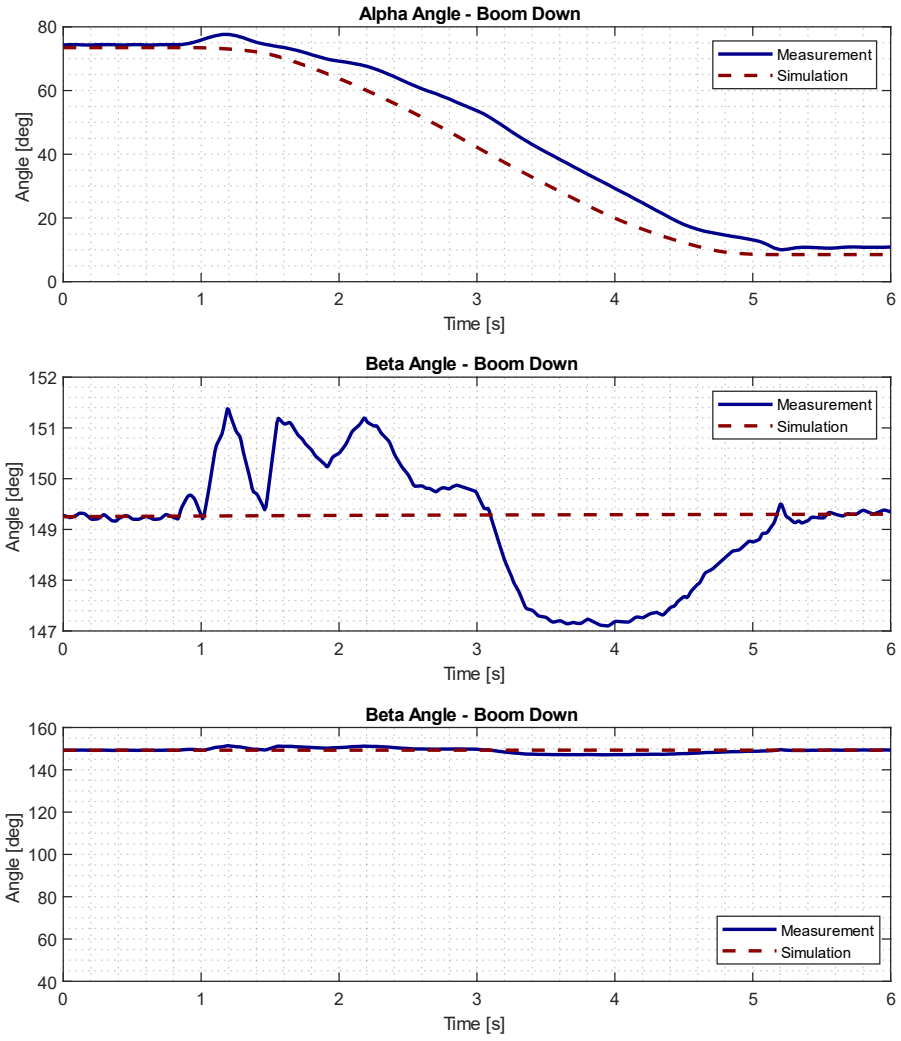

Figure 6.1 Boom down comparison. Mechanics: alpha and beta angles.

The biggest differences are related to the electric motor, as visible in Figure 6.3, even if it is worth remembering that the electric motor is greatly simplified in the model, and it relies on a PI controller to mimic its dynamics. However, looking at the torque, it is visible that for almost a second the simulated torque almost doubles the experimental one. Therefore, following the motor dynamics, the motor velocity varies from the experimental one, even if the velocity difference is a lot smaller than the torque difference.

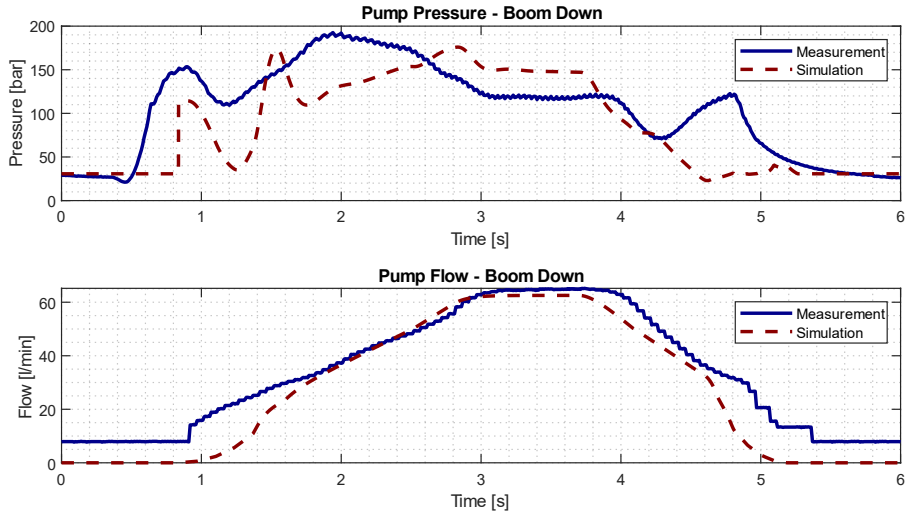

Figure 6.2 Boom down comparison. Hydraulics: pump pressure and pump flow.

Despite the significant difference seen for the hydraulics and the electric motor, the simulation of current and voltage supplied by the energy storage system is closer than expected to the experimental values (Figure 6.4), and this is notably true for the current. Indeed, the current is the last variable computed by the model, so many oscillations are naturally filtered out by the system's dynamics. Similarly, the trend of the voltage drop is well represented, and the discrepancy visible in Figure 6.4 is extremely small in comparison with the value of the nominal voltage.

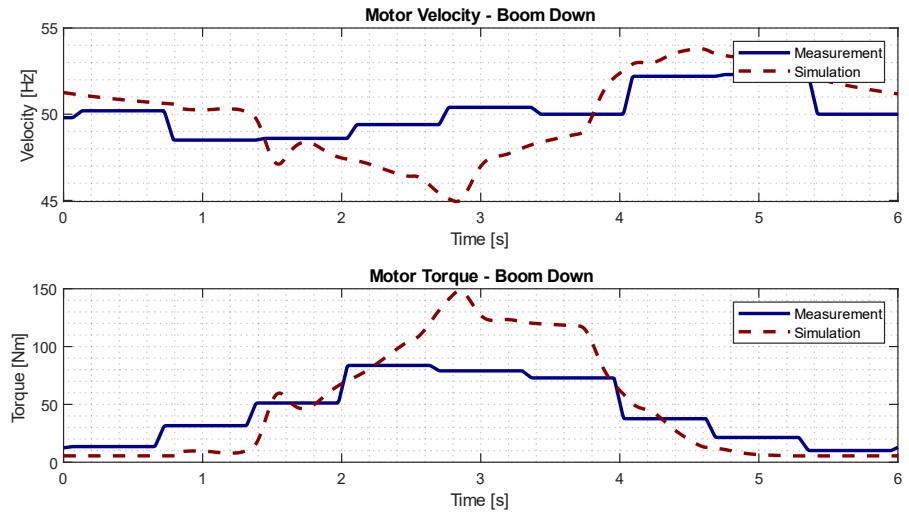

Figure 6.3 Boom down comparison. Electric motor: velocity and torque.

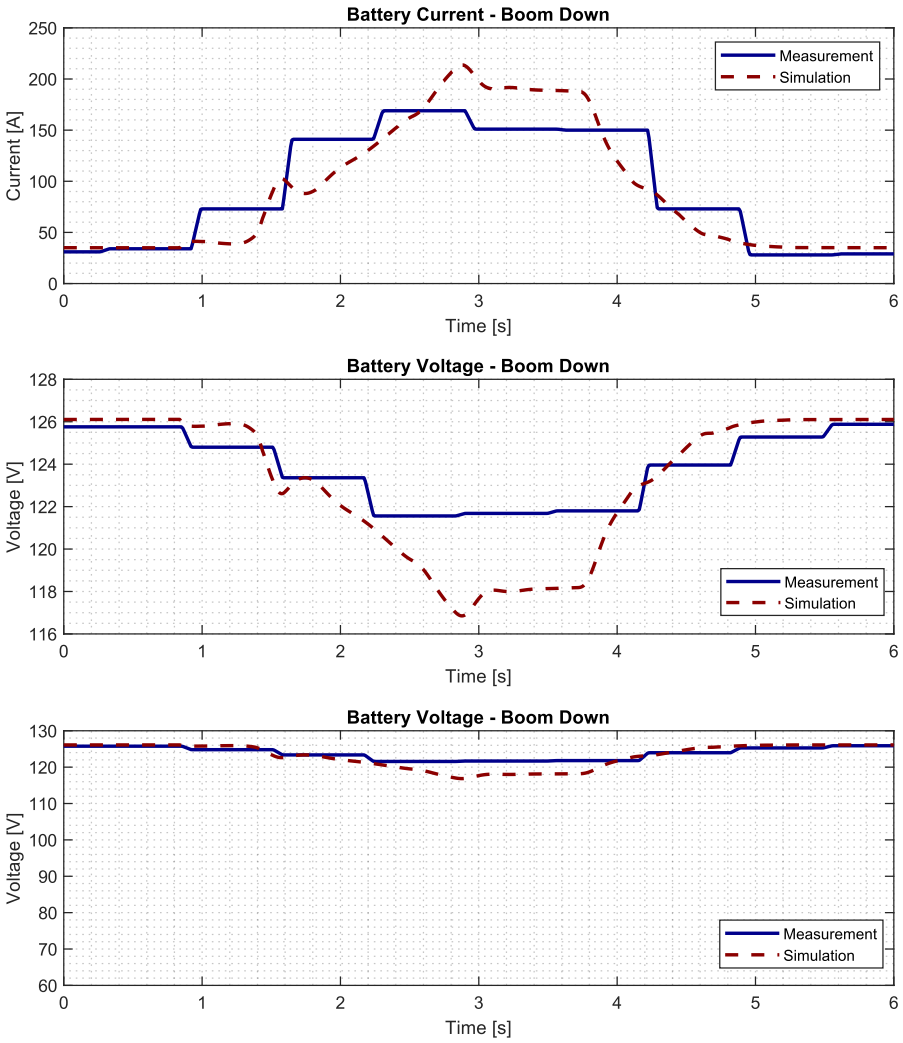

Figure 6.4 Boom down comparison. Energy storage: current and voltage.

The second movement of the boom to care about is its lifting.

Starting again with the two main angles shown in Figure 6.5, it is clearly visible how well reproduced is this movement: looking at the alpha angle, the two curves are very close one each other from start to finish, with the only exception of the final oscillations of the real curve. The reason behind this oscillation is once again the mass of the orange peel grab, which is much more evident for the beta angle and can be neglected from the model.

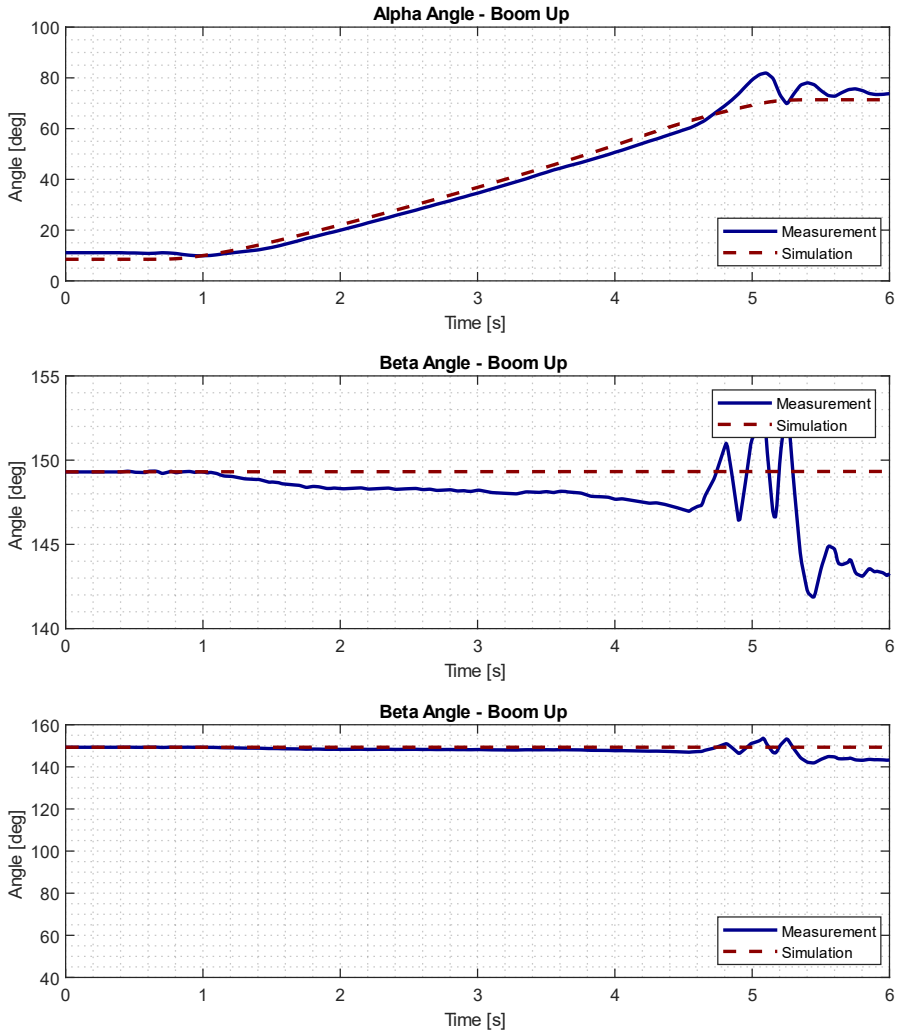

Figure 6.5 Boom up comparison. Mechanics: alpha and beta angles.

A good representation of the angles can be seen also for pressure and flow, as visible in Figure 6.6. Lifting the boom is the most power/energy-intense movement of the machinery, and the model can well reproduce it. As already seen, the first and last parts of the movement are the most complex ones to match, because there are many hydraulic relations between valves, but the final result is more than satisfactory.

It is quite straightforward that having a good match between flow and pressure makes it easier to obtain a decent replica of motor speed and torque (Figure 6.7). Even if there is a 0.5 *s* lag for the motor speed at the beginning of the movement, the simulated velocity catches up with the experimental curve in a decent time range, following its general trend. Also, the curves of the torque are quite similar, with only the ending that differs.

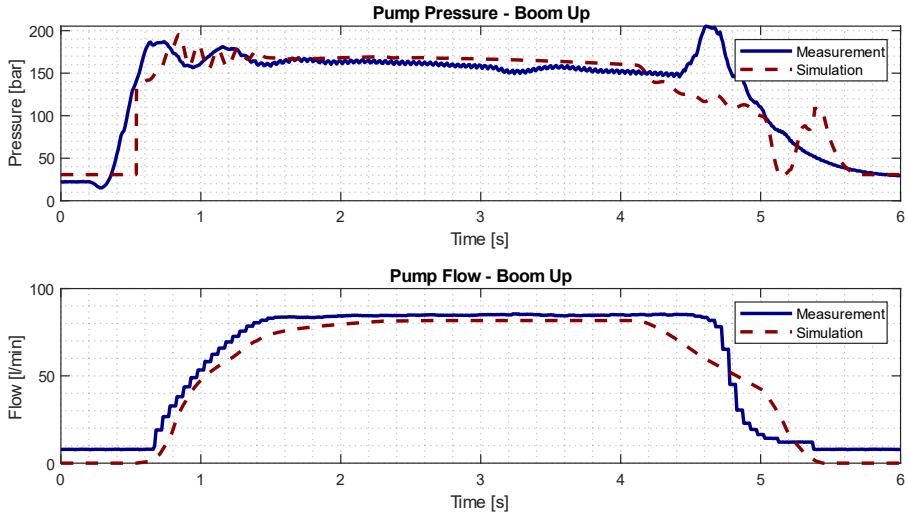

Figure 6.6 Boom up comparison. Hydraulics: pump pressure and pump flow.

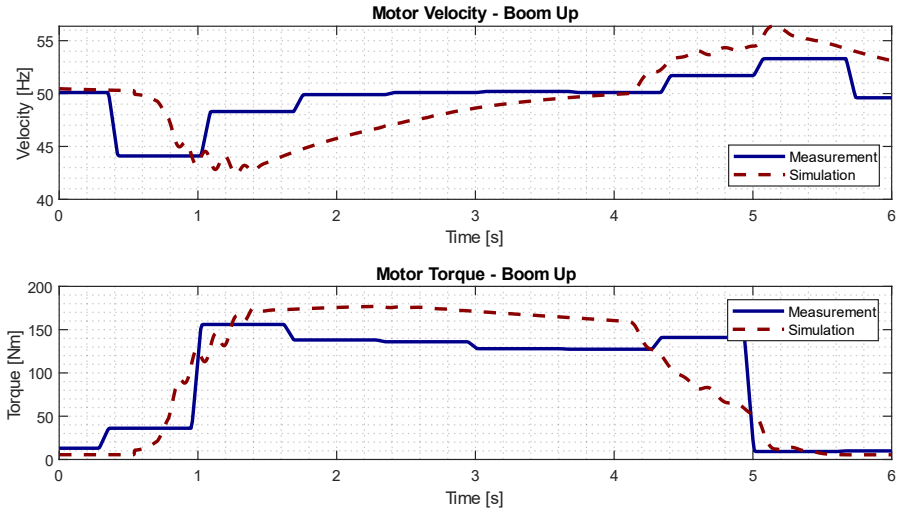

Figure 6.7 Boom up comparison. Electric motor: velocity and torque.

Once again, looking at the results of the energy storage subsystem in Figure 6.8, it is visible that the general trend of the current is quite close to the experimental values. The voltage has a drop bigger than expected, but this can be related to the simplifications inherently included in the 0^{th}-order equivalent circuit model.

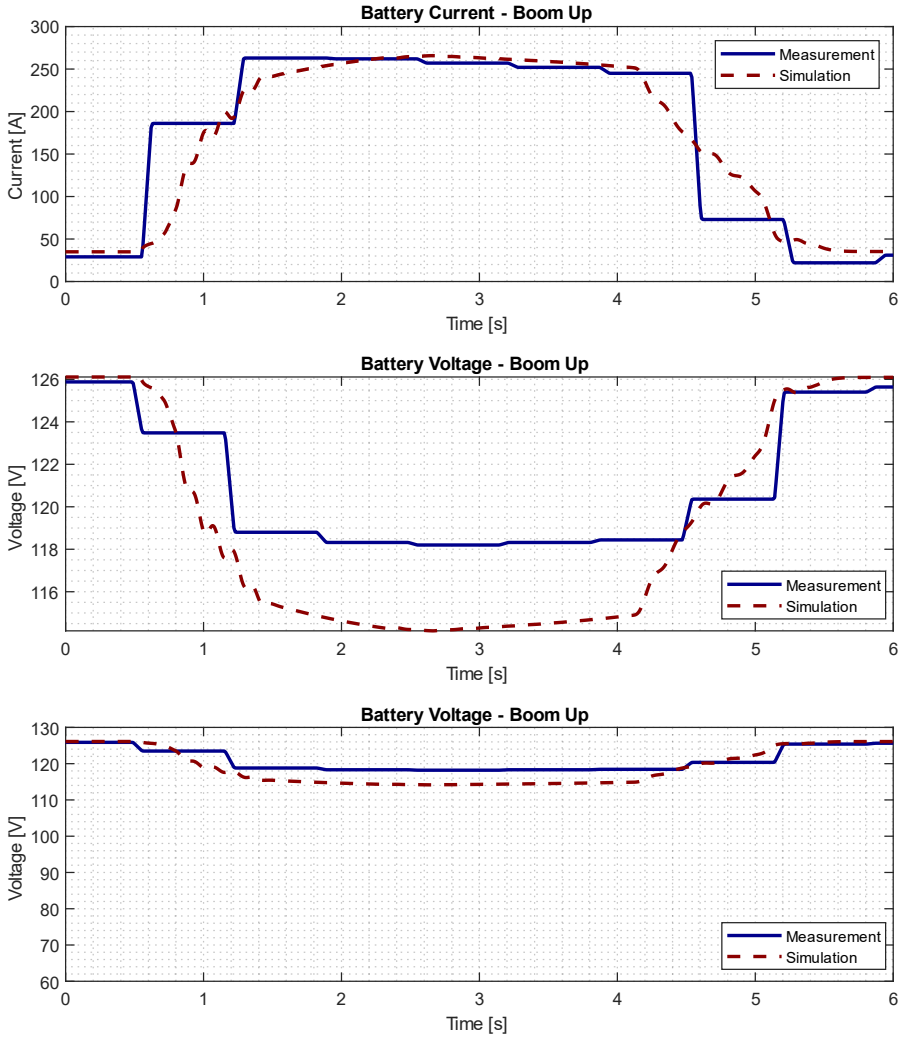

Figure 6.8 Boom down comparison. Energy storage: current and voltage.

6.2 Stick

While for the boom the main angle to check is alpha, beta is the one to consider when talking about the second arm. In this regard, the variation of the two angles while lowering the stick is visible in Figure 6.9. First, alpha seems greatly off target, but this is due only to the scale of the y-axis, indeed there is a constant difference of less than 3° that can be easily neglected. More interesting is beta, because the two curves in the plot cross each other, meaning that the velocity of the two movements are slightly different, with the simulation curve resulting in the slower one. The most probable explanation for this discrepancy is the combination of stiffness and friction of the cylinder and joint and/or the presence of excessive hydraulic resistance.

Once again, the presence of the load-holding valve and its functioning principles while lowering the arm complicates the physical interaction of the hydraulics.

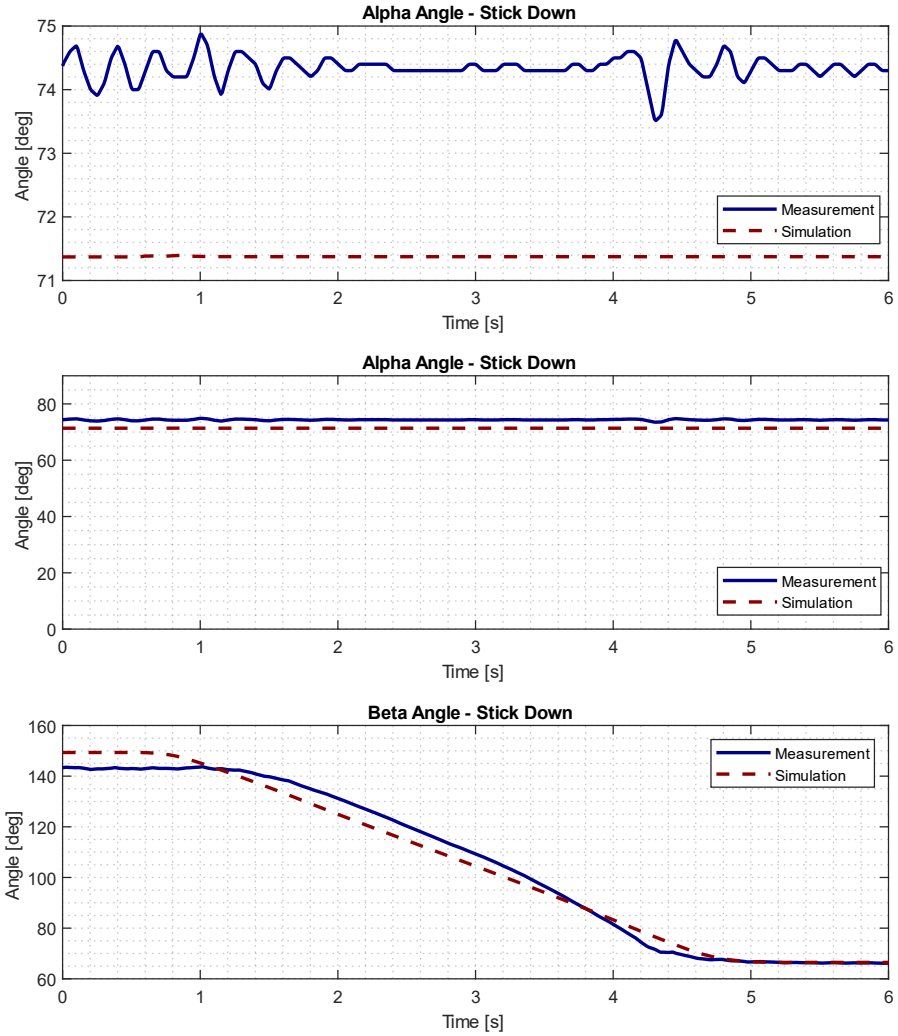

Figure 6.9 Stick down comparison. Mechanics: alpha and beta angles.

The second hypothesis about the excessive hydraulic resistance is confirmed by the curves related to the hydraulic subsystem in Figure 6.10. Indeed, while the simulated flow matches almost perfectly the experimental one in the central part of the movement, the corresponding pump pressure is constantly higher than supposed to be. However, it is interesting to notice how similar are the two pressure peaks in the initial part of the movement, meaning that the model and the real machinery are not completely different. In this regard, it is visible that the simulated pressure has a sharp increase before the measured one. Once again, the discrepancy is due to the absence

of the model of the make-up valves, which, on the contrary, are exploited by the machinery. Indeed, the measurements show a pressure decrease which comes ahead of the sharp simulated spike.

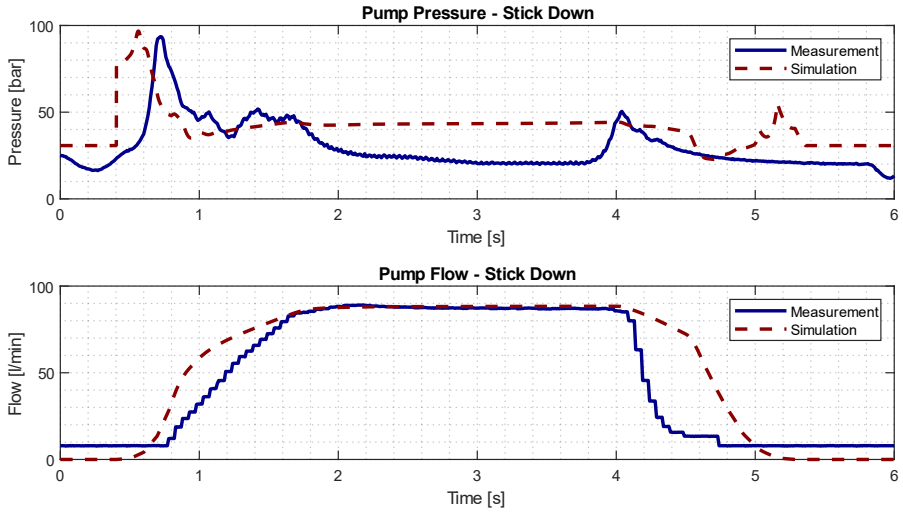

Figure 6.10 Stick down comparison. Hydraulics: pump pressure and pump flow.

Again, the simplified model of the electric motor is not able to accurately reproduce the dynamics of the real component, resulting in a slightly different velocity profile, as visible in Figure 6.11. Nonetheless, looking at the y-axis, it is easy to understand that this difference can be considered marginal. Talking about the torque, it follows the tendency of the pressure, thus it is always higher than the experimental one. Fortunately, the lowering of the stick is a low-demanding movement, so this difference has less influence on the overall energy consumption.

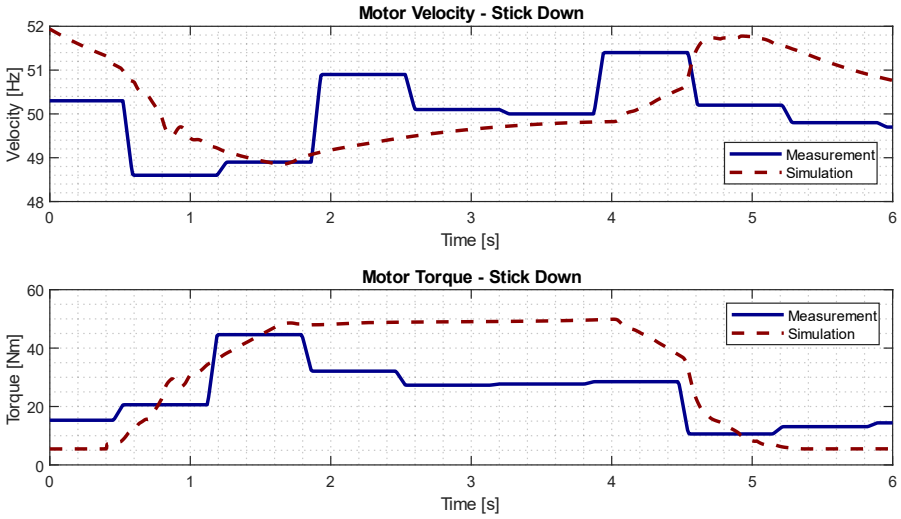

Figure 6.11 Stick down comparison. Electric motor: velocity and torque.

If the pressure and torque are higher than they should be, the same goes for the current, as reported in Figure 6.12. Once again, the simulated voltage drop is higher than the simulated one, remarking the need for a more precise model for the energy storage system.

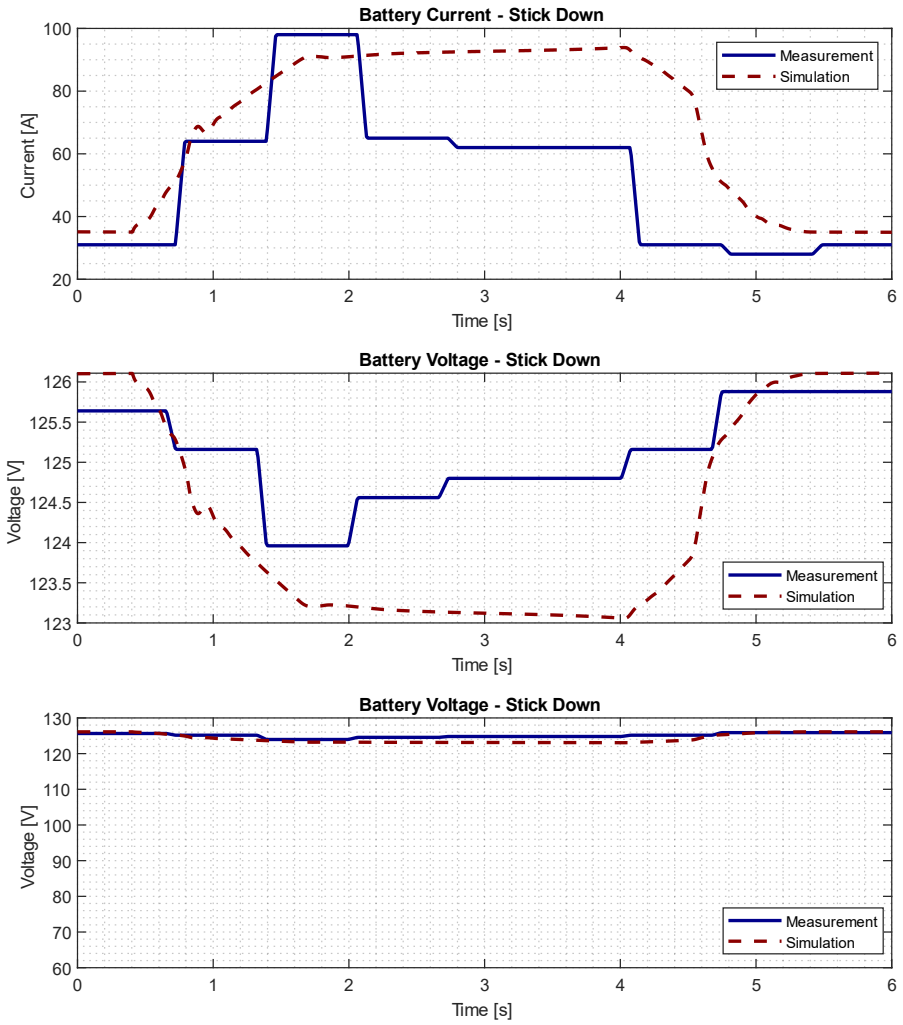

Figure 6.12 Stick down comparison. Energy storage: current and voltage.

The hypothesis that there could be excessive hydraulic resistance in the lowering line of the stick is confirmed by the stick lifting. Indeed, looking at the variation of beta in Figure 6.13, the simulated curve results faster than the real one, excluding the first hypothesis about friction and stiffness.

In Figure 6.14 there are the curves related to the pump pressure and flow, and the results are extremely good. The pressure curves, besides some minor discrepancies at the beginning and the end of the movement, are always close one each other, and it is extremely interesting how both run close to the pressure saturation. Regarding the flow, as for the pressure, there are some differences around $t = 1\ s$ and after $t = 4.5\ s$, but the overall accuracy is decent.

This time, the velocity curves of the electric motor are sufficiently close too (Figure 6.15). Especially at the beginning, there is always a noticeable lag in catching up with the simulated velocity profile, but here the trend is better than for other movements. A possible explanation is that the coefficients of the PI controller mimicking the motor dynamics are more precise at higher torque. In this regard, the simulated torque is always close to the real one, with the only exception of an impulsive peak after $t = 4\ s$, which corresponds to moment where the pump pressure gets close to the relief valve maximum pressure value.

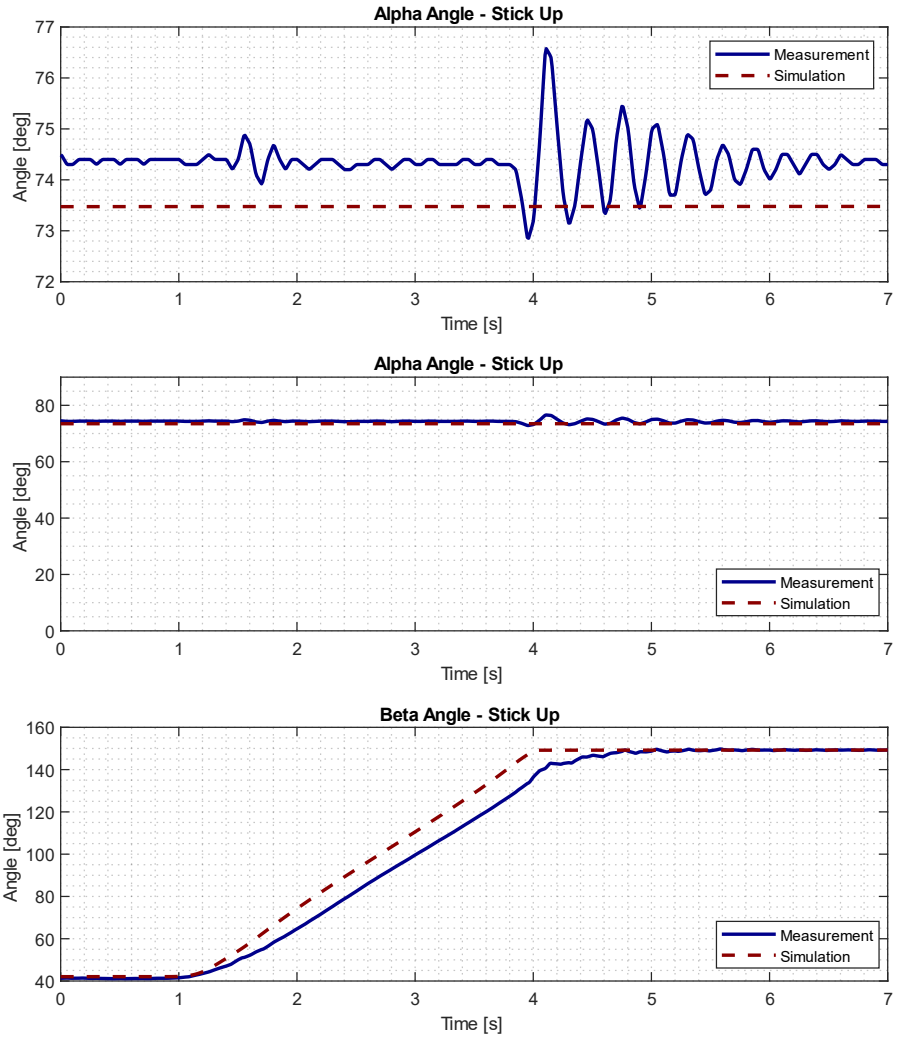

Figure 6.13 Stick up comparison. Mechanics: alpha and beta angles.

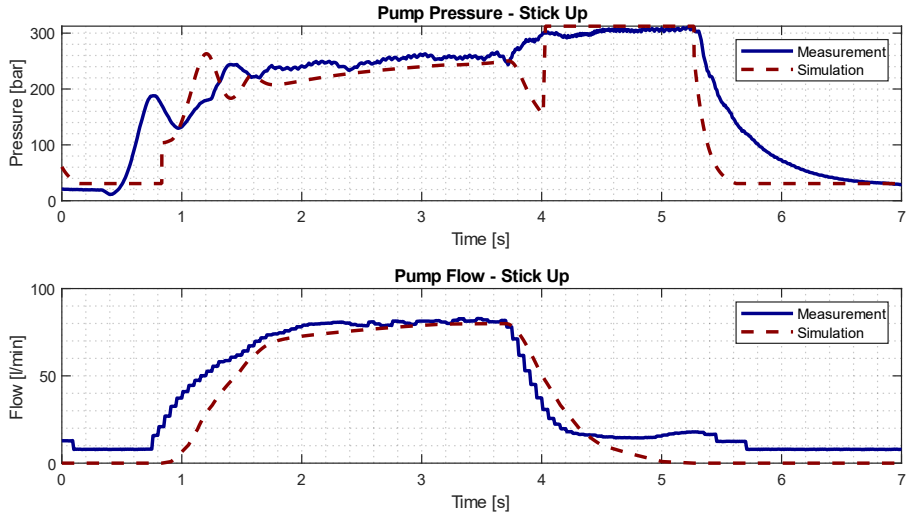

Figure 6.14 Stick up comparison. Hydraulics: pump pressure and pump flow.

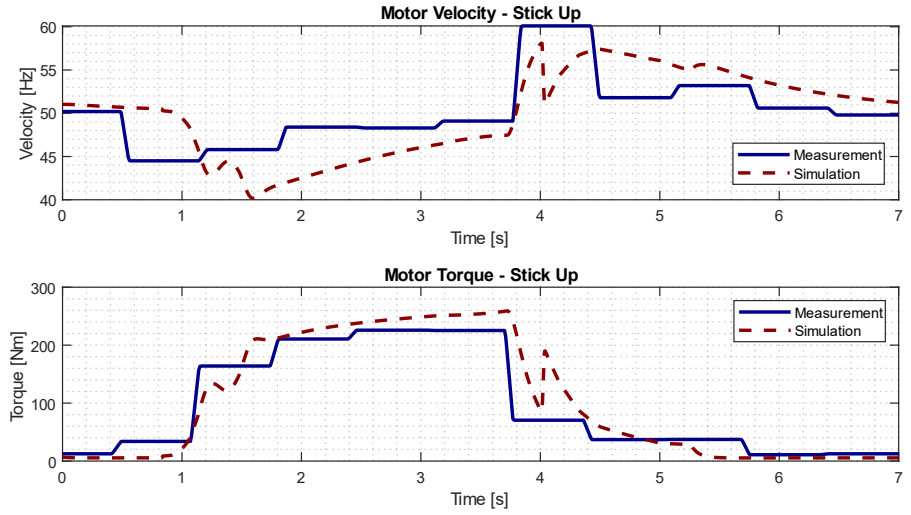

Figure 6.15 Stick up comparison. Electric motor: velocity and torque.

Once again, if pressure and torque are like the experimental ones, the same goes for the current, as clearly visible in Figure 6.16. In this case, even if the values at any moment never match, it is visible how much alike are the trends. For this lifting movement of the stick, not only the current is well simulated, but also the voltage drop, which in the previous tests is always a bit too sharp.

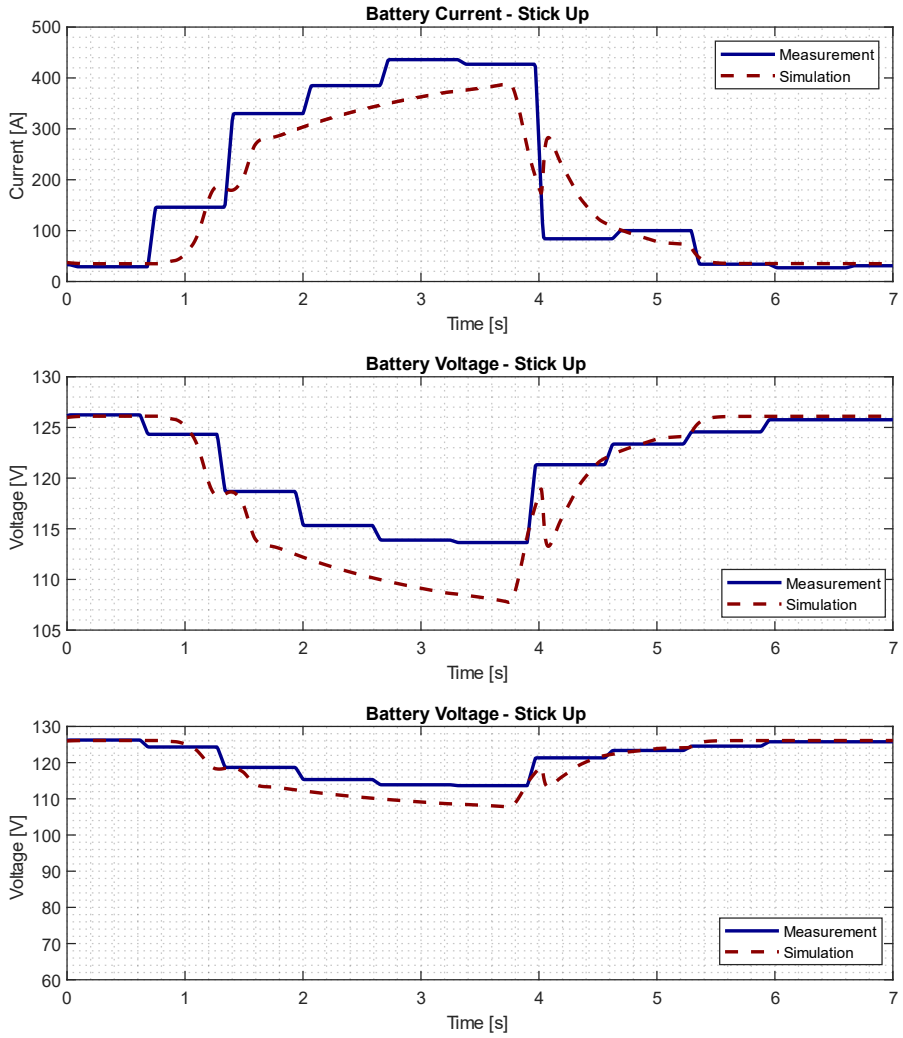

Figure 6.16 Stick up comparison. Energy storage: current and voltage.

6.3 Upper carriage

Even if the swing angle is not measured, the values of pressure, flow, motor velocity, motor torque, current, and voltage, exist, thus the analysis is carried out by comparing these latter values. In this regard, it is worth noticing that all the subsystems' plots for the upper carriage are very similar for both the clockwise and counterclockwise movements. This is due to the almost perfect symmetry of the hydraulic system.

Starting with the hydraulic subsystem, in Figure 6.17 there are the curves of the pump pressure and flow. At the beginning of the movement, despite a good match between the curves of the flow, the pressures rise differently. This visible discrepancy is surely caused by the interactions among the hydraulic

valves, thus more precise data on these components are necessary. On the contrary, there is a good match in the central part, but it loses again accuracy towards the end.

The small accuracy of the motor velocity has already been explained for all the previous movements, while, in Figure 6.18 a good match of the torque curves is shown.

The same goes for the current, as visible in Figure 6.19. As already seen for the lowering of the two arms, being a low-demanding movement, the difference between the simulation and the testing should not ruin the overall power consumption. Nonetheless, the hydraulic system of the upper carriage needs to be better addressed.

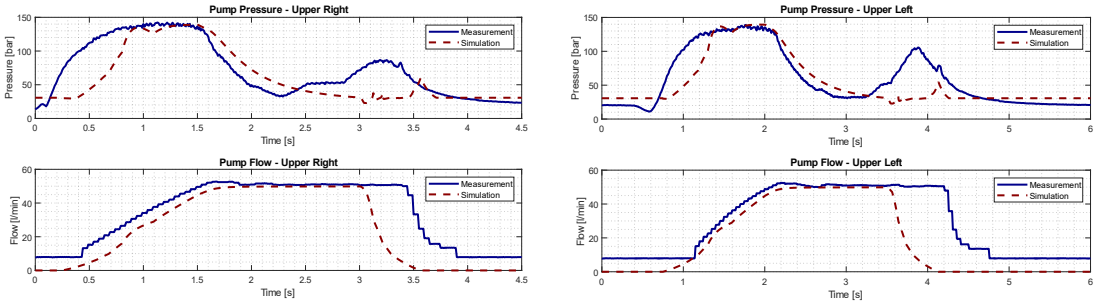

(a) (b)

Figure 6.17 Upper carriage comparison. Hydraulics: pump pressure and pump flow. Clockwise (a), counterclockwise (b).

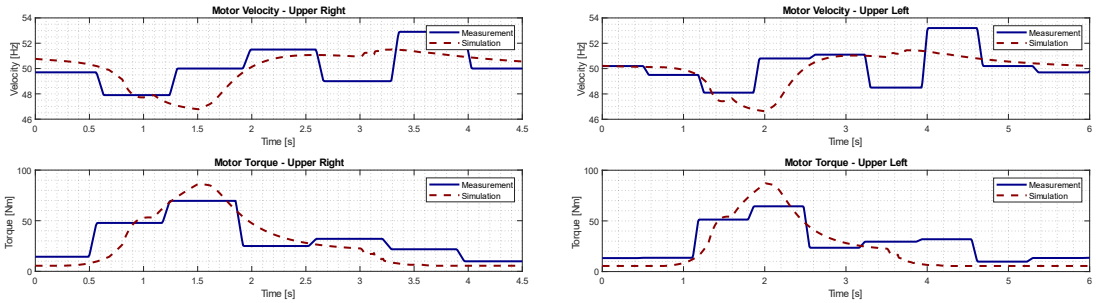

(a) (b)

Figure 6.18 Upper carriage clockwise comparison. Electric motor: velocity and torque. Clockwise (a), counterclockwise (b).

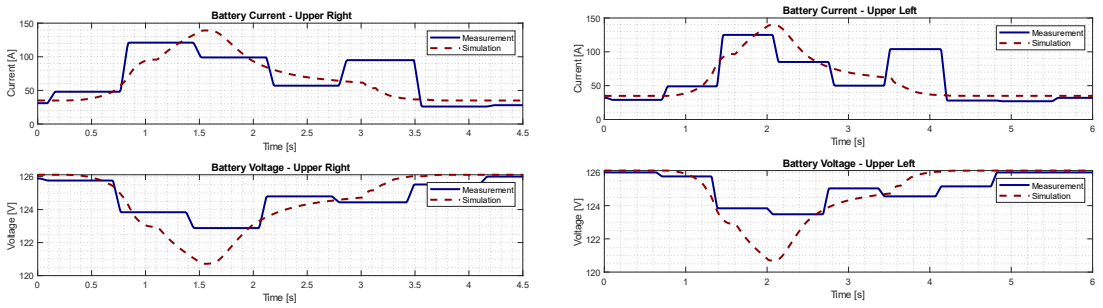

(a) (b)

Figure 6.19 Upper carriage clockwise comparison. Energy storage: current and voltage. Clockwise (a), counterclockwise (b).

6.4 General Discussion and Model Performance

As previously mentioned, achieving a good understanding of the transients of the machinery is the goal of this model, which is designed (almost in its entirety) using industry-oriented modeling software. Moving from a mainly steady-state design to a transient steady-state design is key to allow the investigation of new control strategies, working modes, etc., also for SMEs. Indeed, these companies frequently lack the expertise, time, and resources to build more in-depth model-based designs, but they can take advantage of simplified models.

However, after the display of all the single movements required by the system, one last evaluation must be carried out. It is indeed important to look at the overall power and energy consumption, to see if a more complex use of the machinery, with sequential movements, the model generates similar energy consumption. Furthermore, comparing the power consumption of the real machinery and the simulated one is key for numerically assessing the performance of the model.

To this end, the electric power requested by the battery is computed by combining all the previous tests. This is indeed the last component of the powertrain, thus it considers all the efficiencies/losses of the machinery, for both the model and the real machinery.

The two most common performance indexes are the mean error $\bar{e}$ (Eq. 19) and the correlation r (Eq. 20). The first is the average of the differences

between the simulated values and the measured ones. The latter measures how strongly the two values are related to each other.

$$\bar{e} = \frac{1}{N}\sum_{i=1}^{N}(P_{\mathrm{sim}_i} - P_{\mathrm{real}_i}) \qquad \text{Eq. 19}$$

$$r = \frac{\sum_{i=1}^{N}(P_{\mathrm{sim}_i} - \overline{P_{\mathrm{sim}}})(P_{\mathrm{real}_i} - \overline{P_{\mathrm{real}}})}{\sqrt{\sum_{i=1}^{N}\left(P_{\mathrm{sim}_i} - \overline{P_{\mathrm{sim}}}\right)^2}\sqrt{\sum_{i=1}^{N}\left(P_{\mathrm{real}_i} - \overline{P_{\mathrm{real}}}\right)^2}} \qquad \text{Eq. 20}$$

- P is the power requested by the battery
- $\bar{P}$ is the average value of the power
- N is the number of observations

Considering that the outcome of the model is the assessment of energy consumption, it is useful to evaluate the average discrepancy between the energy consumed by the real machinery and the one simulated by the model. To do so, the Integral Absolute Error (IAE) (Eq. 4) is computed. Due to the formulation of the IAE, the absolute value allows a more precise computation of the error, because the negative and positive errors do not neglect each other's. For the same reason, starting from the IAE, it is possible to assess a constant average value of the power discrepancy of the model in relation to the measurements.

$$\mathrm{IAE} = \int \left|P_{\mathrm{sim}_i} - P_{\mathrm{real}_i}\right| \cdot dt \qquad \text{Eq. 21}$$

All these performance indexes of the model are visible in Table 6.1, while in Figure 6.20 it is shown the error distribution of the model. The combination of Table 6.1 and Figure 6.20 gives an understanding of the overall accuracy of the model. Furthermore, the error distribution and mean error (Figure 6.20) show that the model tends to overestimate power consumption.

$\bar{e}$	r	IAE	$\overline{\mathrm{IAE}}$
$[kW]$	$[\emptyset]$	$[kWh]$	$[kW]$
0.135	0.936	0.041	2.42

Table 6.1 Performance indexes of the model.

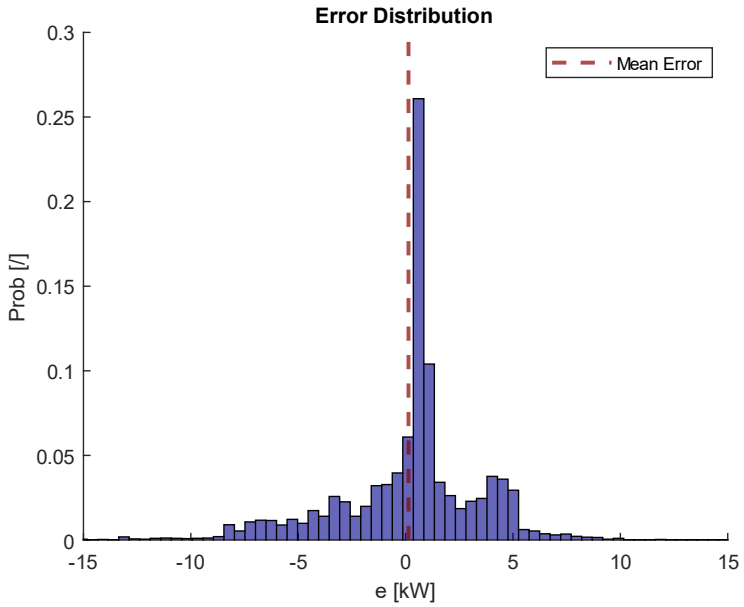

Figure 6.20 Error distribution and mean error of the model.

In general, on the one hand, it is confirmed that the model is not accurate enough to be used as a digital twin. On the other hand, it greatly improves the computation of energy consumption, limiting the use of average values and maximum performance requirements, which are typical of the steady-state approach. Indeed, the model can represent with decent accuracy the movements of the machinery, as well as the variations of the hydraulic and electrical variables.

In conclusion, even considering some inaccuracy, the model is feasible to be used to understand the behavior of the machinery, and to start its optimization by examining the advantages brought by the electrification.[10]

- [10] Some of the main results of this analysis have been published as conference proceedings. Beltrami, D., Ferrari, M., Iora, P.G., Uberti, S. (2024). Application of Physics-Based Modeling Techniques as a Tool to Help the Development of More Electrified Off-Highway Machinery. In: Carfagni, M., Furferi, R., Di Stefano, P., Governi, L., Gherardini, F. (eds) Design Tools and Methods in Industrial Engineering III. ADM 2023. Lecture Notes in Mechanical Engineering. Springer, Cham. https://doi.org/10.1007/978-3-031-52075-4_56 [163]

7 Optimization

The model-based design shifts part of the development of a product from testing to simulation, and this is extremely useful in streamlining the entire process. Indeed, the model-based design allows the simulation of multiple and different tests, investigating methodologies feasibility in the early stages. First, it avoids wasting time on unachievable solutions, second, it is possible to limit experimental campaigns for the more in-depth tuning of the system.

Speaking about the M15e, the model can be initially used to look for working modes based on the machinery as it is. Secondly, it is possible to try alternative solutions, taking advantage of the electric motor speed control.

For both the former and latter analysis, the following steps are needed:

- To recall how the machinery works;
- To understand how the operator interacts with the machinery;
- To create a representative duty cycle.

The M15e is a retrofit of the ICE-powered M15, thus it relies on the same working logic. The rotational velocity of the power source is accelerated from the idle condition to a higher constant speed, turning the hydraulic pump at the same rotational speed. When no power is requested by the functions, to avoid wasting power, the displacement of the pump is turned down to almost zero displacement. The whole control of the displacement is done by the LS system. Indeed, when a power request occurs, the LS system compares the pressure at the outlet of the pump with the pressure down to the DCV, automatically setting the displacement to keep the DCV pressure drop close to the LS margin, which is about 20 bar. Every time a load is applied to the motor, its velocity decreases according to the motor's dynamics, while the controller automatically brings the velocity back to the constant selected reference speed. Thanks to the LS system, the hydraulic system does not suffer from the load-dependency, so, the velocity of the movements and behavior of the machinery are independent from the load.

The load-independency is crucial for the operator, who must control the machinery using the joysticks inside the cab[11]. More precisely, the joystick's basic working mode is to behave as a velocity controller: the higher the shifting of the joystick by the operator, the higher the expected velocity of the movement[12]. The operator is also responsible for selecting the constant reference speed of the power source by turning a specific command: the higher this reference, the higher the maximum hydraulic flow, and the higher the maximum velocity of the actuators.

Therefore, the velocity is controlled by two different inputs, the constant rotational speed of the motor/pump and the shifting of the joysticks. Furthermore, the velocity influences both the time required to complete a task and its energy consumption. For this reason, it is fundamental to create and use a common, representative, and duplicable duty cycle based on a sequence of movements and tasks. With such a duty cycle, the uncertainty of the subjective behavior of the operator is eliminated, and the response of the machinery is the only remaining output.

7.1 The Duty Cycle

The duty cycle visible in Figure 7.1 is created in agreement with Officine Minelli s.r.l., and it represents the conventional use of this type of machinery. The following variables are used to determine the states:

- α is the angle of the boom;
- β is the angle of the stick;
- γ is the angle of the upper carriage;
- the load grabbed by the end effector varies.

- [11] Inside the cab there are two joysticks and two pedals:
  - the right joystick controls the movement of the boom and orange peel grab;
  - the left joystick controls the movement of the stick and rotation of the upper carriage;
- [12] As seen in the chapter Upper Carriage, the upper carriage hydraulic system varies this general behavior, transforming the joystick from a velocity controller to an acceleration controller.

The mass attached to the orange peel grab changes during the duty cycle to simulate the typical use of a hydraulic material handler, but its maximum value can be set using a MATLAB script. More precisely, it varies from a minimum of 400 kg to a maximum of 1600 kg. In the former case, the work with low-density material is simulated (e.g. plastic waste), in the latter it mimics the grab of high-density material (e.g. metallic scrap).

MATLAB Simulink Stateflow [162] is used to implement the duty cycle into the model. As visible in Figure 7.2, the flow diagram inside the model is slightly more complicated than the one visible in Figure 7.1, because it includes more intermediate steps between the four main machinery states.

The duty cycle can be considered as a sequential control chart, with no P, PI, or PID controller to oversee the movements of the duty cycle. Thus, the movements are not optimally controlled, simulating a more realistic behavior.

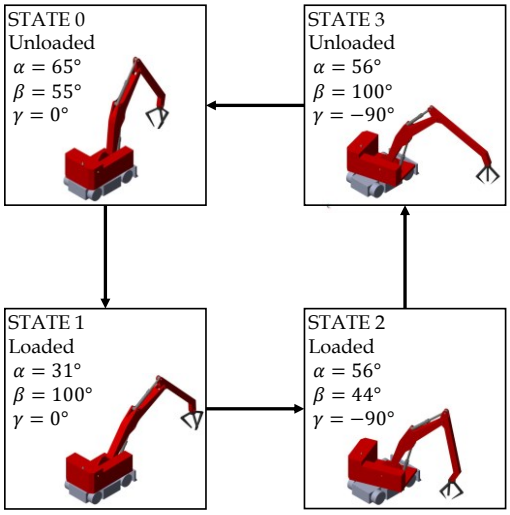

Figure 7.1 Simplified flow chart of the duty cycle.

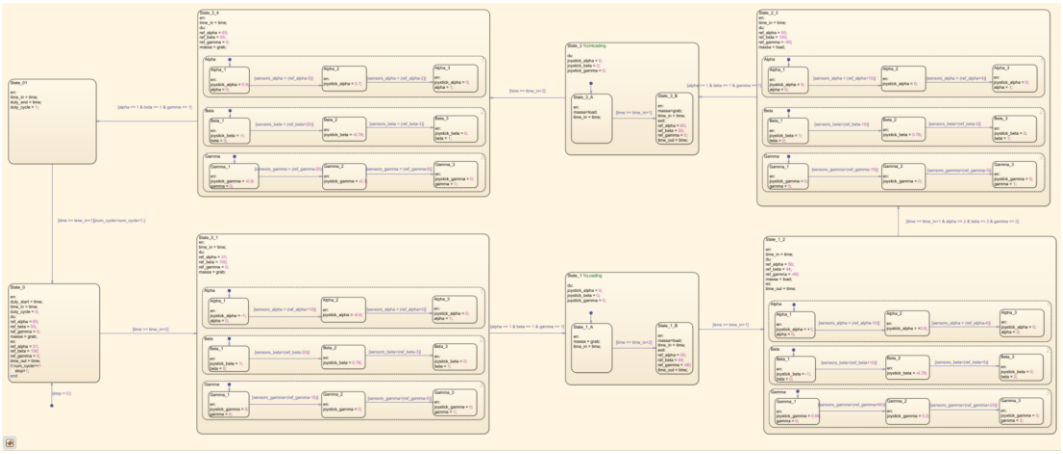

Figure 7.2 Stateflow implementation of the duty cycle.

7.2 Constant Speed Optimization

As mentioned, the first possible investigation regards the optimization of the machinery as it is, simulating the machinery as it is traditionally used. It means that the operator selects a constant speed and moves the joysticks, while everything else is managed by hydraulics[13].

To this end, a MATLAB script is used to sweep two different variables:

- Electric motor speed: $900 \div 2400\ RPM$
- Load: $400 \div 1600\ kg$

The results of these simulations are visible in Figure 7.3 and Figure 7.4.

In Figure 7.3, the x-axis shows different electric motor speeds, while the y-axis shows the time required to complete the duty cycle. The first and most obvious comment highlights that higher electric motor speeds correspond to lower duty cycle times. But, most importantly, it is worth emphasizing that the time required to end the duty cycle is almost completely independent of the load. Indeed, only at higher speeds, there is a noticeable difference in time.

However, higher speeds and lower required times correspond also to higher energy consumption, which is visible in Figure 7.4. Furthermore, it is

- [13] The only exception is the control of the electric motor and battery, which is carried out by the inverter-controller.

shown that the energy consumption increases linearly (more or less) with the load.

From a purely energetic point of view, looking at the two plots in Figure 7.3 and Figure 7.4, the best solution is to lower the electric motor speed to its minimum. Indeed, it does not restrain the machinery from accomplishing its duty cycle, thus it may be viable. However, this type of machinery is used to move high tonnage of material every day, and both operators and waste disposal companies want to move as much material as possible each working shift. So, from the productivity point of view, it may be better to work at high speed.

This type of disparity is typical for many applications, including the off-highway machinery industry. Thus, a balance must be found to combine the two different needs, and model-based design and simulation can help investigate it before moving to real-world testing and tuning.

Looking at the various velocity and energy curves of Figure 7.3 and Figure 7.4 a minimum/optimal working point does not exist. However, it is possible to evaluate a speed, or a small range of speeds, where a balance between energy consumption and duty cycle time can be reasonable.

In this regard, in Figure 7.3 it is visible how much the requested time tends to reach an asymptote at higher rotational speeds. Taking for instance a load of $800\ kg$, there is a 15% time reduction increasing the motor speed from the minimum to the maximum. But, at $1600\ rpm$, the time reduction remains close to 12%. At the same time, the energy consumption from 900 to $2400\ rpm$ increases around 11%, while it is limited to 6% at $1600\ rpm$ (Figure 7.4).

To have a better overview of the results, it is possible to combine the results of Figure 7.3 and Figure 7.4 in the plot visible in Figure 7.5.

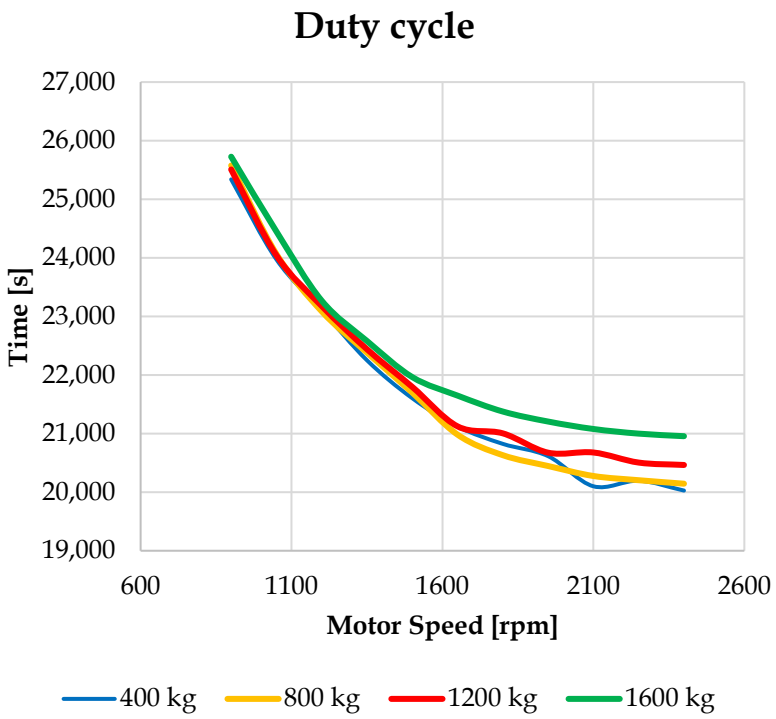

Figure 7.3 Requested time to complete the duty cycle in relation to the constant motor speed of the electric motor.

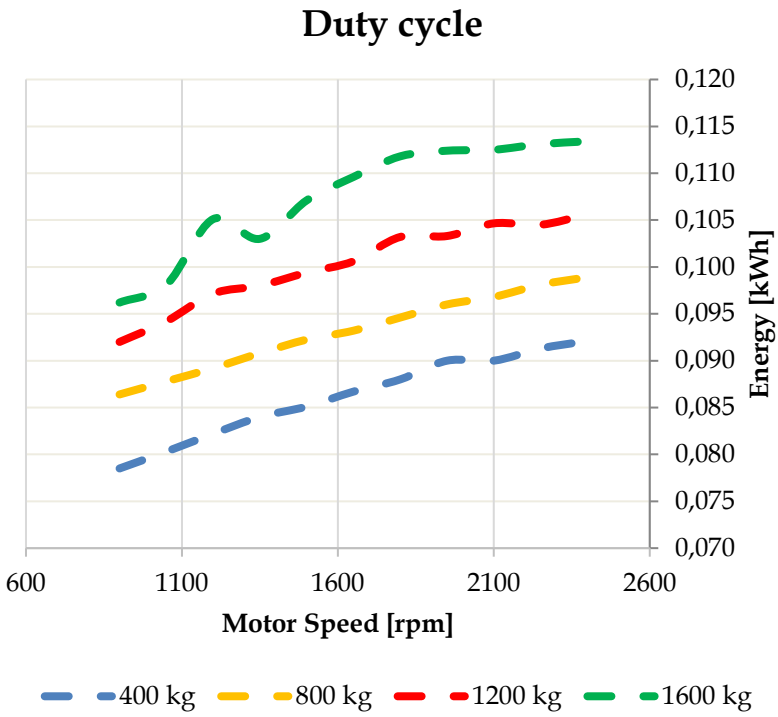

Figure 7.4 Energy consumption of the duty cycle in relation to the constant motor speed of the electric motor.

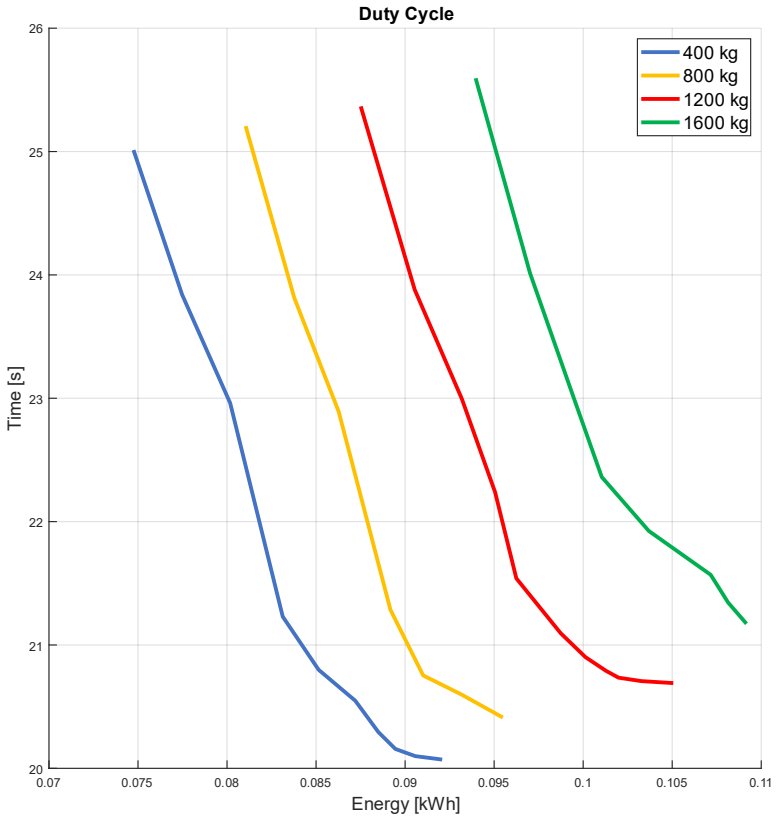

Figure 7.5 Energy consumption and time required by the duty cycle.

It is worth mentioning that this result about the average reference speed around 1600 *rpm* agrees with the empirical evaluations made by the manufacturer. Therefore, the industry-oriented model-based design of the M15e confirms its decent quality of simulating the behavior of the machinery, and this last analytical result carried out by looking at simulated results finds confirmation in the real world.

7.3 Variable Speed Optimization

As already mentioned, one great advantage of electric motors compared to ICEs is their ability to quickly vary the velocity. Moreover, the efficiency of an electric machine is always way higher than an ICE.

Thus, with an electric machine, it is possible to implement a new control variable: the rotational speed. Instead of using the power source at a constant reference speed and delegating the control of the flow to the LS system, the

rotational velocity varies to use the hydraulic pump at its maximum efficiency.

For this reason, the efficiency maps of the hydraulic pump and electric motor are essential, and they are reported in Figure 7.6 and Figure 7.7.

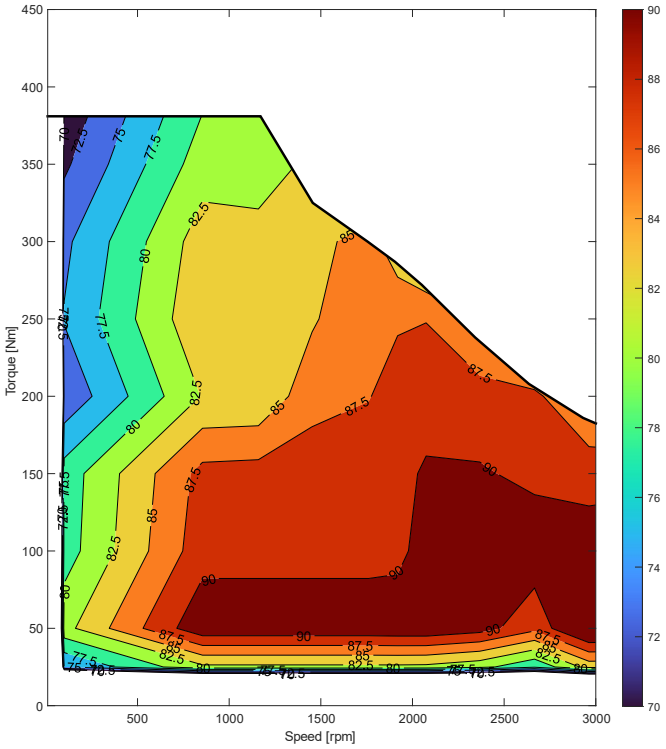

Figure 7.6 Efficiency map of the electric motor.

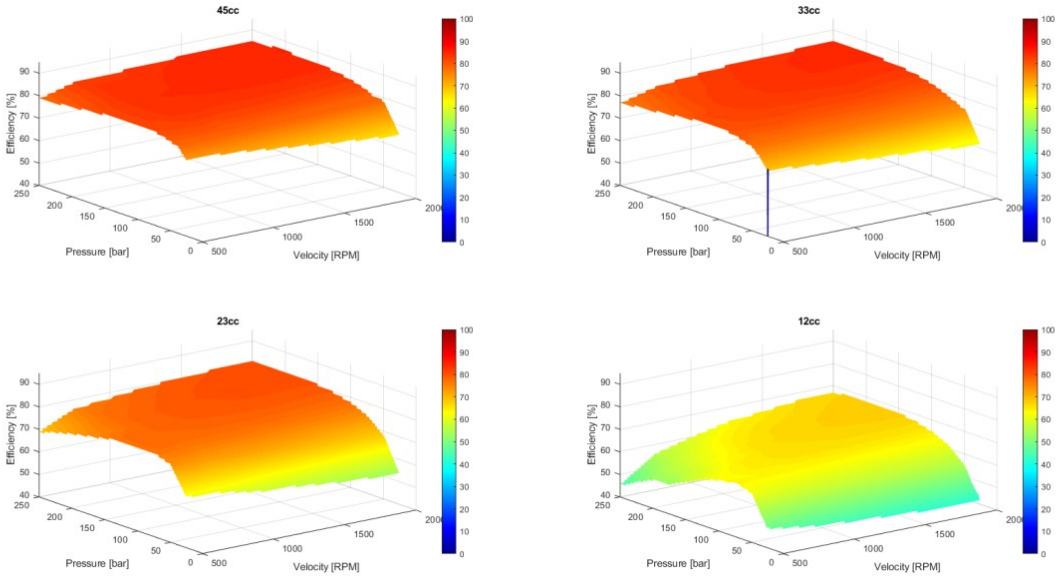

Figure 7.7 Efficiency map of the hydraulic pump.

Knowing the two efficiency maps, it is theoretically possible to compute the optimal working point for any combination of velocity and displacement. But, as mentioned in the chapter Modeling the Machinery, the efficiency map of the electric motor is computed by multiple interpolations of the experimental data received by the electric machine supplier, therefore, this map needs further and more in-depth investigation for this type of optimization. In this regard, more technical data are needed from the supplier.

On the contrary, even ignoring the exact efficiency map of the hydraulic pump mounted on the M15e, the analytical efficiency of the Simscape model proves to be close to the efficiency map of competitors' solutions, where higher displacements correspond to higher efficiencies across the whole range of rotational speeds and pressures.

Looking at the two components' efficiency maps, it is visible that the efficiency range of the hydraulic pump is larger and reaches lower values, while the motor efficiency is constantly higher. Consequently, it is reasonable to prefer the hydraulic pump to work at its best working range, while the electric motor can be controlled across a bigger range without excessively compromising the overall efficiency of the powertrain.

It is essential then to clarify the following:

- an optimal working point cannot be investigated due to the current inaccuracy of the efficiency map of the electric motor;
- the aim is to take advantage of the electric motor's variable speed to improve the overall usage of the machinery, without changing the hydraulics;
- moving the joysticks inside the cab, the operator commands the actuators' velocities. Indeed, the ideal velocity of a linear cylindrical actuator is:

$$v = Q/A \qquad \text{Eq. 22}$$

Where Q is the flow and A is the piston area.

Going backward in the powertrain, the ideal flow Q coming from the pump is:

$$Q = V \cdot n \qquad \text{Eq. 23}$$

Where V is the actual displacement and n is the rotational velocity.

However, between the pump and the actuator, there is the DCV, and every spool of the DCV is characterized by a characteristics curve based on the following orifice equation:

$$Q_{\mathrm{O}} = C_{\mathrm{d}}\, A_{\mathrm{eq,\,O}} \sqrt{\frac{2\Delta p}{\rho}} \qquad \text{Eq. 24}$$

Thus, flow and pressure are not completely independent values, and the main variable linking them one each other is the equivalent area of the spool. This equivalent area of the spool varies based on the spool's linear movement, which is imposed by the shifting of the joystick inside the cab. At the same time, the hydraulic system of the machinery relies on the LS system, which is designed to maintain the LS margin across the DCV.

Knowing these relations and the characteristic curves of the spools, it is possible to create multiple LUTs to find the excepted Q_{DCV}. More precisely, these LUTs are created by considering the following two aspects:

- how much flow is requested by the operator using the joystick;
- how much flow must run through the valve to guarantee the LS margin across the DCV.

At this point, knowing Q_{DCV}, it is possible to compute at each instant, what is the minimum velocity n_{min} such that the displacement is automatically set at its maximum feasible value V_{max}.

In Figure 7.8, there is a simplified flow chart of this optimization, while in Figure 7.9, there is a screenshot of its implementation in the model.

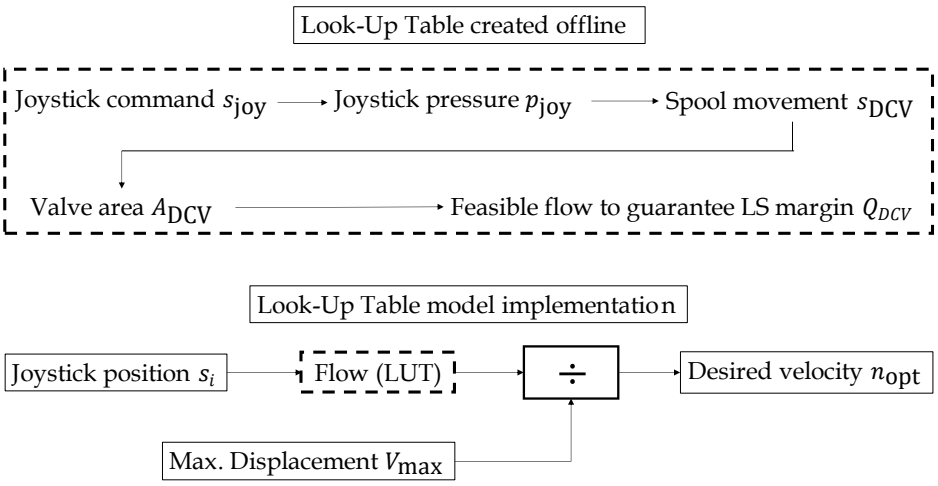

Figure 7.8 Simplified flow chart of the variable speed and displacement optimization.

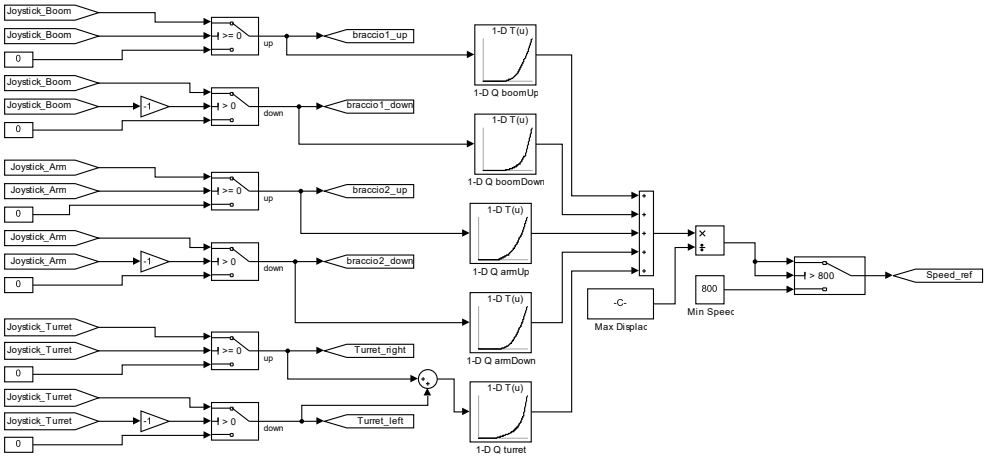

Figure 7.9 Implementation of the LUTs in the M15e.

To get results easily comparable with the optimization at constant speed, a script to sweep the loads is created, and the results are reported in Figure 7.10. There are both the results of the constant speed optimization and these new results about the variable speed optimization. For the latter optimization, it is worth noticing that there is a single test per load. Indeed, the velocity is automatically computed by the model and cannot be manually selected.

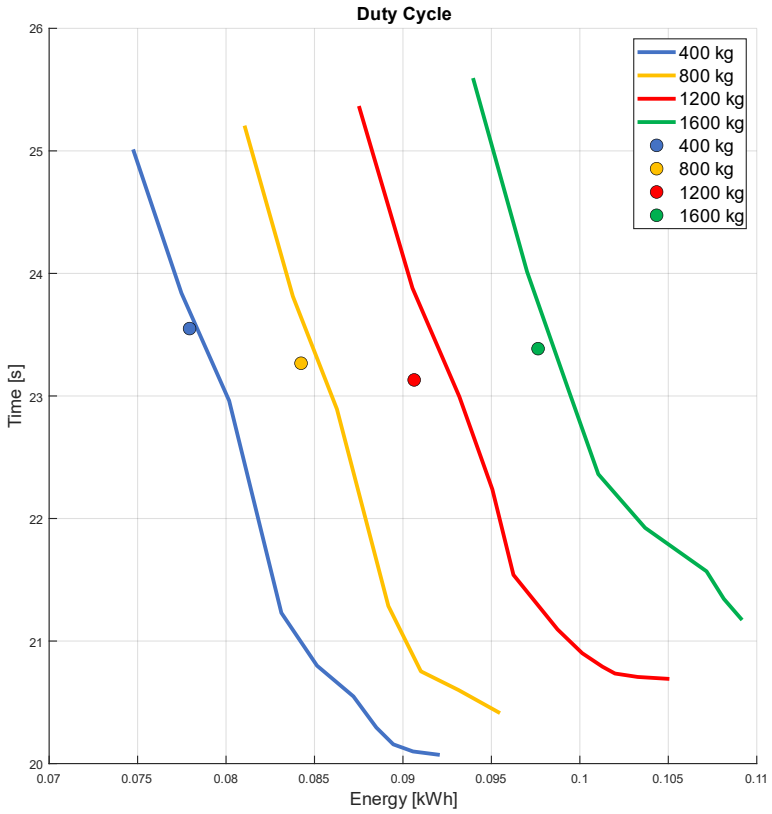

Figure 7.10 Energy consumption and time required by the duty cycle: constant speed optimization (thick line), variable speed optimization (marker).

By implementing the variable motor speed control, it is visible that, for the same amount of time required by the duty cycle, its energy consumption is reduced. Or evenly, the duty cycle is faster for the same energy consumption. This is an extremely interesting result. Indeed, from an energetic point of view, it shows that a simple variation of the traditional control scheme can be enough to reduce the energy consumption of the machinery. Most importantly, this is achieved without changing any component of the hydraulic system.

In fairness, it is important to recognize that the simulated energy consumption reduction is marginal, particularly considering the inaccuracies of the model already discussed in the chapter Results and Discussion. Indeed, both the efficiency map and dynamics of the electric motor need to be improved, as well as some components' details of the hydraulics. Furthermore, with these improvements it will be possible to both enhance this analysis and to combine the efficiency maps of the electric motor and

hydraulic pump, proceeding then with the investigation of the optimal working point.

Lastly, it must be noticed that, losing the possibility to set a velocity reference, the operator cannot decide to favor productivity over energy consumption, or the opposite. Consequently, it may be possible that this type of solution could be interesting only for some working modes, but needs to be excluded upon request. In this regard, keeping the same hydraulics is fundamental and turns out to be a great advantage of the approach used for this optimization.

8 Conclusions

Electrified vehicles have undergone great evolution during the last decades thanks to the increasing attention on environmental sustainability, greenhouse gas emissions, and air pollution. On the one hand, final users are more knowledgeable and sensitive about the topic, on the other hand, governments have been tightening emission regulations.

The electrification of the consumptions for the automotive industry is in broad daylight, but the same process has just started for the off-highway industry.

Indeed, the electrification process can be seen as an enabling technology, but it comes also with new challenges and objectives. For instance, it facilitates new off-highway architectures and the development of both incremental and disruptive technology, enabling the emergence of completely new machinery and companies too.

In this regard, the NRMM industry is characterized by the presence of many SMEs. These often work as system integrators, meaning that they look for off-the-shelf components/systems, and they care about their smooth integration on the final machinery.

This is an important aspect because SMEs are usually more sensitive to changes. On the one hand, if well managed, electrification can bring them great opportunities, especially because small companies can be more agile. On the other hand, they must pay attention not to be cut off the market by larger and richer manufacturers. The latter has indeed more expertise, time, and resources to investigate and optimize hybrid or electric machinery.

Indeed, while the focal point of electrified machinery remains to effectively complete its task, more attention is given to how efficiently this is accomplished. NRMM are indeed purchased to generate value and income, not for leisure or status, thus this market needs to justify the higher cost of acquisition with lower costs of operation, higher productivity, and/or new purposes.

The higher upfront cost of electrified machinery is due to components' cost, and to the investments in research and development to improve and optimize the performance of such components.

For these reasons, the common and most important aspect of the current electrification process is the attempt to maintain reasonable costs by limiting disruptive innovations, for instance, developing retrofitted electric machinery from existing ICE-based ones.

Model-based design has already been gaining acceptance as a cornerstone of engineering, and it can also help SMEs improve their products. Indeed, "modeling and simulation" aims to digitalize as much as possible of the research and development, but it requires moving from steady-state analyses made using spreadsheets to transient-state simulations. This shifting is indeed a priority to better analyze energy consumption and to exploit the benefits of electrification. However, this process is not straightforward, it requires highly specialized employees, and it takes time.

Aware of this situation, more and more software houses are developing tools to ease modeling and simulation, by moving from explicit coding to visual programming to the assembly of pre-compiled components. A clear example of this transition can be seen throughout the portfolio offered by MathWorks with MATLAB, Simulink, and Simscape. Indeed, MATLAB excels in matrix operations, data manipulation, and visualization, but it is not ideal for modeling complex dynamics systems. Simulink is a graphical simulation and model-based design environment based on MATLAB, and it is extremely common for dynamic systems analysis. However, it still needs in-depth mathematical knowledge of the phenomena, and, most importantly, it is necessary to understand and share its visual programming logic. Lastly, Simscape is a tool within the Simulink environment, and its purpose is to simplify the modeling of physical systems. The aim is to shift the attention from block diagram modeling to component-based modeling. Thus, instead of visually coding equations and interactions, there are libraries of physical components where to insert proper physical parameters.

Because moving from steady-state design to transient-state design is essential to investigate electrified machinery and vehicles, and to investigate if industry-based modeling software and approach can help an SME enhance

its electrified machinery, a battery electric hydraulic material handler is modeled, simulated, and tested, and two optimization strategies are investigated.

In particular, the model is created relying as much as possible on the datasheets, greatly decreasing the use of complex mathematical relationships. When needed, independent models are designed to convert data for Simscape applications and/or to understand the components' behaviors. This is fundamental because many subsystems cannot be exactly reproduced using the pre-compiled Simscape component.

An important example of this approach is the model of the LS system, which is the hydraulic feedback that controls the displacement of the hydraulic pump. The precise replica of its hydraulic scheme is impossible on Simscape, thus the model relies on a combination of physical and hydraulic Simscape components to replicate its behavior.

Knowing both the advantages and disadvantages of Simscape, and that the goal is the transition from a spreadsheets-based steady-design to dynamic or transient-state design (and not the design of a digital twin), what's most important to achieve is a general harmony of the trends between experimental results and simulations.

The final result of the model is in line with the original expectations, overall showing a good trend between simulated and experimental results, even if some inaccuracies are present. First, as already explained, hydraulics is extremely difficult to replicate, second, the technical data published on datasheets are not always sufficient to get good results, as is the case for the electric motor.

Nonetheless, the model can represent with decent accuracy the movements of the machinery, as well as the variations of the hydraulic and electrical variables. Moreover, the power and energy consumption are sufficiently well replicated, and this outcome allows the model to be used for the investigation of working modes and control strategies.

These are indeed essential to take advantage of the electrification process, in particular with retrofitted machinery, where the aim is to change as little as possible of the components.

To this end, the first step is to investigate the best constant speed reference to balance the productivity and energy consumption of the machinery, without changing any control. A good balance is found at $1600\ rpm$, and this velocity is confirmed by the manufacturer's empirical experience. Therefore, the industry-oriented model-based design of the M15e confirms its decent quality of simulating the behavior of the machinery in the real world.

The second step is to add the electric motor speed control, and a new strategy is then simulated. In particular, this strategy aims to control the electric motor such that the hydraulic pump works at its maximum efficiency, which is towards higher displacement. This behavior is achieved by knowing the relation between the joysticks inside the cab and the related excepted flow to the actuators. Even if this is a simple improvement, the investigation shows that an energy consumption reduction is possible, but the machinery loses part of its adaptability. Indeed, using this logic, the operator cannot favor productivity over energy consumption (or the contrary). However, because none of the hydraulic components differ, the operator could potentially select if to use the machinery with the traditional control strategy, or with the new one.

In conclusion, the use of retrofitted machinery is surely a viable solution for SMEs to learn the ropes of electrification, and to get used to this new technology. However, to remain competitive, the design of the retrofits must be carried out with a new design paradigm. Indeed, moving from steady-state design to transient-state design is fundamental to benefit of the advantages enabled by the electrification.

Industry-oriented modeling software can actually be used to address this task. Even if a more in-depth, mathematical, and data-based approach is needed to get to a digital twin, a model built with software like Simscape can already give useful indications of the transients of the machinery. These indications can then be used to investigate the general behavior of the machinery, to develop new working modes or control strategies, etc., streamlining the development of more electrified machinery.

References

1. Morris C (2023) As The Off-Road Vehicle Market Rushes To Electrify, Standards are Lagging Behind. Charged - Electric Vehicle Magazine 28–33
2. European Parliament (2016) Regulation (EU) 2016/1628 of the European Parliament and of the Council
3. Malavatu J, Kandke SR, Gupta S, Agrawal B (2019) Design Challenges in Electrification of Off-highway Applications. 2019 IEEE Transportation Electrification Conference, ITEC-India 2019. https://doi.org/10.1109/ITEC-India48457.2019.ITECIndia2019-247
4. Haycraft WR (2011) History of Construction Equipment. J Constr Eng Manag 137:720–723. https://doi.org/10.1061/(ASCE)CO.1943-7862.0000374
5. Sanders RW (1998) Vintage Farm Tractors. The Ultimate Tribute to Classic Tractors, First Edition. Barnes & Noble Books
6. Caterpillar Caterpillar | Company History Timeline. https://www.caterpillar.com/en/company/history/history-timeline.html. Accessed 24 Aug 2023
7. History - Komatsu Germany GmbH – Mining Division, Düsseldorf. https://www.komatsu.eu/en/company/komatsu-germany-mining/history. Accessed 24 Aug 2023
8. Hagan R, Markey E, Clancy J, et al (2022) Non-Road Mobile Machinery Emissions and Regulations: A Review. Air 2023, Vol 1, Pages 14-36 1:14–36. https://doi.org/10.3390/AIR1010002
9. Yan F, Winijkul E, Streets DG, et al (2014) Global emission projections for the transportation sector using dynamic technology modeling. Atmos Chem Phys 14:5709–5733. https://doi.org/10.5194/acp-14-5709-2014
10. Merkisz J, Lijewski P, Fuc P, et al (2016) Development of the methodology of exhaust emissions measurement under RDE (Real Driving Emissions) conditions for non-road mobile machinery (NRMM) vehicles. IOP Conf Ser Mater Sci Eng 148:012077. https://doi.org/10.1088/1757-899X/148/1/012077

11. Zhang Q, Yang L, Ma C, et al (2020) Emission characteristics and chemical composition of particulate matter emitted by typical non-road construction machinery. Atmos Pollut Res 11:679–685. https://doi.org/10.1016/j.apr.2019.12.018
12. Desouza CD, Marsh DJ, Beevers SD, et al (2020) Real-world emissions from non-road mobile machinery in London. Atmos Environ 223:117301. https://doi.org/10.1016/j.atmosenv.2020.117301
13. Lovarelli D, Bacenetti J (2019) Exhaust gases emissions from agricultural tractors: State of the art and future perspectives for machinery operators. Biosyst Eng 186:204–213. https://doi.org/10.1016/J.BIOSYSTEMSENG.2019.07.011
14. Public Buyers Community (2022) Joint Statement of Demand of Zero Emission Construction Sites Working. https://public-buyers-community.ec.europa.eu/resources/joint-statement-demand-zero-emission-construction-sites-working-group. Accessed 22 Aug 2023
15. Dieselnet (2021) Emission Standards. https://dieselnet.com/standards/eu/nonroad.php#intro. Accessed 21 Aug 2023
16. The European Parliament and the Council of the European Union (2016) Regulation (EU) 2016/ 1628 of the European Parliament. Official Journal of the European Union
17. Dallman T, Menon A (2016) Technology pathways for diesel engines used in non-road vehicles and equipment. International Council on Clean Transportation (ICCT)
18. International Council on Clean Transportation (2016) European Stage V non-road emission standards
19. EPA (1999) EPA Nonregulatory Nonroad Duty Cycles. In: Environmental Protection Agency. https://www.epa.gov/moves/epa-nonregulatory-nonroad-duty-cycles#individual. Accessed 22 Jan 2021
20. JCMAS (2007) JCMAS H020:2007. Earth-moving machinery – Fuel consumption on hydraulic excavator – Test Procedure
21. DLG-PowerMix: Tractor output, efficiency and fuel consumption - dlg.org. https://www.dlg.org/en/agriculture/tests/dlg-powermix/. Accessed 12 Jun 2023

22. Brenna M, Foiadelli F, Leone C, et al (2018) Feasibility Proposal for Heavy Duty Farm Tractor. In: 2018 International Conference of Electrical and Electronic Technologies for Automotive. IEEE, pp 1–6
23. Troncon D, Alberti L, Mattetti M (2019) A Feasibility Study for Agriculture Tractors Electrification: Duty Cycles Simulation and Consumption Comparison. In: 2019 IEEE Transportation Electrification Conference and Expo (ITEC). IEEE, pp 1–6
24. Dalboni M, Santarelli P, Patroncini P, et al (2019) Electrification of a Compact Agricultural Tractor: A Successful Case Study. In: 2019 IEEE Transportation Electrification Conference and Expo (ITEC). IEEE, pp 1–6
25. Bertini A, Ceraolo M, Lutzemberger G (2015) Systematic approach in the hybridization of a hydraulic skid loader. Autom Constr 58:144–154. https://doi.org/10.1016/j.autcon.2015.07.013
26. Bertini A, Ceraolo M, Lutzemberger G (2012) Development of a hybrid skid loader through modelling. 2012 IEEE International Energy Conference and Exhibition, ENERGYCON 2012 1022–1027. https://doi.org/10.1109/EnergyCon.2012.6347719
27. Alan C, Ali S, Alaa H, Eric B (2014) Optimal sizing of an energy storage system for a hybrid vehicle applied to an off-road application. In: 2014 IEEE/ASME International Conference on Advanced Intelligent Mechatronics. IEEE, pp 775–780
28. Nevrly J, Fichta M, Jurik M, et al (2020) Battery Electric Drive of Excavator Designed with Support of Computer Modeling and Simulation. Proc West Mark Ed Assoc Conf 58:25. https://doi.org/10.3390/wef-06927
29. Schneider S, Vincenz D (2018) SUNCAR Elektrobagger. Oberbüren, Switzerland
30. Vauhkonen N, Liljeström J, Maharjan D, et al (2014) Electrification of excavator. Proceedings of the International Conference of DAAAM Baltic 2014-Janua:305–310
31. Salomaa V (2017) Efficiency Study of an Electro-Hydraulic Excavator. Master's Thesis. Tampere University of Technology, Tampere, Finland

32. The MathWorks Inc MATLAB. https://www.mathworks.com/products/matlab.html. Accessed 23 Aug 2023
33. The MathWorks Inc Simulink - MATLAB. https://www.mathworks.com/products/simulink.html?s_tid=hp_products_simulink. Accessed 23 Aug 2023
34. The MathWorks Inc Simscape - MATLAB. https://www.mathworks.com/products/simscape.html. Accessed 23 Aug 2023
35. Li K (2019) GitHub - Quarter Car. https://github.com/kattly/Quarter_Car. Accessed 23 Aug 2023
36. Lin T, Lin Y, Ren H, et al (2020) Development and key technologies of pure electric construction machinery. Renewable and Sustainable Energy Reviews 132:110080. https://doi.org/10.1016/j.rser.2020.110080
37. Liebherr Liebherr Mining Goes Electric - Liebherr. https://www.liebherr.com/en/ita/latest-news/news-press-releases/detail/liebherr-mining-goes-electric.html. Accessed 5 Mar 2021
38. He X, Jiang Y (2018) Review of hybrid electric systems for construction machinery. Autom Constr 92:286–296. https://doi.org/10.1016/j.autcon.2018.04.005
39. Lukic SM, Emadi A (2004) Effects of Drivetrain Hybridization on Fuel Economy and Dynamic Performance of Parallel Hybrid Electric Vehicles. IEEE Trans Veh Technol 53:385–389. https://doi.org/10.1109/TVT.2004.823525
40. Soma A, Bruzzese F, Mocera F, Viglietti E (2016) Hybridization Factor and Performance of Hybrid Electric Telehandler Vehicle. IEEE Trans Ind Appl 52:5130–5138. https://doi.org/10.1109/TIA.2016.2595504
41. Filla R (2009) Hybrid Power Systems for Construction Machinery: Aspects of System Design and Operability of Wheel Loaders. In: Volume 13: New Developments in Simulation Methods and Software for Engineering Applications; Safety Engineering, Risk Analysis and Reliability Methods; Transportation Systems. ASMEDC, pp 611–620

42. Iora PG (2016) Tecnologie per la Mobilità Sostenibile: Veicoli elettrici, ibridi e a fuel cell. Società Editrice Esculapio, Bologna
43. Emadi A (2014) Advanced Electric Drive Vehicles, 1st Editio. CRC Press
44. Henze V (2022) Lithium-ion Battery Pack Prices. In: BloombergNEF. https://about.bnef.com/blog/lithium-ion-battery-pack-prices-rise-for-first-time-to-an-average-of-151-kwh/. Accessed 29 Aug 2023
45. Ding Y, Cano ZP, Yu A, et al (2019) Automotive Li-Ion Batteries: Current Status and Future Perspectives. Electrochemical Energy Reviews 2:1–28. https://doi.org/10.1007/s41918-018-0022-z
46. Yang XG, Liu T, Wang CY (2021) Thermally modulated lithium iron phosphate batteries for mass-market electric vehicles. Nat Energy 6:176–185. https://doi.org/10.1038/s41560-020-00757-7
47. Wang H, Wang Q, Hu B (2017) A review of developments in energy storage systems for hybrid excavators. Autom Constr 80:1–10. https://doi.org/10.1016/j.autcon.2017.03.010
48. Wang J, Yang Z, Liu S, et al (2016) A comprehensive overview of hybrid construction machinery. Advances in Mechanical Engineering 8:168781401663680. https://doi.org/10.1177/1687814016636809
49. Hui S, Lifu Y, Junqing J (2010) Hydraulic/electric synergy system (HESS) design for heavy hybrid vehicles. Energy 35:5328–5335. https://doi.org/10.1016/j.energy.2010.07.027
50. Lin T, Wang L, Huang W, et al (2017) Performance analysis of an automatic idle speed control system with a hydraulic accumulator for pure electric construction machinery. Autom Constr 84:184–194. https://doi.org/10.1016/j.autcon.2017.09.001
51. Rajashekara K (2013) Present Status and Future Trends in Electric Vehicle Propulsion Technologies. IEEE J Emerg Sel Top Power Electron 1:3–10. https://doi.org/10.1109/JESTPE.2013.2259614
52. Un-Noor F, Padmanaban S, Mihet-Popa L, et al (2017) A Comprehensive Study of Key Electric Vehicle (EV) Components, Technologies, Challenges, Impacts, and Future Direction of Development. Energies (Basel) 10:1217. https://doi.org/10.3390/en10081217
53. Moreda GP, Muñoz-García MA, Barreiro P (2016) High voltage electrification of tractor and agricultural machinery – A review. Energy

Convers Manag 115:117–131. https://doi.org/10.1016/j.enconman.2016.02.018

54. An K, Kang H, An Y, et al (2020) Methodology of Excavator System Energy Flow-Down. https://doi.org/10.3390/en13040951
55. Love LJ (2012) Estimating the Impact (Energy, Emissions and Economics) of the US Fluid Power Industry. Oak Ridge, TN (United States)
56. Ohira S, Suehiro M, Ota K, Kawamura K (2013) Use of emission rights for construction machinery to help prevent global warming. Hitachi Review 62:123–130
57. Padovani D, Rundo M, Altare G (2020) The Working Hydraulics of Valve-Controlled Mobile Machines: Classification and Review. J Dyn Syst Meas Control 142:. https://doi.org/10.1115/1.4046334
58. Axin M (2015) Mobile Working Hydraulic System Dynamics. Linköpings universitet. Institutionen för ekonomisk och industriell utveckling.
59. Cetinkunt S, Pinsopon U, Chen C, et al (2004) Positive flow control of closed-center electrohydraulic implement-by-wire systems for mobile equipment applications. Mechatronics 14:403–420. https://doi.org/10.1016/S0957-4158(03)00067-9
60. Vacca A, Franzoni G (2021) Hydraulic Fluid Power - Fundamentals, Applications, and Circuit Design, First Edit. John Wiley and Sons Ltd, Chichester, UK
61. Jensen S A Shifting Fluid Power Industry | OEM Off-Highway. In: OEM Off-HighwayOEM Off-Highway. https://www.oemoffhighway.com/fluid-power/article/21244542/a-shifting-fluid-power-industry. Accessed 17 Feb 2021
62. Minav T, Papini L, Jarf A, et al (2016) Direct Driven Hydraulics: What can possibly go wrong? -A thermal analysis. In: 2016 XXII International Conference on Electrical Machines (ICEM). IEEE, pp 1618–1624
63. Minav TA, Heikkinen JE, Pietola M (2015) Electric-driven Zonal Hydraulics in Non-Road Mobile Machinery. In: New Applications of Electric Drives. InTech
64. Zhang S, Minav T, Pietola M (2017) Decentralized Hydraulics for Micro Excavator. In: Proceedings of 15:th Scandinavian International

Conference on Fluid Power, 15th Scandinavian International Conference on Fluid Power, Fluid Power in the Digital Age, SICFP'17, June 7-9 2017 - Linköping, Sweden. pp 187–195

65. Zhang S, Minav T, Pietola M, et al (2019) The effects of control methods on energy efficiency and position tracking of an electro-hydraulic excavator equipped with zonal hydraulics. Autom Constr 100:129–144. https://doi.org/10.1016/j.autcon.2019.01.003
66. Michel S, Weber J (2017) Investigation of Self-Contamination of Electrohydraulic Compact Drives. In: The 10th JFPS International Symposium on Fluid Power. The Japan Fluid Power System Society, Fukuoka
67. Minav T, Heikkinen J, Schimmel T, Pietola M (2019) Direct Driven Hydraulic Drive: Effect of Oil on Efficiency in Sub-Zero Conditions. Energies 2019, Vol 12, Page 219 12:219. https://doi.org/10.3390/EN12020219
68. Minav T, Bonato C, Sainio P, Pietola M (2014) Direct Driven Hydraulic Drive. In: The 9th International Fluid Power Conference. IFK, Aachen, Germany, pp 508–517
69. Ketelsen S, Padovani D, Andersen TO, et al (2019) Classification and Review of Pump-Controlled Differential Cylinder Drives. Energies 2019, Vol 12, Page 1293 12:1293. https://doi.org/10.3390/EN12071293
70. Minav T, Heikkinnen J, Pyne S, et al (2020) Analysis of novel zonal two-cylinder actuation system for heavy loads. In: Volume 1 - Symposium. Technische Universität Dresden, pp 99–103
71. The European Commission NorrDigi revolutionary Energy Saver | Norrdigi Project | H2020 | CORDIS | European Commission
72. Gøytil PH, Padovani D, Hansen MR (2020) A Novel Solution for the Elimination of Mode Switching in Pump-Controlled Single-Rod Cylinders. Actuators 9:20. https://doi.org/10.3390/act9010020
73. Ketelsen S, Schmidt L, Donkov VH, Andersen TO (2018) Energy Saving Potential in Knuckle Boom Cranes using a Novel Pump Controlled Cylinder Drive. Modeling, Identification and Control: A Norwegian Research Bulletin 39:73–89. https://doi.org/10.4173/mic.2018.2.3

74. Minav T, Zhang S, Pietola M (2017) Eliminating Sizing Error in Direct-Driven Hydraulics. In: The 10th JFPS International Symposium on Fluid Power, JFPS2017At: Fukuoka, Japan
75. Fassbender D, Zakharov V, Minav T (2021) Utilization of electric prime movers in hydraulic heavy-duty-mobile-machine implement systems. Autom Constr 132:103964. https://doi.org/10.1016/j.autcon.2021.103964
76. Opdenbosch P, Sadegh N, Book W, Enes A (2011) Auto-calibration based control for independent metering of hydraulic actuators. In: 2011 IEEE International Conference on Robotics and Automation. IEEE, pp 153–158
77. Kim H, Choi J, Yi K (2012) Development of supervisory control strategy for optimized fuel consumption of the compound hybrid excavator. Proceedings of the Institution of Mechanical Engineers, Part D: Journal of Automobile Engineering 226:1652–1666. https://doi.org/10.1177/0954407012447019
78. Borghi M, Zardin B, Pintore F, Belluzzi F (2014) Energy Savings in the Hydraulic Circuit of Agricultural Tractors. Energy Procedia 45:352–361. https://doi.org/10.1016/j.egypro.2014.01.038
79. Xu B, Shen J, Liu S, et al (2020) Research and Development of Electro-hydraulic Control Valves Oriented to Industry 4.0: A Review. Chinese Journal of Mechanical Engineering 33:29. https://doi.org/10.1186/s10033-020-00446-2
80. Zhang Q, Kong X, Yu B, et al (2020) Review and Development Trend of Digital Hydraulic Technology. Applied Sciences 10:579. https://doi.org/10.3390/app10020579
81. Wang H, Chen Z, Huang J, et al (2022) Development of High-Speed On–Off Valves and Their Applications. Chinese Journal of Mechanical Engineering 35:67. https://doi.org/10.1186/s10033-022-00720-5
82. Green M, Macpherson J, Caldwell N, Rampen WHS (2018) DEXTER: The Application of a Digital Displacement® Pump to a 16 Tonne Excavator. In: BATH/ASME 2018 Symposium on Fluid Power and Motion Control. American Society of Mechanical Engineers, pp 45–54
83. Pellegri M, Green M, Macpherson J, et al (2020) Applying a multi-service digital displacement® pump to an excavator to reduce valve

losses. In: Volume 2 - Conference. Technische Universität Dresden, pp 59–68

84. Gehm R Volvo CE and Norrhydro digital hydraulics. https://www.sae.org/news/2020/12/volvo-ce-and-norrhydro-digital-hydraulics. Accessed 25 Mar 2021
85. Beltrami D, Iora P, Tribioli L, Uberti S (2021) Electrification of Compact Off-Highway Vehicles—Overview of the Current State of the Art and Trends. Energies (Basel) 14:5565. https://doi.org/10.3390/en14175565
86. Grayson W Bobcat's Electric Excavator Retrofit A First Step Toward An All-Electric Future | Equipment World. In: Equipment World. https://www.equipmentworld.com/alternative-power/battery-electric/video/14972534/bobcats-electric-excavator-retrofit-a-first-step-toward-an-allelectric-future. Accessed 11 Mar 2021
87. ISO (2018) ISO - ISO 6469-3:2018 - Electrically propelled road vehicles — Safety specifications — Part 3: Electrical safety. https://www.iso.org/standard/68667.html. Accessed 12 Mar 2021
88. Bilo J, Burghoff H-G, dos Santos H, Engbring J (2016) 48 Volt Electrical Systems – A Key Technology Paving to the Road to Electric Mobility. Frankfurt
89. Fischer H-M, Dorn L, ZVEI (2013) Voltage Classes for Electric Mobility
90. Frost and Sullivan (2019) Global Off-Highway Vehicle Electrification Trends, Forecast to 2030. Santa Clara, CA, USA
91. CEMA aisbl (2019) European Agricultural Machinery Industry: CEMA Priorities and key figures. Brussels
92. JCB JCB 525-60E | Electric Telehandler. https://www.jcb.com/en-gb/products/telescopic-handlers/525-60e-hi-viz. Accessed 16 Apr 2021
93. E-mining AG Products | E-mining AG. https://www.emining.ch/en/products. Accessed 16 Apr 2021
94. ZF Friedrichschafen ZF eTRAC Driveline System for Electric Vehicles. https://www.oemoffhighway.com/drivetrains/product/21126638/zf-friedrichshafen-ag-zf-etrac-driveline-system-for-electric-vehicles. Accessed 11 Mar 2021
95. Boasch Rexroth AG (2018) Electrification of Mobile Applications. Lohr am Main, Germany

96. Deutz AG (2018) E-DEUTZ Market Positioning. Cologne, Germany
97. Buning EA (2010) Electric Drives in Agricultural Machinery-Approach from the Tractor Side. Journal of Agricultural Engineering 47:30
98. Caban J, Vrabel J, Šarkan B, et al (2018) Analysis of the market of electric tractors in agricultural production. MATEC Web of Conferences 244:03005. https://doi.org/10.1051/matecconf/201824403005
99. Fendt Fendt e100 Vario | Fendt FutureFarm - Fendt. https://www.fendt.com/it/e100-vario. Accessed 1 Apr 2021
100. Rigitrac Rigitrac SKE 40 Electric - Rigitrac Website! https://www.rigitrac.ch/produkte-1/rigitrac-ske-40-electric/. Accessed 1 Apr 2021
101. Monarch Tractor Monarch Tractor Electric Tractor. https://www.monarchtractor.com/. Accessed 1 Apr 2021
102. Farmtrac Farmtrac - Trattori. https://www.farmtracitalia.it/trattori. Accessed 20 Apr 2021
103. Van Leeuwen LB (2020) Hydrogen or battery tractors: what potential for sustainable grape growing? IVES Technical Reviews, vine and wine. https://doi.org/10.20870/IVES-TR.2020.4381
104. Allen J John Deere develops fully electric, autonomous tractor | Industrial Vehicle Technology International. In: IVT International. https://www.ivtinternational.com/news/agriculture/john-deere-develops-fully-electric-autonomous-tractor.html. Accessed 18 May 2021
105. E-OX EOX - 175. https://www.e-ox.nl/eox-175. Accessed 20 Apr 2021
106. Li T, Huang L, Liu H (2019) Energy management and economic analysis for a fuel cell supercapacitor excavator. Energy 172:840–851. https://doi.org/10.1016/j.energy.2019.02.016
107. TU Dresden Rigitrac EWD 120. https://tu-dresden.de/ing/maschinenwesen/int/ast/ressourcen/dateien/forschung/files/flyer_rigitrac.pdf?lang=en. Accessed 8 Apr 2021
108. Pialorsi R (2019) Stato dell'arte dei veicoli elettrici e studio dell'elettrificazione di un veicolo industriale con trasmissione meccanica. Master's Thesis. Università degli Studi di Brescia, Brescia, Italy

109. DULEVO Scopri la nuova spazzatrice stradale elettrica DZero2. https://dzero2.dulevo.com/it/index.xhtml. Accessed 2 Apr 2021
110. Boschung (2021) Urban-Sweeper S2.0 - Electric Street Sweeper releasing 0 (zero) emissions. https://www.boschung.com/product/urban-sweeper-s2-0/. Accessed 2 Apr 2021
111. Uberti S, Azzini G, Beltrami D, et al (2020) Modelling of a 15-kW Electric Utility Vehicle and Range Assessment through Driving Cycle Analysis Based on GPS Experimental Data. In: SAE Technical Papers
112. Morris C Charged EVs | Dennis Eagle's new electric refuse trucks hit the streets, earn rave reviews - Charged EVs. In: Charged EVs. https://chargedevs.com/newswire/dennis-eagles-new-electric-refuse-trucks-hit-the-streets-earn-rave-reviews/. Accessed 21 Apr 2021
113. Serrao L, Rizzoni G (2008) Optimal control of power split for a hybrid electric refuse vehicle. In: 2008 American Control Conference. IEEE, pp 4498–4503
114. Serrao L, Hubert CJ, Rizzoni G (2007) Dynamic Modeling of Heavy-Duty Hybrid Electric Vehicles. In: Volume 16: Transportation Systems. ASMEDC, pp 121–128
115. Sullivan J (2016) Gas Versus Electric Forklifts – Which Is Better? In: Toyota Material Handling Nothern California. https://www.tmhnc.com/blog/gas-versus-electric-forklifts-which-is-better. Accessed 6 Apr 2021
116. Fu S, Chen H, Ren H, et al (2020) Potential Energy Recovery System for Electric Heavy Forklift Based on Double Hydraulic Motor-Generators. Applied Sciences 10:3996. https://doi.org/10.3390/app10113996
117. Electric Motor Engineering Partnership for the industrial full electric loader - Electric Motor Engineering. https://www.electricmotorengineering.com/partnership-for-the-industrial-full-electric-loader/. Accessed 20 Apr 2021
118. Keränen TM, Karimäki H, Viitakangas J, et al (2011) Development of integrated fuel cell hybrid power source for electric forklift. J Power Sources 196:9058–9068. https://doi.org/10.1016/j.jpowsour.2011.01.025
119. Hosseinzadeh E, Rokni M, Advani SG, Prasad AK (2013) Performance simulation and analysis of a fuel cell/battery hybrid forklift truck. Int J

Hydrogen Energy 38:4241–4249. https://doi.org/10.1016/j.ijhydene.2013.01.168

120. H2ports First application of hydrogen technologies in port handling equipment in Europe. https://h2ports.eu/wp-content/uploads/2020/03/H2PORTS-Brochure.pdf. Accessed 26 Aug 2021
121. JCB 19C-1 JCB E-TECH | JCB.com. https://www.jcb.com/it-it/products/mini-escavatori/19c-1e. Accessed 6 Apr 2021
122. Tobroco Giant Electric loaders from Tobroco-Giant can be used all year long. https://www.tobroco-giant.com/en/products/wheel-loaders/giant-g2200e-x-tra/. Accessed 6 Apr 2021
123. Volvo CE Volvo CE unveils 100 percent electric compact excavator prototype : Volvo Construction Equipment. https://www.volvoce.com/global/en/news-and-events/press-releases/2017/volvo-ce-unveils-100-percent-electric-compact-excavator-prototype/. Accessed 26 Apr 2021
124. Volvo CE Volvo CE unveils the next generation of its electric load carrier concept : Volvo Construction Equipment. https://www.volvoce.com/global/en/news-and-events/press-releases/2017/conexpo-vegas-2017/volvo-ce-unveils-the-next-generation-of-its-electric-load-carrier-concept/. Accessed 21 Apr 2021
125. Inoue H (2008) Introduction of PC200-8 Hybrid Hydraulic Excavators
126. Edamura M, Ishida S, Imura S, Izumi S (2013) Adoption of electrification and hybrid drive for more energy-efficient construction machinery
127. Kobelco Europe HYBRID - Kobelco Construction Machinery Europe B.V. https://www.kobelco-europe.com/innovation/hybrid/. Accessed 8 Apr 2021
128. Goodenough B, Czarnecki A, Robinette D, et al (2023) Reducing Fuel Consumption on a Heavy-Duty Nonroad Vehicle: Conventional Powertrain Modifications
129. Ishida K, Higurashi M (2015) Hybrid wheel loaders incorporating power electronics

130. MathWorks (2020) Mechanical Joints. In: MathWorks. https://it.mathworks.com/help/sm/ug/joints.html. Accessed 30 Oct 2023
131. MathWorks (2020) Solid CAD. In: MathWorks. https://it.mathworks.com/help/sm/ref/filesolid.html?searchHighlight=File%20Solid&s_tid=srchtitle_support_results_1_File%20Solid. Accessed 30 Oct 2023
132. MathWorks (2020) Rigid Transform. In: MathWorks. https://it.mathworks.com/help/sm/ref/rigidtransform.html?searchHighlight=Rigid%20Transform&s_tid=srchtitle_support_results_1_Rigid%20Transform. Accessed 30 Oct 2023
133. Midac Batteries Midac MDL/MBS. http://www.midacbatteries.com/it/batterie_motive/73/2/mdlmbs.html. Accessed 27 Sep 2023
134. Sato S, Kawamura A (2022) A new estimation method of state of charge using terminal voltage and internal resistance for lead acid battery. In: Proceedings of the Power Conversion Conference-Osaka 2002 (Cat. No.02TH8579). IEEE, pp 565–570
135. Nakajo K, Kumarasinghe S, Shimamura Y, et al (2016) On-line measurement system for internal resistance in lead acid battery. In: 2016 55th Annual Conference of the Society of Instrument and Control Engineers of Japan (SICE). IEEE, pp 103–108
136. Zapi S.p.A. (2015) Datasheet - ZAPI AC3. Zapi S.p.A.
137. MathWorks (2020) Mapped Motor and Drive Electronics. In: MathWorks. https://it.mathworks.com/help/autoblks/ref/mappedmotor.html. Accessed 30 Oct 2023
138. MathWorks (2020) Hydraulic Fluid Component. https://it.mathworks.com/help/hydro/ref/hydraulicfluid.html?s_tid=doc_ta. Accessed 9 Oct 2023
139. Conqord Oil S.r.l. (2020) Datasheet - Q8 Handel. Q8 Oils
140. Linde Hydraulics Gmbh & Co. (2020) Datasheet - Linde HPR. Linde Hydraulics Gmbh & Co.
141. AlfaBiotech S.p.A. (2018) Datasheet - AlfaBiotech. AlfaBiotech S.p.A.

142. MathWorks (2020) Hydraulic Pipeline Component. In: MathWorks. https://it.mathworks.com/help/hydro/ref/hydraulicpipeline.html. Accessed 9 Oct 2023
143. MathWorks (2020) Hydraulic Var-Disp Bidirectional Pump. In: MathWorks. https://it.mathworks.com/help/hydro/ref/variabledisplacementpump.html. Accessed 9 Oct 2023
144. Kauranne H (2022) Effect of Operating Parameters on Efficiency of Swash-Plate Type Axial Piston Pump. Energies (Basel) 15:4030. https://doi.org/10.3390/en15114030
145. MathWorks (2020) Hydraulic Double Acting Cylinder. In: MathWorks. https://it.mathworks.com/help/hydro/ref/doubleactinghydrauliccylinder.html. Accessed 12 Oct 2023
146. MathWorks (2020) Prismatic Joint. In: MathWorks. https://it.mathworks.com/help/sm/ref/prismaticjoint.html. Accessed 12 Oct 2023
147. MathWorks (2020) Hydraulic Pressure Relief Valve. In: MathWorks. https://it.mathworks.com/help/hydro/ref/pressurereliefvalve.html. Accessed 19 Oct 2023
148. Linde Hydraulics Gmbh & Co. (2020) Datasheet - Linde VW. Linde Hydraulics Gmbh & Co.
149. Linde Hydraulics Gmbh & Co. (2020) Datasheet - Linde Spool 6610007590 - 1. Linde Hydraulics Gmbh & Co.
150. Linde Hydraulics Gmbh & Co. (2020) Datasheet - Linde Spool 6610007590 - 2. Linde Hydraulics Gmbh & Co.
151. Linde Hydraulics Gmbh & Co. (2020) Datasheet - Linde Spool 6610007590 - 3. Linde Hydraulics Gmbh & Co.
152. MathWorks (2020) Hydraulic Generic Variable Orifice. In: MathWorks. https://it.mathworks.com/help/hydro/ref/variableorifice.html. Accessed 16 Oct 2023
153. Doke J (2020) GRABIT GUI. In: Matlab Central File Exchange. https://it.mathworks.com/matlabcentral/fileexchange/7173-grabit. Accessed 17 Oct 2023
154. MathWorks (2020) Hydraulic Double-Acting Valve Actuator. In: MathWorks.

https://www.mathworks.com/help/hydro/ref/hydraulicdoubleactingvalveactuator.html. Accessed 18 Oct 2023

155. MathWorks (2020) Hydraulic 2-Way Directional Valve. In: MathWorks. https://it.mathworks.com/help/hydro/ref/2waydirectionalvalve.html. Accessed 19 Oct 2023
156. Linde Hydraulics Gmbh & Co. (2020) Datasheet - Linde HMF. Linde Hydraulics Gmbh & Co.
157. MathWorks (2020) Pressure Compensator. In: MathWorks. https://it.mathworks.com/help/hydro/ref/pressurecompensator.html. Accessed 30 Oct 2023
158. Bosch Rexroth Oil Control SpA (2016) Datasheet - Bosch Rexroth VBC-33. Bosch Rexroth Oil Control SpA
159. Hydrotechnik (2021) Datasheet - Hydrotechnik QT4xx. Hydrotechnik
160. Hydrotechnik (2021) Datasheet - Hydrotechnik PR 1xx. Hydrotechnik
161. PEAK System (2021) Datasheet - PEAK PCAN-USB. PEAK System
162. MathWorks (2023) Stateflow Documentation. In: MathWorks. https://it.mathworks.com/help/stateflow/index.html?searchHighlight=stateflow&s_tid=srchtitle_support_results_1_stateflow. Accessed 26 Oct 2023
163. Beltrami D, Ferrari M, Iora PG, Uberti S (2024) Application of Physics-Based Modeling Techniques as a Tool to Help the Development of More Electrified Off-Highway Machinery. pp 497–504

List of Figures

List of Tables

Ringraziamenti

Per la seconda volta in vita mia "voglio iniziare un discorso in modo squisitamente egocentrico ringraziando me stesso per aver resistito fino alla fine di questo percorso, per averlo vissuto appieno e per aver sempre cercato di vedere il lato positivo di ogni esperienza fatta, gioiosa o meno che fosse. Fine dell'egocentrismo". (cit. la mia tesi magistrale)

Voglio continuare ringraziando la mia famiglia, perché senza il loro sostegno probabilmente non avrei avuto il coraggio di iniziare questa strana avventura chiamata "dottorato di ricerca". Grazie papà Ennio per il gusto delle piccole cose, grazie mamma Caterina per l'empatia, grazie Laura per la costanza e grazie Marco per la leggerezza. Poi mi sento di scrivere qui quello che ripeto spesso al mio amato nonno Luciano (a cui so di dover molta della mia dedizione al lavoro): io non so se svolgere il dottorato sia stata la scelta migliore che potessi fare, quantomeno sotto al profilo lavorativo e di carriera, ma sono felice di averla presa. Volevo scoprire cosa significasse "fare ricerca", ed un pochino penso di averlo capito. Pensavo potesse essere una cosa divertente, e penso lo sia stato. Volevo testarmi in un ambiente e paese diverso, e direi che anche questo l'abbia portato a casa. Ma soprattutto, volevo e voglio cercare una mia dimensione, e su questo punto ho perlomeno stretto il campo. Per cui, va bene così. Soprattutto perché ho la certezza che questo tempo non sia stato sprecato.

Finisco la parte più romantica ringraziando le tante persone con cui ho condiviso un pezzo di questo percorso, a Gavardo, Brescia, Columbus ed ovunque sia stato. Eviterò l'elenco di nomi perché sono davvero troppi e non voglio rischiare di dimenticarmene qualcuno. Però grazie a tutti e tutte.

Per quanto riguarda i ringraziamenti formali, penso di dover iniziare con colui che è stato letteralmente il mio compagno di scrivania. Per cui, grazie Marco. Nonostante le nostre grandi differenze, siamo una discreta squadra. Grazie inoltre al team di Technox. Nonostante il nostro lavoro fosse ben separato e non mi doveste nulla, siete sempre stati disponibili ad aiutarmi, spiegarmi, e anche a proteggermi da qualche errore che prevedevate stessi per compiere.

Grazie poi, probabilmente sopra ogni cosa, al Prof. Stefano Uberti e al Prof. Paolo Iora. Grazie di aver lavorato per me e con me perché questo percorso fosse realizzabile, di avermi consigliato al meglio delle vostre possibilità, e grazie di avermi capito.

Infine, un ringraziamento alle due istituzioni che mi hanno ospitato: grazie all'Università degli Studi di Brescia, a cui sono affezionato nonostante tanti screzi, e grazie al Center for Automotive Research di Columbus, dove mi sono sentito ben accolto fin dal primo giorno e dove ho pianto all'ultimo.

Chiudo riprendendo una frase in cui mi sono ritrovato durante le magistrali e nella quale continuo a rivedermi anche alla fine del dottorato:

"senza fretta, ma senza sosta"
(Johann Wolfgang Goethe)

Davvero grazie a tutti e tutte. Sono una persona fortunata.